Theses and Dissertations

5-2012

Molecular Dynamics Study of Diffusion of O2 Penetrates in Uncrosslinked Polydimethysiloxane (PDMS), Crosslinked PDMS, and PDMS-based Nanocomposites

Varun Ullal
University of Arkansas, Fayetteville

Follow this and additional works at: http://scholarworks.uark.edu/etd

Part of the Dynamics and Dynamical Systems Commons, Nanoscience and Nanotechnology Commons, and the Nanotechnology Fabrication Commons

Recommended Citation

Ullal, Varun, "Molecular Dynamics Study of Diffusion of O2 Penetrates in Uncrosslinked Polydimethysiloxane (PDMS), Crosslinked PDMS, and PDMS-based Nanocomposites" (2012). *Theses and Dissertations*. 417.
http://scholarworks.uark.edu/etd/417

MOLECULAR DYNAMICS STUDY OF DIFFUSION OF O$_2$ PENETRATES IN UNCROSSLINKED POLYDIMETHYSILOXANE (PDMS), CROSSLINKED PDMS, AND PDMS-BASED NANOCOMPOSITES

MOLECULAR DYNAMICS STUDY OF DIFFUSION OF O_2 PENETRATES IN
UNCROSSLINKED POLYDIMETHYSILOXANE (PDMS), CROSSLINKED PDMS, AND
PDMS-BASED NANOCOMPOSITES

A thesis submitted in partial fulfillment
of the requirements for the degree of
Master of Science in Mechanical Engineering

By

Varun N. Ullal
University of Arkansas
Bachelor of Science in Mechanical Engineering, 2008

May 2012
University of Arkansas

ABSTRACT

Molecular dynamics simulations are used to study diffusion of O_2 molecules in pure polydimethysiloxane (PDMS), crosslinked PDMS, and PDMS-based nanocomposites. The PDMS chains and penetrates are modeled using a hybrid interatomic potential which treats the Si-O atoms along the chain backbone explicitly while coarse-graining the methyl side groups and penetrates. By tracking the diffusion of penetrates in the system and subsequently computing their mean-squared displacement, diffusion coefficients are obtained. In pure PDMS models of varying molecular weight, diffusivity of the O_2 penetrates is found to have an inverse relationship with chain length. Simulation models with longer chains have more entanglements which restrict the evolution of free volume in the system necessary for diffusion of the penetrants, thus reducing their diffusivity. In agreement with experiment, the crosslinked models studied in this work maintain a PDMS to crosslink molecule weight ratio of 5:1 or 10:1. In order to satisfy this weight ratio criterion, the crosslinked models in this study are oversaturated (number of crosslink molecule ends exceeds PDMS chain ends). Despite crosslinking, the presence of these unbonded crosslink molecules in the system enhances diffusivity for the crosslinked cases in comparison to the pure PDMS models. In the nanocomposite models, diffusivity of O_2 has an inverse relationship with volume fraction. Nanoparticles act as geometric obstacles for diffusion of the atmospheric penetrates, reducing the available porosity for diffusion. In models with the smallest gap between nanoparticles, a "crossover" behavior is observed at the lowest temperatures examined, resulting in diffusivities higher than the crosslinked and pure PDMS models. This is attributed to the preferential diffusion of the penetrants through localized regions of low density within the PDMS matrix. The creation of these low density regions is due to a combination of the limited mobility of the PDMS chains at

temperatures near glass transition and the close proximity of nanoparticles at 20% volume fraction. For all models, the role of temperature on diffusion is captured using the Williams-Landel-Ferry (WLF) equation. The relationship between WLF parameters and molecular weight or nanoparticle volume fraction is studied.

This thesis is approved for recommendation
to the Graduate Council.

Thesis Director:

_____
Dr. Douglas E. Spearot

Thesis Committee:

_____
Dr. Po-Hao Adam Huang

_____
Dr. Ajay Malshe

THESIS DUPLICATION RELEASE

I hereby authorize the University of Arkansas Libraries to duplicate this thesis when needed for research and/or scholarship.

Agreed   _____

Varun N. Ullal

Refused   _____

Varun N. Ullal

ACKNOWLEDGMENTS

TABLE OF CONTENTS

LIST OF TABLES

LIST OF FIGURES

LIST OF VARIABLES

Note: Variables listed in order of appearance.

F	Force
m	Mass
a	Acceleration
U	Interatomic Potential
r	Position
k_b	Force constant for bonds
b	Instantaneous bond length
b_0	Equilibrium bond length
k_a	Force constant for angles
θ	Instantaneous value of the angle
θ_0	Equilibrium angle conformation
k_d	Force constant for dihedrals
n	Multiplicity factor
φ	Dihedral angle
$\varepsilon_{\alpha\beta}$	Lennard Jones well-depth
$\sigma_{\alpha\beta}$	Equilibrium separation distance of the LJ potential
r_s	Separation Distance
q_α, q_β	Partial charges
ε_0	Permittivity of free space

"." or "dot"	First derivative with respect to time
p_i	Momentum
ψ	Thermostatting constant
v_T	Thermostatting rate
V	Volume
t	Time
h	Barostatting rate
R_0	Center of mass of the system
A	Pre-factor for "soft" potential
r_c	Cutoff distance
K	Force constant
R	Radius of the repulsive sphere
J	Diffusion Flux
D	Diffusivity or diffusion coefficient
D_0	Diffusion constant
Q	Activation Energy
T_g	Glass Transition Temperature
C_1, C_2, y_0	WLF parameters. C_1 and C_2 are material constants whereas y_0 is a shift variable.

Chapter I: INTRODUCTION

I.1 Corrosion and its Costs

Corrosion is generally defined as the deterioration of a substance or its properties due to the environment [1, 2]. The use of metals in early civilizations, combined with their extensive prevalence and consumption in the industrial era, often creates the tendency to associate corrosion exclusively to metals. Thus, corrosion is more often specifically defined as the gradual chemical alternation of metallic materials by an oxidizing process [3]. Metals are extracted from various naturally occurring chemical compounds (ores) in the earth's crust. This extraction process requires the provision of energy to obtain metals from these original compounds. Thus, corrosion serves to degenerate metals to their true or primary form upon exposure to the environment [1-3]. It is therefore important to note that while adequate steps can be taken to prolong the life of materials exposed to corrosive environments, corrosion itself is inevitable. The rapid technological advances relating to civil infrastructure and innovations in the field of materials science has facilitated the use of engineering materials in inimical environments, raising the annual costs of corrosion damage from $5.5 billion (2.1% of Gross National Product) in 1949 [4] to $552 billion (6% of Gross National Product) in 2001 [1]. The major contributing factor to the aforementioned annual cost is the maintenance and replacement of operationally deficient infrastructure.

I.2 Existing Maintenance Methods

Traditionally, the four corrosion maintenance techniques employed to maintain civil infrastructure are: corrective, preventive, predictive, and reliability-centered maintenance [5].

Corrective maintenance involves repairing/replacing defective components after system/component failure has occurred. The application of stringent guidelines on safety and the high costs associated with such maintenance renders it unacceptable for civil infrastructure. The service/repair of equipment based on a regular schedule irrespective of damage is constituent of preventative maintenance. Predictive maintenance requires monitoring the structure to observe changes in properties, and once detected, maintenance is performed on the required parts. Thus, the actual condition of the part serves as a reminder for maintenance operations instead of a defined time interval. Lastly, reliability-centered maintenance aims to improve the three other types of maintenance by utilizing a structured approach to study the reliability history of the component combined with risk-based analysis [6]. The ideal method would serve three causes: economic, improved safety and reliability, and conservation [4]. The economic aspect underlines the inexpensive nature of the method combined with its efficacy to reduce incurred direct and indirect costs. The safety and reliability aspects would reduce or eliminate catastrophic failure due to corrosion, which results in personal injuries, unscheduled shutdowns, environmental contamination, etc. [1, 4]. The limited supply of metal resources, their wastage due to corrosion resulting from improper design, and the corresponding losses of energy associated with production of metal structures constitutes the conservation aspect [4]. To meet the requirements of a predictive maintenance based approach, a MEMS-based corrosion sensor is currently under development by Pan and Huang [7] to provide an economical and reliable alternative for an early detection and abatement of corrosion damage.

This aforementioned corrosion sensor incorporates metallic nanoparticles in a polydimethylsiloxane (PDMS) matrix as shown in Fig. 1. During exposure to the environment, atmospheric penetrants will diffuse through the permeable PDMS membrane and corrode the

2

metallic nanoparticles. This corrosion modifies the electrical conductance of the film. This change in conductance can be monitored and associated with the level of corrosion of the nanoparticles; however, this step requires a detailed understanding of the rate of diffusion of the penetrants through the matrix [8].
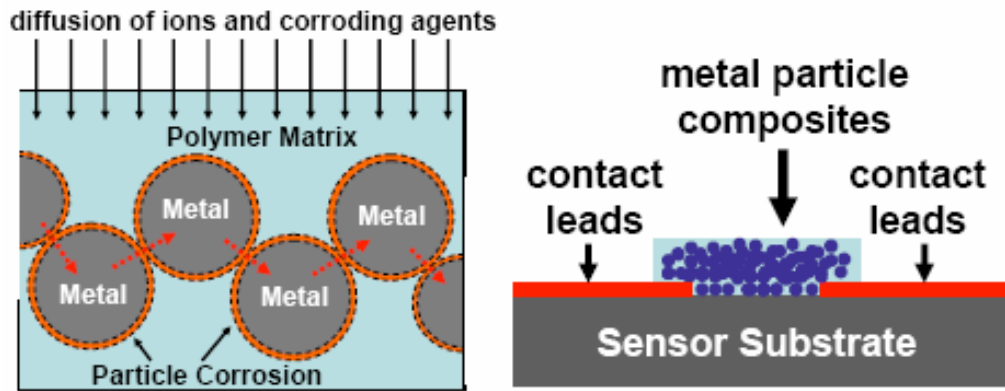
Figure 1. Schematic of the MEMS-based corrosion sensor proposed by Pan and Huang [7].

I.3 Thesis Objective and Tasks

In this thesis, molecular dynamics (MD) simulations will be used to study diffusion of O_2 molecules in pure polydimethysiloxane (PDMS), crosslinked PDMS, and PDMS-based nanocomposite systems. Diffusion is an atomic level mechanism, thus MD is the appropriate tool for this study. Additionally, MD allows for the explicit modeling of the nanoscale details pertaining to the polymer structure and metal/polymer interfaces [8, 9]. Previous work on this subject aimed to study the effect of uncrosslinked PDMS chain length on the diffusion mechanism of the penetrants and characterize a relationship between the diffusion coefficient and temperature using MD simulations [8]. A later study in an uncrosslinked PDMS melt with nanocomposites kept the chain length constant (339 repeating units of the monomer

[SiO(CH$_3$)$_2$]), while varying the number of PDMS chains and the volume fraction of the nanoparticles to analyze their explicit effects on the diffusion mechanism [10]. Thus, a natural progression of the two studies mentioned above would be to assess the influence of cross-linking on diffusion of the penetrants in PDMS and PDMS-based nanocomposite cases. Therefore, the specific tasks in this thesis are:

1. *Create a quantitative test matrix.* The diffusion of the penetrants in the polymer membrane could be affected by temperature, density, chain length, crosslink density, volume fraction of the nanoparticles, weight ratio of the PDMS chains and crosslinker molecules, etc. With such an enormous number of variables, a thorough study should be constructed to identify the individual contributions of each defined primary variable on diffusion. Therefore, setting up a systematic matrix is of primordial importance. In this study, the number of PDMS chains in the matrix is constant (50) regardless of the configuration. A detailed discussion of the test matrix is provided in Chapter III.

2. *Create and validate an algorithm for crosslinking.* A dynamic crosslinking approach, similar to the one employed by Heine et al. [11], based on a predefined cutoff distance is employed to simulate the crosslinking procedure. This approach, where all eligible pairs inside a defined cutoff are reacted simultaneously, avoids computational limitations associated with one crosslink per iteration type approaches making it suitable for larger systems. The allowance of sufficient relaxation time in between successive crosslink iterations avoids adversely affecting the system bonds,

4

angles, and dihedrals ensuring a lower energy cross-linked structure. In order to validate that the created crosslinked structure is valid, the bond and angle distributions in the system are studied using histograms along with determining glass transition temperature of the melt. Further discussion of this subject is provided in Chapter III.

3. *Study the effects of chain length and unbonded crosslink molecule ends on the diffusion mechanism.* Experiments generally tend to employ a system oversaturated with crosslinking molecules by weight (number of crosslinking molecule ends exceed the number of PDMS chain ends) resulting in either unbonded crosslink ends or entirely unbonded crosslink molecules depending on the weight ratio. The effects of the presence of excessive crosslinking molecules along with chain length of PDMS on the diffusion mechanism of the penetrants are analyzed. Crosslinking tends to restrict mobility of the system obstructing diffusion pathways while unbonded crosslinking molecules, which are extremely mobile owing to their low molecular weights, could result in increased diffusion. Further discussion pertaining to this subject is provided in Chapter IV.

4. *Create a crosslinked model of a PDMS-based nanocomposite.* The presence of metallic nanoparticles creates an added obstruction to the diffusion of atmospheric penetrants through the matrix. This study embeds eight copper nanoparticles in the cubic simulation cell. The copper atoms are placed in a simple cubic arrangement in this initial study. Further discussion on this subject is presented in Chapter III.

5. *Evaluate factors that will affect diffusion in the nanocomposite case.* PDMS exhibits properties dependent on chain length. The factors that might affect diffusion in the nanocomposite case would be chain length, volume fraction of copper nanoparticle inclusions, number of unbonded crosslink molecules, the gap spacing between the copper nanoparticles, etc. Comparisons between pure PDMS models, crosslinked PDMS models, and PDMS models with embedded metallic nanoparticle models can be made systematically to improve understanding of the factors that affect diffusion mechanisms of the penetrants. These results are presented in Chapter IV.

I.4 Polydimethylsiloxane

PDMS is a silicon-based organic polymer belonging to the family of polysiloxanes. It contains a flexible silicon-oxygen (Si-O) backbone. Two methyl sidegroups are attached to each silicon atom in the center of the chain as shown in Figure 2. The valence of silicon is four, therefore to ensure connection of atoms by a single covalent bond, the silicon atoms at each end of the chain are connected to three methyl sidegroups. This type of structure is representative of the pure PDMS molecules conducted in this study.
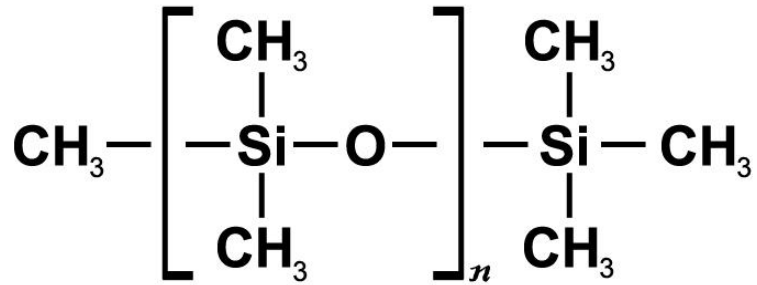
Figure 2. Schematic of a PDMS repeating unit.

The flexibility of the backbone lends PDMS its amorphous structure. The major interest in PDMS stems from the vast availability of silicon and the plethora of beneficial properties it displays translates into wide-ranging industrial applications. These properties include high flexibility, high permeability to gas, low internal pressure, low bulk viscosity, low chemical reactivity, low entropy of dilution, and small temperature variation of thermal constants (except for thermal expansivity). Its low glass transition temperature (-125 C) [12] allows operability of its elastomeric property in a vast array of temperature ranges. Common applications include silicone-based lubricants, defoaming agents, coatings, heat transfer fluids, etc. [13]. Its chemical inertness and non-toxic nature make it an ideal candidate in MEMS applications.

Crosslinking is defined as the formation of a bond formed between polymer chains, either between different chains or between different parts of the same chain. It alters the viscous gel-like behavior of PDMS, providing a solid elastomeric state. The elastic characteristics of the final structure depend on the cure conditions and the degree of crosslinking. It is important to note that the systems observed in this study have both physical entanglements and chemical crosslinks. The advantages of crosslinking include improved tensile strength, better crush resistance, improved fluid characteristics, and improved mechanical properties at higher

temperatures with negligible changes to the electrical properties and thermal stability [14]. A chemically modified form of PDMS is used to generate crosslinks due to the inertness of PDMS with the aforementioned structure and chemistry. This study uses silanol (containing SiOH groups) terminated PDMS chains. The silane-terminated crosslinking molecule used in this study is tetrakis (dimethylsiloxy) silane. The structure of both molecules is shown in Figure 3.
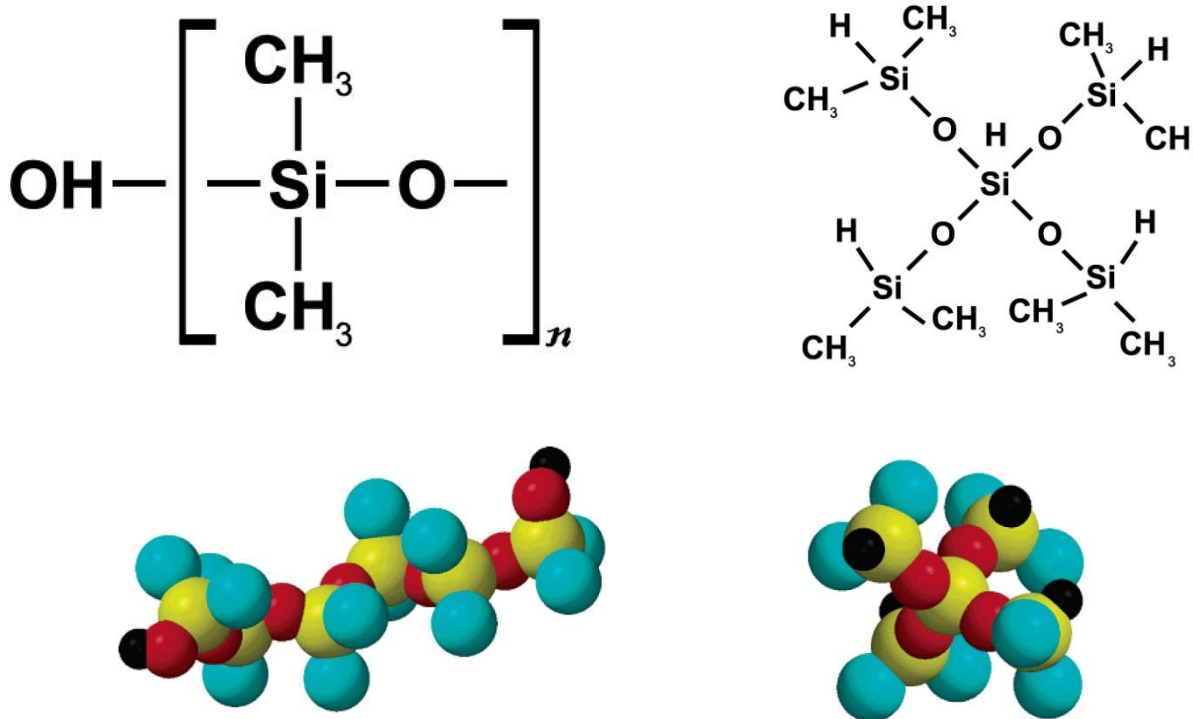
Figure 3. Schematic of a silanol terminated PDMS repeating unit (left) and silane crosslink molecule [11].

The crosslinking reaction is performed by forming a bond between a terminal SiH atom on the crosslink molecule to the nearest OH end of the PDMS chain. It is important to know that at chain lengths greater than 340 repeating units [15], owing to chain length, the creation of physical entanglements between PDMS chains create characteristics that mimic crosslinked networks.

In summary, this work is a natural progression of the two aforementioned studies [8, 10] to assess the influence of cross-linking on diffusion of the penetrants in pure PDMS and PDMS-based nanocomposite cases. The use of PDMS in this study is specifically to take advantage of an array of beneficial properties, in particular its permeability. In the nanocomposite cases, Cu is used as the nanoparticle because (1) manufacturability (2) the ease of its oxide formation and (3) the availability of a robust potential to describe its interactions with other atoms in the system.

I.5 Organization of the Thesis

The remainder of this thesis is organized as follows. Chapter II provides a description and background of MD simulations, the interatomic potential used to realistically model the physical system being studied, and the time integration algorithms used to integrate the equations of motion and propagate the system in time. Chapter III provides an introduction to Monte Carlo methods and discusses the Coupled-Decoupled Configurational-Bias Monte Carlo method used to generate initial conformations for the uncrosslinked, crosslinked, and nanocomposite models; along with a summary for the specifics of creation of the aforementioned systems. A literature review for MD studies of glass transition temperature and crosslinking is provided along with discussion about the crosslinking algorithm, validation of the crosslinked models created in this study, and factors affecting glass transition temperature. Chapter IV provides a brief discussion on diffusion, obtaining diffusion coefficients from MD, and the type of fitting procedure used in this study. Also, diffusion results in the pure, crosslinked, and PDMS-based nanocomposite systems at various temperatures are presented along with analysis on the effects of chain length, weight ratio and nanoparticle volume fraction on the diffusivity for these systems. The

Williams-Landel-Ferry (WLF) equation is used to characterize the role of temperature on diffusion; analysis on the variation of the WLF parameters with chain length, weight ratio, and nanoparticle volume fraction is also presented. Chapter V summarizes the conclusions and recommendations for future work. Although MD studies of diffusion in PDMS have been performed previously, the uniqueness of this study rests in a systematic evaluation on the effects of crosslinking and nanoparticle concentration on diffusivity for the systems studied here.

Chapter II   BACKGROUND

This chapter provides a brief overview of the importance of computer simulations, the molecular dynamics method and its constituents, and the MD techniques employed in this study. It also contains a brief overview of the interatomic potential that is used in this work.

Atomistic simulations are conducted to understand the interactions between molecules and their structure at nano length and time scales [16]. They act as a bridge by providing a direct route from microscopic to macroscopic properties of experimental interest. The use of a realistic physical model can also result in simulations being complementary to experiments. The feasibility of modeling extreme pressure or temperature conditions using atomistic simulation makes it a more attractive option than experiments, where it may be difficult to work under such conditions [16, 17]. Molecular dynamics (MD) and Monte Carlo (MC) are two main types of atomistic simulation techniques and a multitude of hybrid techniques result from their combination [16].

II.1 Introduction to Molecular Dynamics

Molecular dynamics is a computational method where the time evolution of an interacting set of atoms is computed by integrating a prescribed set of equations of motion. For an isolated system, the evolution of atomic positions can be described using Newton's Second Law of Motion,

$$\vec{F}_i \; = \; m\,\vec{a}_i \tag{1}$$

Here, m is the mass, F_i is the force acting on the atom, and a_i is its acceleration. The above equation characterizes the motion for an isolated system devoid of interactions with its surroundings. The two most important characteristics of the equations of motion are the conservation law and time-reversibility. Since the forms of the kinetic and potential energies are time independent, the resulting Hamiltonian (operator associated with system energy, typically a sum of kinetic and potential energies of the system) is constant and through a simple derivation force can be expressed as:

$$\vec{F}_i = -\frac{\partial U(\vec{r}_N)}{\partial r_i} \tag{2}$$

Therefore, the resolved force on each atom resulting from its interaction with other atoms in the system is simply the gradient of the potential energy of the system. For large systems, analytical solutions of the equations of motion are not possible, and therefore numerical methods are used. Speed, reasonable accuracy for large time-steps, time reversibility, and energy conservation are important criteria for good algorithms to integrate the equations of motion. The most widely used method to solve the equations of motion in molecular dynamics is the velocity-Verlet finite difference algorithm as it meets the aforementioned criteria. This algorithm will be discussed in greater detail in Chapter II.3.2

A macroscopic piece of matter contains atoms on the order of 10^{23}, which are many orders of magnitude larger than what MD simulations can handle currently due to the limitations of computational power. Therefore, due to this limitation, simulations have an increased ratio of surface atoms to total atoms resulting in the dominance of surface effects [18]. Periodic boundary conditions, a schematic of which is shown in Figure 4, can be used to nullify these surface effects. The translationally rigid replication of the cubic simulation box throughout

space to form an infinite lattice is the result of using PBC [17, 18]. Therefore, if an atom leaves the simulation box during the course of the simulation, its incoming image can be used to determine its interactions [16, 17]. This essentially allows the employment of smaller systems to capture bulk properties. The employment of the minimum image criteria ensures that only one among all the pairs of atom i in the box will interact with the closest image of atom j.
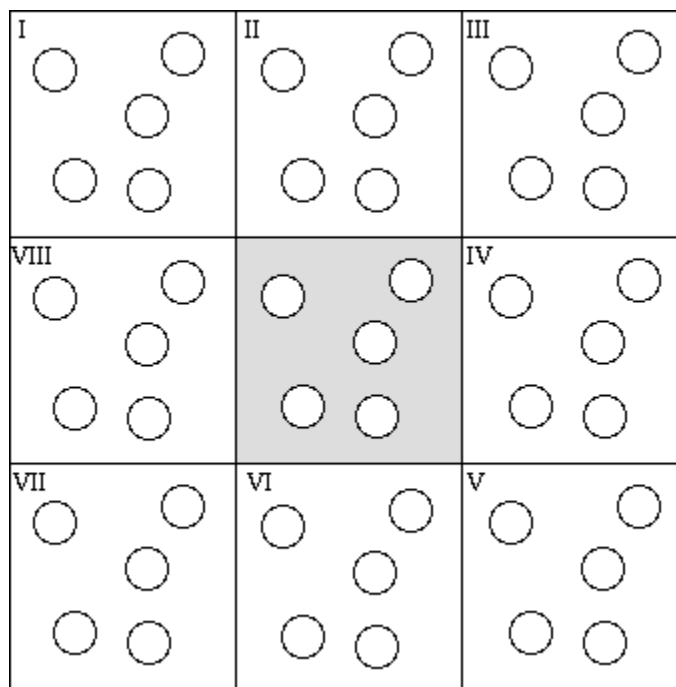
Figure 4: Schematic of the effective replication of the simulation cell using PBC's [19].

As aforementioned, MD involves the solution of the classical equations of motion of an interacting set of atoms. These interactions create forces causing the atoms to move creating a trajectory in a 6N-dimensional phase space (3N positions and 3N momenta) [18]. The creation of MD trajectories allows us to sample different phase space configurations. Such a collection of configurations which have different microscopic properties but an identical macroscopic or thermodynamic state is defined as an ensemble. If we could track the system for an infinite time enabling the system to access all parts of phase space at a given set of initial conditions (ergodic

system), a sampling of all these configurations with the appropriate statistical weight and averaging a given property becomes the ensemble average of the system. This enables a connection between macroscopic ensembles containing a large number of particles and the microscopic time-dependent properties of a single molecule [20]. Since the time evolution for a given set of positions and velocities is completely determined, MD is termed as a deterministic technique [18].

II.2 Ensembles

As mentioned above, an ensemble is a collection of points in phase space that conform to a particular thermodynamic state. There three most commonly used ensembles in MD are:

- Microcanonical Ensemble (NVE) – The thermodynamic state characterized by a fixed Number of atoms, Volume and Energy.
- Canonical Ensemble (NVT) - Number of atoms, Volume and Temperature of the system are constant.
- Isobaric-Isothermal Ensemble (NPT) - Number of atoms, Pressure and Temperature of the system are kept constant.

II.3 Constituents of MD Simulations in this Study

A MD study can typically be partitioned into two basic stages. First, a model for the interatomic interactions of the system is created. This serves as the potential energy function from which the forces on the particles are obtained. Second, an iterative procedure is used to solve the equations of motion for the specified initial atomic and boundary conditions which

14

generate the sample trajectory. This trajectory is then used to evaluate various static and dynamic averages of interest [21]. Since the aim of MD simulations is to capture the interaction between atoms and their evolution in time by integrating the equations of motion, the following can be considered its two main constituents: Interatomic Potential and Time Integration Algorithms.

II.3.1 Interatomic Potential

The objective of MD simulations is to accurately model a physical system. This is done in MD with the use of an interatomic potential, which is a function of the atomic positions of all atoms in the system. Therefore, an interatomic potential handles all the essential physics of a system. For polymer systems, it can be divided into intermolecular and intramolecular interactions. Intermolecular interactions or non-bonded interactions include van der Waals and Coulombic interactions. The intramolecular interactions include bond stretch, angle bending, and dihedral angle torsion within a polymer chain. The total potential energy of the system is a sum of the intermolecular and intramolecular contributions.
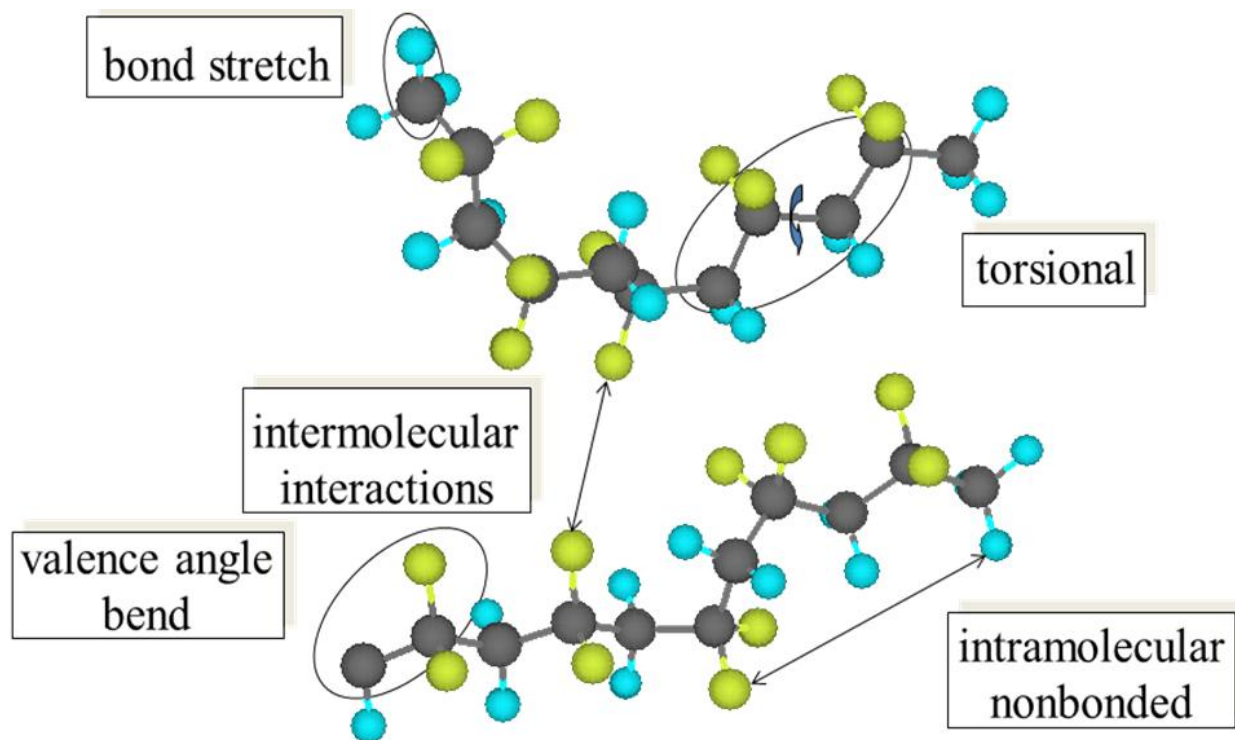
Figure 5: Bonded and non-bonded interactions in a polymer system [22].

There are several interatomic potentials, ranging from explicit atom models to united atom models, which have been proposed to model PDMS. Explicit atom (EA) model, like the name suggests, models every type of atom in the system independently. Using such a model typically results in excellent agreement of properties with real PDMS however such explicit modeling of atoms results in an increase in simulation cost. United atom (UA) models for PDMS treat methyl (CH_3) side-groups as a single atom, resulting in a reduction of atoms in the monomer from ten to four [23]. This can be verified from Figure 2 in Chapter I.

The idea behind the development of the hybrid/UA model by Frischnecht et al. [23] was to retain as much of the EA/Class II (CII) forcefield within the united atom framework while achieving a significant improvement over existing UA/Class I (CI) models for PDMS [23]. Class I potentials are relatively simple potential energy functions consisting of mainly bond,

angle, dihedral, non-bonded, and improper contributions to the total energy. Class II potentials are more complex containing the previously mentioned CI contributions to the total energy along with cross terms (bond-angle, angle-dihedral, etc.) bond, angle, and torsional potentials are represented by the class I form of the intermolecular potential. The bond and angle potentials have a harmonic form as they can be viewed as springs around an equilibrium value. Torsional interactions, which define twisting of two adjacent planes of atoms about each other, are modeled using a sinusoidal function. The intramolecular potentials, displayed in Figure 6, are as follows:

$$U_{bond}(l) = k_b (b - b_0)^2 \tag{3}$$

$$U_{angle}(\theta) = k_a (\theta - \theta_0)^2 \tag{4}$$

$$U_{torsion}(\phi) = k_d [1 + \cos(n\phi)] \tag{5}$$

where k_a, k_b, and k_d are the respective force constants for bond, angle and dihedrals in the system, b and θ refers to the instantaneous values of bonds and angles respectively, l_0 and θ_0 are the equilibrium bond length and bending angle, and n is the multiplicity factor. It is important to note that the anharmonic bond and angle potentials and cross-terms such as bond angle interactions, which are part of the EA/CII potential, are not included contributions to the intramolecular interactions in the hybrid/UA model.

The intermolecular interactions include van der Waals and Coulomb contributions, which act on all atoms on different chains and on atoms further apart than third nearest neighbors on the same chain. The nonbond potential is defined as:

$$U_{vdw}^{LJ}(r) = 4\,\varepsilon_{\alpha\beta}\left[\left(\frac{\sigma_{\alpha\beta}}{r_{sep}}\right)^{12} - \left(\frac{\sigma_{\alpha\beta}}{r_{sep}}\right)^{6}\right] \qquad (6)$$

when α or $\beta = CH_3$

$$U_{vdw}^{II}(r) = \varepsilon_{\alpha\beta}\left[2\left(\frac{\sigma_{\alpha\beta}}{r_{sep}}\right)^{9} - 3\left(\frac{\sigma_{\alpha\beta}}{r_{sep}}\right)^{6}\right] \qquad (7)$$

when α and $\beta = Si$ or O

$$U_{coulombic}(r) = \frac{q_{\alpha}\,q_{\beta}}{4\,\pi\,\varepsilon_0\,r_{sep}} \qquad (8)$$

where $\varepsilon_{\alpha\beta}$ is the Lennard-Jones (LJ) well depth, $\sigma_{\alpha\beta}$ is the equilibrium separation distance of the LJ potential, r_{sep} is the separation distance between a pair of atoms, q_{α} and q_{β} are partial charges of the atoms, and ε_0 is the permittivity of free space. The LJ 9-6 form was used to model Si, O, and Si-O van der Waals interactions. This is similar to the EA/CII model and helps capture the flexible Si-O backbone of PDMS. A standard 12-6 for of the LJ potential is used to model interactions involving the methyl groups. This mixing of the 12-6 and 9-6 forms of LJ to model PDMS in this model results in it being called the hybrid/UA model [23]. Figure 6 provides a schematic of the force field interactions, with covalent bonds depicted with solid lines and nonbonded interactions depicted with a dashed line.

18
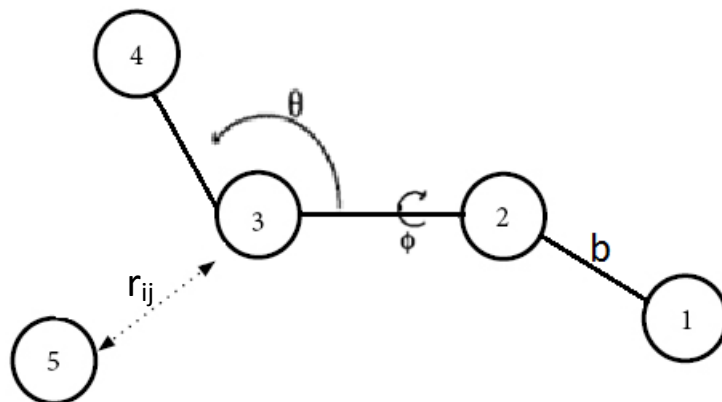
Figure 6: Schematic of bonded and nonbonded interactions.

For models in this thesis which incorporate Cu nanoparticles, the van der Waals interactions between the copper atoms are modeled using the two-body LJ 12-6 potential by Erkoc et al. [24]. Although a more robust potential is essential to study the properties of metals accurately, the LJ potential is sufficient to model the interactions between the metallic nanoparticles and PDMS. Van der Waals interactions between the penetrates, polymer, and metallic nanoparticles are also modeled with the 12-6 form of the LJ potential using the Berthelot mixing rules [23]. The parameters used in the hybrid coarse-grained model are listed in Table 1 and the van der Waals parameters to particle/penetrate interactions are listen in Table 2. A 12 Å cutoff radius is used for the van der Waals interactions.

Bonds	r_0 (Å^2)	k_b (kcal/mol Å^2)
Si-O	1.64	350.12
Si-CH$_3$	1.90	189.65

Angles	θ_0 (deg)	k_a (kcal/mol deg^2)
Si-O-Si	146.46	14.14
O-Si-O	107.82	94.50
CH$_3$-Si-CH$_3$	109.24	49.97
O-Si-CH$_3$	110.69	49.97

Dihedrals	n	k_d (kcal/mol)
Si-O-Si-O	1	0.225
Si-O-Si-CH$_3$	3	0.01

Pair	ε (kcal/mol)	σ (Å)
Si-Si	0.1310	4.29
Si-O	0.0772	3.94
Si-CH$_3$	0.1596	3.83
O-O	0.0800	3.30
O-CH$_3$	0.1247	3.38
CH$_3$-CH$_3$	0.1944	3.73

Table 1: Intermolecular and intramolecular parameters for the hybrid coarse-grained model [23].

Pair	ε (kcal/mol)	σ (Å)
Si-O$_2$	0.3624	3.41
O-O$_2$	0.2134	3.19
CH$_3$-O$_2$	0.2100	3.66
O$_2$-O$_2$[25]	0.2246	3.43
Si-Cu	2.3479	2.86
O-Cu	1.3898	2.65
CH$_3$-Cu	1.3023	3.06
O$_2$-Cu	1.4550	2.88
Cu-Cu[24]	9.4267	2.34

Table 2: Calculated van der Waals for O$_2$ penetrates and Cu particle using Berthelot mixing rule.

The role of charged particles is modeled using the Coulombic function in the hybrid/UA model. A cutoff radius of 12 Å is used for long range interactions instead of the Ewald sum or similar methods in this study. The explicit modeling of hydrogen atoms is crucial for accurately generating details of the structure and chain dimensions of PDMS. This is because hydrogen atoms provide a screening effect for partial charges in the EA/CII model which cannot be replicated with a coarse-grained approximation. Although the hybrid/UA model provides a better prediction of structural factors (mean squared radius of gyration and end to end distance) and system pressure at equilibrium when compared to existing UA/CI models, it is unlikely that any coarse-grained approximation can accurately provide structural conformation provided by the explicit atom models. In order to account for these screening effects partially, the charge on the methyl groups is zeroed and the charges are reduced in the hybrid/UA model from the values used in the EA/CII model. Thus, by setting $q_{CH3} = 0$ and $q_{Si} = - q_O = 0.3$, relatively good agreement with the EA/CII model for the structure, pressure, and chain dimensions is obtained [23]. Owing to the models' improved compressibility and chain dimensions, Frischknecht et al. recommend the hybrid/UA model for any application in which chain dimensions play a significant role [23]. A previous study on uncrosslinked PDMS [8] used the hybrid/UA forcefield developed by Frischnecht et al. [23]. In order to maintain consistency between the uncrosslinked and crosslinked studies of PDMS, this thesis employs the same potential.

II.3.2 Time Integration Algorithms

A system, whose equations of motion are specified using Eq. (1), corresponds to an isolated system from the environment. While studying the behavior of a system in an isolated

system has its merits, no connection is made to temperature or volume changes due to pressure in microcanonical studies. Experiments are often conducted at defined temperatures and pressures and therefore their boundary conditions are different from the systems in the microcanonical ensemble. In order to overcome this discrepancy, extended systems capable of interacting with their surrounding environment (nonequilibrium molecular dynamics) are introduced. This relationship between the behavior of the system and the environment is described by additional differential equations which are coupled to an augmented version of Newton's equations of motion [26]. The NVT and NPT ensembles are classified under the nonequilibrium MD umbrella.

In this study simulations are performed in both the NVT and NPT ensembles. The NVT ensemble is primarily used for construction runs while equilibration and diffusion calculations are performed in the NPT ensemble, using the Nose-Hoover thermostat and barostat which equilibrates the system to the desired temperature and pressure.

II.4 NVT Ensemble

In this study, NVT calculations are performed using the extended system approach and the equations of motion are augmented by the addition of a frictional coefficient, ζ, which essentially couples the system to an external heat bath. The initial formulation by Nose was simplified by Hoover, eliminating the scaling of variables in both space and time, and time development of positions can be expressed as:

$$\dot{r}_i = \frac{\vec{p}_i}{m} \tag{9}$$

where r_i and p_i are positions and corresponding momenta of the particles and the 'dot' denotes first derivative with respect to time. The equations of motion of the real particles (alternate form of Equation 1)

$$\dot{\vec{p}}_i (r) = \vec{F} (r) \qquad \text{10)}$$

are extended by the aforementioned frictional term

$$\dot{\vec{p}}_i (r) = \vec{F} (r) - \zeta \, \vec{p}_i (r) \qquad \text{11)}$$

with

$$\dot{\zeta} (t) = v_T^2 \left[\frac{T_{system}}{T_{equilibrium}} - 1 \right] \qquad \text{12)}$$

In Eq. 15, $T_{equilibrium}$ is the temperature of the external heat bath and v_T is the thermostating rate. As briefly described in Chapter II.1, analytical solutions to the equations of motion of large systems are not possible and this study employs the velocity Verlet algorithm. The time integration algorithm is responsible for integrating the equations of motion of the interacting atoms and computing their trajectory. These integration algorithms are often based on finite difference methods. This involves the writing of Taylor expansions for each of the points on a grid, with the time step being the distance between consecutive grid points. Thus, with the knowledge of positions and velocities at time t, an attempt to obtain the above mentioned properties is made for a later time, $t + \partial t$ [17]. It is important to note that truncation errors and round off errors are a common consequence of such algorithms. Truncation errors are not implementation dependent; they are intrinsic to the algorithm as finite difference methods are

based on the truncation of Taylor expansions at some term [18]. For an isolated system, this velocity Verlet finite difference algorithm is characterized by the following equations:

$$r(t + \partial t) = r(t) + v(t) \partial t + \frac{1}{2} a(t) \partial t^2 \tag{13}$$

$$v(t + \partial t) = v(t) + \frac{1}{2} [a(t) + a(t + \partial t)] \partial t \tag{14}$$

The above equations are further split into three equations:

$$v\left(t + \frac{1}{2} \partial t\right) = v(t) + \frac{1}{2} a(t) \partial t \tag{15}$$

$$r(t + \partial t) = r(t) + v\left(t + \frac{1}{2} \partial t\right) \partial t \tag{16}$$

$$v(t + \partial t) = v\left(t + \frac{1}{2} \partial t\right) + \frac{1}{2} a(t + \partial t) \partial t \tag{17}$$

In order to reduce the error inherent to finite difference methods, the Velocity Verlet algorithm divides the integration into half time steps. In Eq. (15), the half step velocity at $t + 0.5 \partial t$ is calculated using force and velocity at time t. This half step velocity is then used to determine the full step position of the atoms in the system by Eq. (16). The new forces resulting from the updated full step positions are then used to calculate the full step velocities by Eq. (17) [17, 27].

Using the aforementioned equations (Eq. 9-12) and implementing them in the velocity-Verlet algorithm mentioned in Eq. 13-17 results in the following step by step solution to the Hoover NVT equations of motion.

I.   Apply temperature constraint

$$\zeta\left(t + \frac{\Delta t}{2}\right) = \zeta(t) + \frac{\Delta t}{2}\dot{\zeta}(t)$$

where $\dot{\zeta}(t)$ is defined in Eq. 12

II.   Adjust velocities

$$\tilde{v}(t) = v(t)\left[\exp\left[-\frac{\Delta t}{2}\zeta\left(t + \frac{\Delta t}{2}\right)\right]\right]$$

III.   Update velocities (half-step)

$$v\left(t + \frac{\Delta t}{2}\right) = \tilde{v}(t) + \frac{\Delta t}{2m}F(t)$$

IV.   Update positions (full-step)

$$r(t + \Delta t) = r(t) + \Delta t\, v\left(t + \frac{\Delta t}{2}\right)$$

V.   Compute "new" forces at F (t+Δt)

VI.   Update velocities (full-step)

$$v\left(t + \Delta t\right) = v\left(t + \frac{\Delta t}{2}\right) + \frac{\Delta t}{2m}F(t + \Delta t)$$

VII.   Adjust the newly obtained velocities

$$\tilde{v}(t + \Delta t) = v(t + \Delta t)\left[\exp\left[-\frac{\Delta t}{2}\zeta\left(t + \frac{\Delta t}{2}\right)\right]\right]$$

VIII.   Calculate a new temperature at T (t+Δt)

IX.   Update the friction thermostat variable

$$\zeta \left(t + \Delta t \right) = \zeta \left(t + \frac{\Delta t}{2} \right) + \frac{\Delta t}{2} \dot{\zeta} \left(t + \Delta t \right)$$

II.5 NPT Ensemble

The equations of motion for the NPT ensemble can be obtained as an extension of the Nose-Hoover equations for the NVT ensemble. A friction coefficient is introduced to couple the system pressure or stress to an external reservoir in the extended system methodology. The changes in pressure are accomplished by adjusting the box volume. This change in box volume is influenced by the imbalance between the internal and desired system pressure. The system temperature and pressure are coupled to the equations of motion in an NPT ensemble as shown in the following equations presented by Melchionna et al. [28]:

$$\dot{\bar{r}}_i = \frac{\bar{p}_i}{\bar{m}_i} + \eta \left(\bar{r}_i - R_0 \right)$$

$$\dot{\bar{p}}_i = \bar{F}_i - \left(\eta + \zeta \right) \bar{p}_i$$

$$\dot{\zeta} = v_T^{\ 2} \left(\frac{T(t)}{T_{ext}} - 1 \right)$$

$$\dot{\eta} = \frac{v_P^2}{NkT_{ext}} V \left(P(t) - P_{ext} \right)$$

$$\dot{V} = dV\eta$$

18)

In the above equations, r_i is the position of atom i, R_0 is the center of mass of the system, p_i refers to the momentum of atom i, F_i is the resolved force on atom i, ζ , and η are thermostatting and barostatting constants, v_p and v_T are thermostatting and barostatting rates, T (t) and P (t) are the instantaneous temperature and pressure, and T_{ext} and P_{ext} are the temperature and pressure of the external bath. The above equation (18) can then be implemented in the velocity-Verlet algorithm mentioned in Eq. 13-17 to obtain step by step solutions to the Hoover NPT equations of motion. This implementation is not discussed here and is beyond the scope of this thesis.

Chapter III   CONSTRUCTION AND VALIDATION OF ATOMISTIC MODELS

This chapter provides an introduction to Monte Carlo (MC) methods, a literature review of studies using MC, and the details on the specific type of MC algorithm used in this study. A detailed description of the methodology used to create the pure, crosslinked, and nanocomposite based-PDMS models is also provided. Also, a description of crosslinking algorithms, literature reviews of MD studies involving crosslinking, and a validation of the crosslinked model is provided. An overview of the calculation of glass transition temperature using MD simulations and its significance in validating crosslinked models is also provided.

III.1   Introduction to Monte Carlo

The initial system consisting of pure PDMS chains or chemically modified PDMS chains with crosslinker molecules are generated using a Monte Carlo (MC) molecular simulation code called Towhee. Monte Carlo is a stochastic method in which material properties are computed by appropriate sampling within a given ensemble. The method is deemed stochastic due to its use of probability and random numbers to generate a set of solutions to a given problem. In general, given some probability measure (π) in a configuration space S, the aim of MC methods is to generate many random samples from π [29]. This requires an effective sampling of the configuration space. In a simple MC scheme, the points in configuration space are sampled uniformly resulting in the sampling of random regions in configuration space which the system rarely occupies. This tends to lower the efficiency of Monte Carlo methods. Importance sampling, a technique that samples from regions of configuration space that make a major contribution to the ensemble, improves the efficiency of MC methods [30, 31]. The stochastic

process that samples each state of the system with the appropriate frequency is accomplished by the creation of the Markov chain. The two requirements of the Markov chain are: The outcome of each trial must belong to a finite set of outcomes (i.e. sampling must be done in configuration space) and that the outcome of a trial depends only on the outcome of a previous trial [30]. The basic MC approach by Metropolis et al. [32] the following scheme is proposed [30, 31]:

I.   Select a particle a particle at random, and calculate its potential energy $\bar{U}$ (m).

II.   Give the particle a random displacement, $n = m + \Delta$, and calculate its new potential energy $\bar{U}$ (n).

III.   If the change in potential energy $\Delta\bar{U}_{mn}$ i.e. $\bar{U}$ (m) $-$ $\bar{U}$ (n) $<= 0$, then accept move. If $\bar{U}$ (m) $-$ $\bar{U}$ (n) $>= 0$, then accept move with a probability (ρ_n / ρ_m).

While the original Metropolis scheme performs single particle trial moves, in some cases, performing moves in which the coordinates of many particles are changed is more efficient. Therefore this scheme is inefficient for polymer simulations where topological constraints (chains cannot cross) dictate the natural dynamics. In order to improve sampling efficiency, Rosenbluth and Rosenbluth [33] introduced a biased sampling method for polymers, where idealized chain molecule conformations were generated on a lattice using a self-avoiding random walk. The ensemble averages were then calculated using a specially weighted average.

III.2   Configurational Bias Monte Carlo

The Configurational Bias Monte Carlo (CBMC) builds on the Rosenbluth sampling scheme. The CBMC is a dynamic MC scheme that enables the attainment of large conformational changes in a single trial move that affects a large number of monomeric units

[31, 34]. In this scheme, instead of random changes to the coordinates of a molecule, the molecular conformation is generated in a stepwise fashion such that the addition of the next monomeric unit is in a direction that has a large Boltzmann weight [31]. The trial conformation's probability of acceptance is given by the ratio of the Rosenbluth weights of the new and old conformations. It is important to note that the original Rosenbluth scheme was devised for polymers on a lattice however; the CBMC can be extended to chain molecules in continuous space [31].

Since a specific formulation (coupled-decoupled CBMC) of CBMC is used in this study to generate initial chain configurations, it is beneficial to understand the basic CBMC algorithm implementation before analyzing the coupled-decoupled CBMC (CD-CBMC). In general, CBMC algorithms are implemented in three steps: (1) generating a set of trial positions using an arbitrary probability distribution, (2) selecting one of the several generated trial positions with a given probability for further growth over a number of growth steps until the recreation of the entire molecule, and (3) accepting or rejecting the regrown molecule with a given probability [35].

$$p_{arb}^{trial} \, (\, r_i \,) \; = \; f \, (\, r \neq r_i \,) \tag{19}$$

$$P_{select} \, (\, r_i \,) \; = \; \frac{\left\{ \left(\dfrac{p_{trial}^{ideal} \, (\, r_i \,)}{p_{trial}^{arb} \, (\, r_i \,)} \right) \times w_{bias} \, (\, r_i \, , r_{exist} \,) \times \exp \left[-\beta \, U \, (\, r_i \,) \right] \right\}}{W_k} \tag{20}$$

$$P_{accept} \, (\, r_m \, ,....., r_z \,) \; = \; Min \left[1, \frac{\prod_{k=1}^{n_{step}} W_k^{new}}{\prod_{k=1}^{n_{step}} W_k^{old}} \times \frac{\prod_{s=m}^{z} w_{bias} \, (r_s \, , r_{exist} \,)^{old}}{\prod_{s=m}^{z} w_{bias} \, (r_s \, , r_{exist} \,)^{new}} \right] \tag{21}$$

30

In Eq (19), the function 'f' depends on anything that is known (position of atoms already grown, etc.) prior to the generation of trial positions for the appropriate range of r_i. In Eq (20), the selection of one of the generated trial positions is a function of the potential energy of the trial position [U (r_i)], the ideal probability distribution (distribution obtained in an ideal system where U is zero for all values of r_i), and the Rosenbluth Weight (W_k) [35]. Also, the biasing function [(w_{bias} (r_i, r_{exist}))] must be non-zero and is dependent on either the positions of the existing atoms that were generated in previous growth steps or those whose positions are not being sampled in this CBMC move [34]. The Rosenbluth weight is computed from the sum of the trials as described by Eq (22)

$$W_k = \sum_{j=1}^{n_{trial}^k} \left(\frac{p_{trial}^{ideal} (r_i)}{p_{trial}^{arb} (r_i)} \right) \times w_{bias} (r_i, r_{exist}) \times \exp \left[-\beta U (r_i) \right] \qquad (22)$$

In Eq (20), $r_m, \ldots, r_z$ is the set of all atom positions generated during a CBMC move consisting of n_{step} growth steps. Upon completion of the total number of growth steps, the Rosenbluth weight of the new trial conformation of the chain is calculated. The old Rosenbluth weight is calculated in a similar fashion, except that the actual old position of each atom appears once in the growth process and is always the trial selected for further growth [35].

III.3 Coupled-Decoupled Configurational Bias Monte Carlo

As aforementioned, this study uses the CD-CBMC formulation for the generation of initial polymer conformations. The original CD-CBMC algorithm by Martin and Siepmann [36], which generates configurations by coupling nonbonded and torsional selections while splitting

angle bending into decoupled selections, was augmented by introducing flexible bond lengths as an additional decoupled selection proposed by Martin and Thompson [37] to generate chain conformations in this study. For the decoupled selections, one selection (such as bond length) is made (solely on the basis of bond energy) and then that value is used in all subsequent selections (such as bending angles, torsion angles and nonbonded interactions). Terms are considered to be coupled when the Rosenbluth weight of the first term appears in the acceptance probability of the second thereby requiring a full selection procedure of the first term for every trial of the second term [35]. Therefore, instead of uniform sampling of the volume of a sphere of radius r_{max} (maximum bond length) centered on an existing atom that is bonded to the trial atom, the trial generation process is divided into parts like bond lengths, bending angles, dihedrals, and nonbonded interactions. This is followed by sampling the degree of freedom related to each of these interactions such that the selections are either decoupled or coupled. The algorithm therefore consists of decoupled bond length selection, decoupled bending A selection, decoupled bending B selection, and dihedral angle selection coupled to nonbonded selection. This is done with the following equations [35]:

$$
P_{select}^{bond}(l_{ga,f}(i)) = \frac{\left(\dfrac{p_{trial}^{ideal}(l_{ga,f}(i))}{p_{trial}^{arb}(l_{ga,f}(i))}\right) \times \exp\left[-\beta U_{bond}(l_{ga,f}(i))\right]}{W_{bond}(n,a)}
\tag{23}
$$

$$
W_{bond}(n,a) = \sum_{i=1}^{nch\_vib} \left(\frac{p_{trial}^{ideal}(l_{ga,f}(i))}{p_{trial}^{arb}(l_{ga,f}(i))}\right) \times \exp\left[-\beta U_{bond}(l_{ga,f}(i))\right]
\tag{24}
$$

$$
P_{select}^{bendA}(\theta_{ga,f,p}(i)) = \frac{\left(\dfrac{p_{trial}^{ideal}(\theta_{ga,f,p}(i))}{p_{trial}^{arb}(\theta_{ga,f,p}(i))}\right) \times \exp\left[-\beta U_{bend}(\theta_{ga,f,p}(i))\right]}{W_{bend}^{A}(n,a)}
\tag{25}
$$

32

$$W_{bend}^{A}(n,a) = \sum_{i=1}^{nch\_bend\_a} \left(\frac{p_{trial}^{ideal}(\theta_{ga,f,p}(i))}{p_{trial}^{arb}(\theta_{ga,f,p}(i))} \right) \times \exp\left[-\beta U_{bend}(\theta_{ga,f,p}(i)) \right] \quad (26)$$

$$P_{select}^{bendB}(\theta_{gb,f,ga}(i)) = \frac{\left(\frac{p_{trial}^{ideal}(\theta_{gb,f,ga}(i))}{p_{trial}^{arb}(\theta_{gb,f,ga}(i))} \right) \times \exp\left[-\beta U_{bend}(\theta_{gb,f,ga}(i)) \right] \times \exp\left[\beta U_{imp}(\theta_{f,gb,ga,p}(i)) \right]}{W_{bend}^{B}(n,b)} \quad (27)$$

$$W_{bend}^{B}(n,b) = \sum_{i=1}^{nch\_bend\_b} \left(\frac{p_{trial}^{ideal}(\theta_{gb,f,ga}(i))}{p_{trial}^{arb}(\theta_{gb,f,ga}(i))} \right) \times \exp\left[-\beta U_{bend}(\theta_{gb,f,ga}(i)) \right] \times \exp\left[\beta U_{imp}(\theta_{f,gb,ga,p}(i)) \right] \quad (28)$$

$$P_{select}^{nb}(\phi_{g1,f,p,q}(j)) = \frac{\exp\left(-\beta \sum_{c=1}^{n_h(n)} U_{nb}^{part}(r_a(i)) \right) \frac{\frac{p_{trial}^{ideal}(\phi_{g1,f,p,q}(j))}{p_{trial}^{arb}(\phi_{g1,f,p,q}(j))} w_{bias}^{fe}(j) \exp\left[-\beta \sum_{a=1}^{n_g(n)} U_{con}(\phi_{g1,f,p,q}(j)) \right]}{W_{dihed}(i)}}{W_{nb}(n)} \quad (29)$$

$$U_{con}(\phi_{g1,f,p,q}) = \sum_{c \neq f} U_{bond}(l_{ga,c}) + \sum_{c \neq f} U_{bend}(\theta_{ga,c,d}) + \sum U_{bend}(\theta_{c,ga,d}) + \sum U_{tor}(\phi_{ga,c,d,e})$$
$$+ \sum U_{tor}(\phi_{c,ga,d,e}) + \sum U_{imp}(\phi_{ga,f,c,d}) + \sum_{c \neq f} U_{imp}(\phi_{ga,f,p,qb}) \quad (30)$$

$$W_{dihed}(i) = \frac{p_{trial}^{ideal}(\phi_{g1,f,p,q}(j))}{p_{trial}^{arb}(\phi_{g1,f,p,q}(j))} w_{bias}^{fe}(j) \exp\left[-\beta \sum_{a=1}^{n_g(n)} U_{con}(\phi_{g1,f,p,q}(j)) \right] \quad (31)$$

$$W_{nb}(n) = \sum_{i=1}^{nch\_nb} \left[\exp\left(-\beta \sum_{a=1}^{n_g(n)} U_{nb}^{part}(r_a(i)) \right) W_{dihed}(i) \right] \quad (32)$$

In Equations 23-32, all the variables containing U (U_{bond}, U_{bend}, U_{imp}, etc.) are obtained by breaking down the potential energy function or interatomic potential. In Equation 23, $l_{ga,f}$ is the bond distance between the existing (growing from atom f) and the newly generated atom (g_a). Upon completion of the selection of one bond length (described by Equation 24) using the arbitrary trial distribution (Equations 19-21) from the *nch_vib* generated trial bond lengths for each generated atom, the decoupled bending angle A selection proceeds. In Equation 25, $\theta_{ga, f, p}$

represents the angle formed between the newly generated atom (g_a), the existing atom (f), and an atom which is previous to the existing atom (p). Note that if p is existent (either because it was grown in an earlier CBMC step or it is not selected for regrowth during the current step) then it is randomly chosen from the list of existing atoms bonded to f. Otherwise, if p is non-existent, atoms grown during the current step are selected to be the p atom [35]. Equation 26, performs a similar selection process as Equation 24, for the $\theta_{ga, f, p}$ angles and upon their determination, the pseudo-dihedral angles between the atoms are sampled. In Equation 27, $\varphi_{gb, f, p, ga}$ is the pseudo-dihedral angle between the planes formed by the g_a-f-p and the g_b-f-p atom triplets. Equation 28 performs the sampling for the selected pseudo-dihedral angles for each of the generated atoms. The next step involves a coupled dihedral and nonbonded selection. Equations 29-32 proceed by conducting a full dihedral selection (computationally non-expensive compared to the nonbonded selections) for each trial of the nonbonded selection [35].

III.4   Pure PDMS models

The pure PDMS models consist of 50 trimethyl terminated PDMS chains. Recall from Chapter I that trimethyl terminated PDMS chains consist of a Si-O backbone with two methyl groups attached to the center Si atoms while the terminal Si atoms have three methyl groups. In order to understand the effect of entanglement length, this study considers chains above and below the entanglement molecular weight of 24,500 g/mol [15]. The chains considered in this study have molecular weights of 5,000 g/mol, 10,000 g/mol, 20,000 g/mol, and 40,000 g/mol. These conformations are created using the Coupled-Decoupled CBMC formulation described above in an NVT ensemble at a temperature of 300 K in a low density simulation box. Three

independent conformations of the PDMS system are created with different initial random conformations of the chains. The CBMC simulations were run for 5 cycles, where a cycle equals N moves, with N being the number of molecules in the system (50 in this case). Although typical CBMC simulations employ a much higher number of cycles, the purpose of using CBMC in this study is to simply generate an accurate structure conforming to the equilibrium bond, angle, and dihedral configurations specified in the interatomic potential.

III.4.1 Preliminary Simulation Setup for Pure PDMS Models

Upon completion of the Towhee runs, a data file with atomic coordinates of all the atoms in the system is generated and imported into LAMMPS (Large-scale Atomic/Molecular Massively Parallel Simulator) [38], a classical molecular dynamics code. An energy minimization is then performed on the imported structure using the Polak-Ribiere version of the conjugate gradient (CG) method [39]. Energy minimization is a numerical procedure to determine local or global minimum on the potential energy surface from a higher energy initial conformation. Therefore, a stepwise modification of the molecular geometry is undertaken to reduce the overall energy of the molecular system during energy minimization.

After minimization, a "soft" purely repulsive potential containing the following form is applied to all non-bonded interactions in the system,

$$E = A \left[1 + \cos\left(\frac{\pi \, r_{sep}}{r_c} \right) \right] , \; r < r_c \tag{33}$$

In the above equation, A is the pre-factor containing energy units; r_c is the cutoff distance, and r_{sep} is the separation distance between the interacting atoms. The above equation is not

undefined as r goes to zero, and hence is useful for pushing apart overlapping atoms. The atomic interactions with a soft potential allow considerable changes in chain configuration ensuring randomization of the system. This mitigates potential problems arising from the employment of low MC cycles employed in Towhee. This procedure is performed for 1 nanosecond at 300 K in a NVT ensemble during which the value of A is kept constant at zero and the cutoff is specified as 6 Å. A subsequent short equilibration, with r_c of 6Å and A varied from 1 to 500 kcal/mol, is performed for 10 picoseconds at 300 K in a NVT ensemble using the soft potential [11]. Although the configuration of the chains stays locked during this run, they are rapidly pushed apart from each other as the interactions harden with increasing time. Upon completion of this run, the LJ parameters specified in Table 2 are "turned on" to characterize the non-bonded interactions along with Coulombic interactions with a cutoff radius of 12 Å. This equilibration is performed for 1 nanosecond in a NPT ensemble, where a Nose-Hoover barostat and thermostat is used to maintain the system pressure at 1 atomosphere and 300 K respectively. Such an equilibration is important as it enables the system to evolve out of the low density initial conformation and attain its equilibrium density. Upon completion of the NPT equilibration, the system is ready to undergo the diffusion part of the simulation.
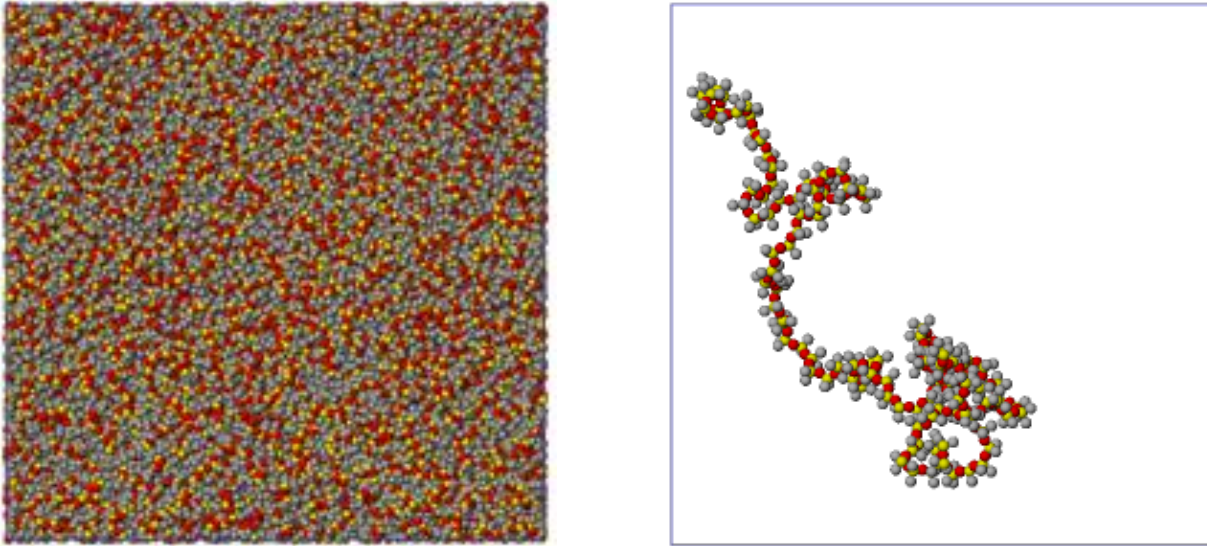
Figure 7: Illustration of a fully dense pure PDMS system (left) and a single chain of molecular weight 10,000 g/mol generated using Ovito [40].

III.4.2 Diffusion Simulation Setup for Pure PDMS Models

Simulations of diffusion in this study are performed at target temperatures ranging from 225 K to 400 K in 25 K increments in an NPT ensemble with the system pressure kept constant at 1 atm. Also, the number of diffusing species (O_2) is kept constant at 100 united atom penetrants for each of the eight target temperatures specified above. The system is then aligned with the desired target temperature and allowed to reach equilibrium density at this target temperature in a NPT ensemble over a period of 100 picoseconds. Penetrants are then introduced into the system at random (overlaps with PDMS chains are avoided) at the target temperature. Another NPT equilibration is performed for 500 picoseconds in order to allow the randomly introduced penetrants to diffuse evenly throughout the system. Finally a NPT production run is performed for 1 nanosecond with the time origin for the diffusion calculation reset every 100 picoseconds during the production run. In this study, Mean-Squared

Displacement (MSD) presented as an ensemble average over the penetrates will be used to study diffusivity. Further details regarding the extraction of diffusion coefficients are incorporated in following sections.
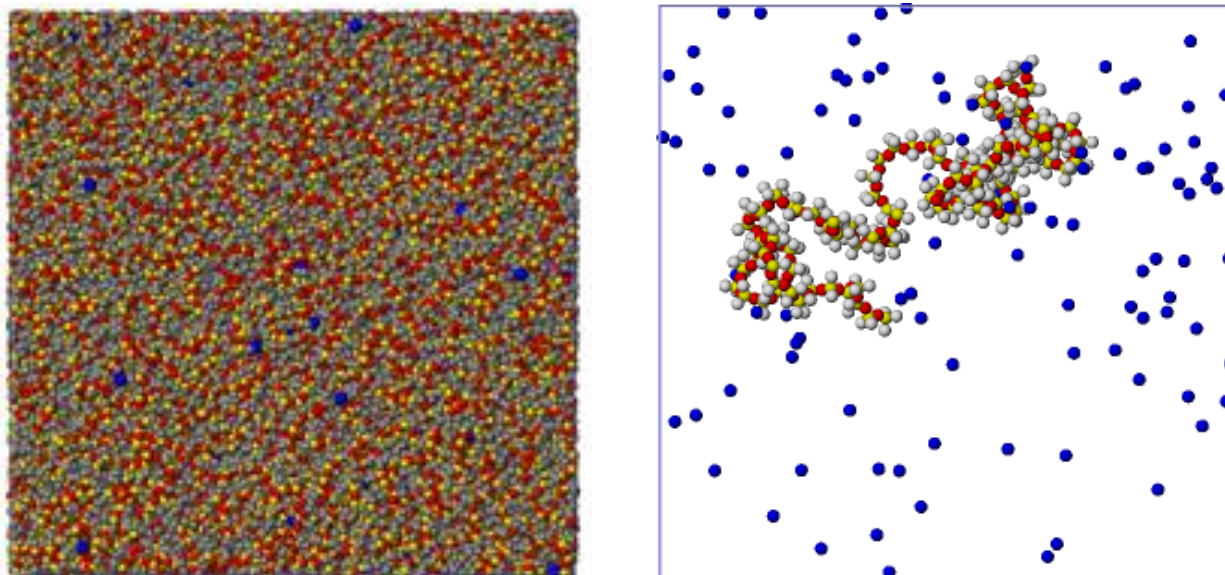
Figure 8: Pure PDMS system (M_g = 10,000 g/mol) with O_2 penetrates in blue which are enlarged to show detail (left). Single Chain PDMS (M_g = 10,000 g/mol) with 100 O_2 penetrates (right).

In summary, Chapter III.4 and its subsections provide the following information: (1) creation of the pure PDMS systems using CD-CBMC, (2) preparing the system for the diffusion runs by performing a two-step equilibration using a "soft" potential followed by an NPT equilibration, (3) using MSD to calculate diffusion coefficients. This information is provided concisely in Figure 9, which summarizes the simulation procedure utilized in this study. Note that Figure 9 also displays information on crosslinked PDMS and nanocomposite-based PDMS systems, which will be discussed in detail in Chapters III.5 and its subsections and Chapter III.10 respectively.
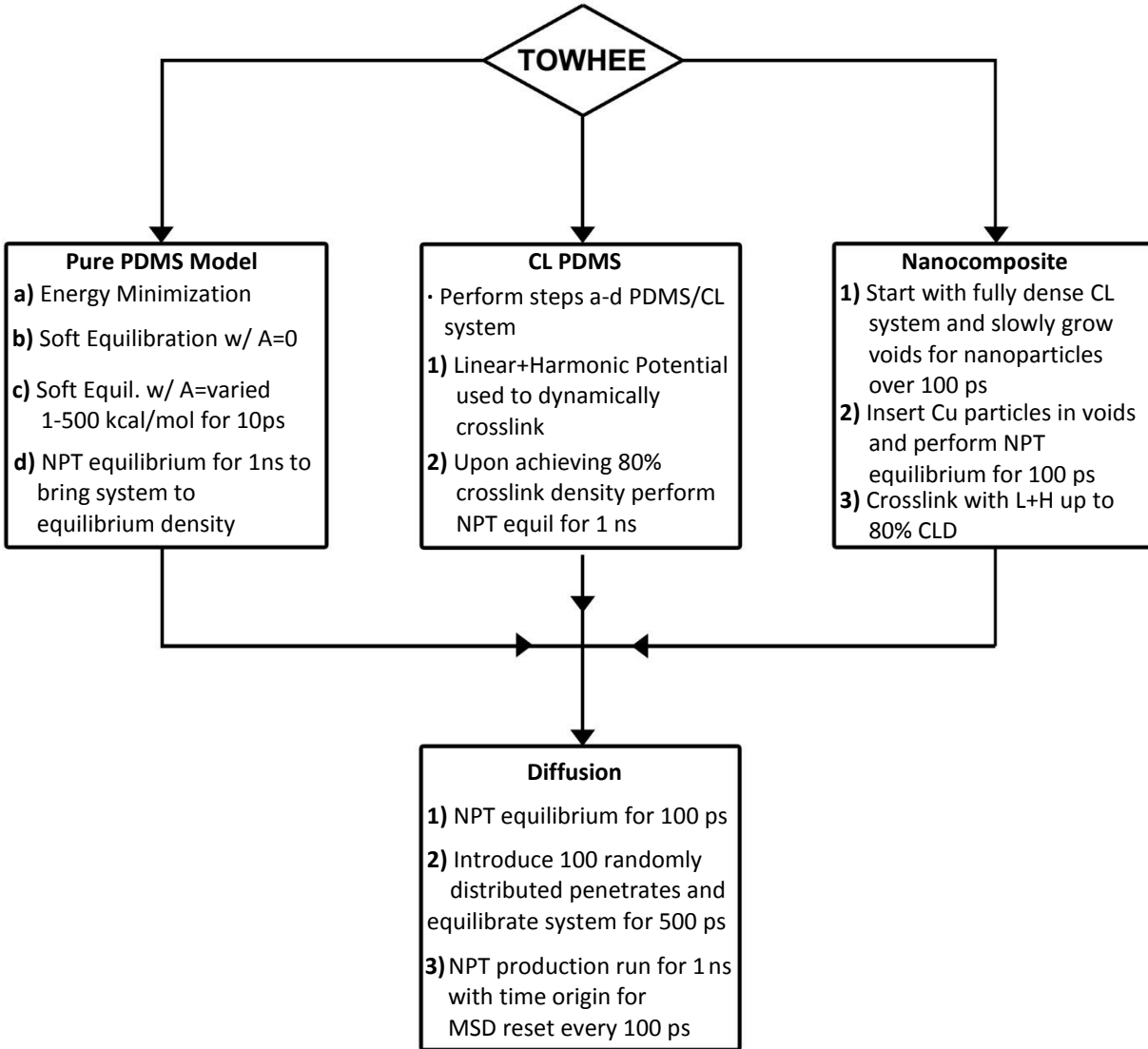
Figure 9: Flowchart depicting the construction and simulation procedure for all systems.

III.5 Crosslinked Polymers

The following subsections provide a detailed literature review of early MC algorithms and MD simulation of crosslinking in PDMS and other polymers and the crosslinking algorithm employed in this study

III.5.1 Background

As mentioned in Chapter I, crosslinking is defined as the formation of a bond between polymer chains, either between different chains or between different parts of the same chain. In this study, the crosslinking reaction is performed by forming a bond between a terminal SiH atom on the crosslink molecule to the nearest OH end of the PDMS chain.

The use of computer models to analyze crosslinked networks can be traced back to the 1980s. Eichinger et al. [41] developed a coarse-grained non-lattice MC algorithm to construct polymer networks and predict material behavior. The simulations of radiation cure of polymers, mechanical properties, critical gel points, etc. were conducted using their algorithm [42]. Lattice MC algorithms by Shulz and Frisch [43] have been employed to study interpenetrating polymer network formation and swelling behavior of polymer networks [42]. In these initial studies, the simultaneous crosslinking during the network formation process without the allotment of sufficient relaxation time resulted in large internal strains creating unnatural bond, angle, and dihedral distributions in the final crosslinked configurations. Note that simultaneous crosslinking causes deviation of the system from an equilibrium state and relaxation time can essentially be thought of the time required to reestablish this state of equilibrium. Doherty et al. [42] used molecular dynamics simulations to progressively perform crosslinking and

polymerization reactions. The crosslinking process was initiated by selecting a predefined number of reactive sites arbitrarily or specifically. A reaction radius was established and a covalent bond was formed between the two reactive sites when they are within the specified reaction radius at the reference temperature. The formation of a bond is followed by a significant lowering of the simulation temperature and restoration to the reference temperature is done over several picoseconds. The lowering of the simulation temperature during crosslinking is critical as it enables an efficient relaxation of the geometry in the vicinity of the crosslink. The resulting relaxed topology and chemically reasonable densely crosslinked atomistic networks provided impetus to the use of MD to study crosslinked networks.

Heine et al. [11] conducted molecular dynamics simulations of network formation in the united atom framework. This study, which evaluated structural and mechanical properties of crosslinked PDMS, employed a dynamic crosslinking approach based on a cutoff distance criteria. The relaxation of the crosslinked topology was achieved by a modified potential which was harmonic at distances below the specified cutoff and linear at large distances. Studies by Tsige et al. [44] and Tsige and Stevens [45] used a dynamic crosslinking approach to study the role of crosslinker functionality on adhesion and network connectivity on the mechanical properties of highly crosslinked networks respectively. Komarov et al. [46] developed a hybrid MC/MD simulation method to create highly crosslinked polymer networks and predict their structural and thermophysical properties. This involves four procedures beginning with the mapping of the polymerizing monomers into a coarse-grained model. Recall from Chapter II, coarse-graining allows the simulation of dense macromolecular systems to be more tractable by reducing the degrees of freedom and complexity of the interactions. Monte Carlo simulations of these coarse-grained approximations are then used to undertake the crosslinking procedure. This

41

is primarily done to take advantage of the MC algorithms which allow a faster relaxation to an equilibrium conformation for networks as compared to MD. The third and fourth steps are the reverse mapping of the coarse-grained model to its fully atomistic representation followed by simulation of the atomistic model through MD. Varshney et al. [47] conducted a MD study on epoxy based networks with a special emphasis on the crosslinking procedure. These simulations also studied the structural properties and volume shrinkage as a function of degree of curing. Comparisons between the total energy of the resulting crosslinked topology and computational time were made with the four different crosslinking approaches pursued in this study to generate highly crosslinked polymer networks. The generation of a relaxed topology is ensured through a multistep relaxation process during the crosslinking process. Li and Stratchan [48] conducted MD studies on thermosetting polymers to understand the role of the crosslinking procedure on the internal strain of the resulting topology and the role of chemical kinetics on the resulting properties. The charge distribution is altered as a result of the crosslinking reactions and updating them to account for changes in chemistry and topology is extremely important. Both studies [15, 16] account for the change in charge distribution in the local vicinity of crosslinks, although a detailed analysis of charge evolution during crosslinking is provided in the latter. The prediction of structure and thermo-mechanical properties in the work of Li and Stratchan is performed in three stages: polymerization, annealing (to obtain glass transition temperature and thermal expansion coefficient), and mechanical testing using non-equilibrium MD to determine elastic constants. Although both studies [47, 48] used epoxy resin EPON-862 with curing agent DETDA as the model system, the procedure could hypothetically be extended to generate other crosslinked systems. A recent study on the same epoxy/curing agent system conducted by Nouri et al. [49] proposed a methodology that required no change in bond data nor control over the

crosslinking process during the interaction between the epoxy and the curing agent. The existing methods [47, 48] to model the epoxy/curing agent system use a combination of harmonic and LJ potentials requiring the simulation to keep track of the distance between potential bond partners to determine the type of interaction. This could be a time consuming affair requiring greater computational effort. Also, once the eligible bond partners are within equilibrium bond lengths, separation is not possible. In order to use a single potential before and after bond creation, a LJ potential with modified parameters is used. These parameters for the modified LJ potential were determined using Quantum Mechanics (QM)/ Molecular Mechanics (MM) methods. While the method simplifies the programming algorithm which subsequently increases the calculation speed, it may result in a minor error in the calculation of the interaction force. However, according to the authors, this is negligible with respect to the size of the model.

III.5.2 Crosslinking Algorithm

The chemical reaction of a tetra-functional crosslinker with a silanol terminated PDMS chains in the presence of a catalyst can be described by the following equation:

$$RH + HO-Si(CH_3)_2 \, R^{'} \longrightarrow R-O-Si(CH_3)_2 \, R^{'} + H_2 \uparrow \qquad (34)$$
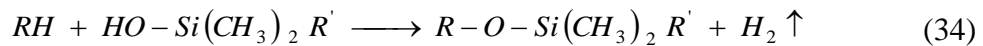
where R represents the crosslinker molecule and R' represents the PDMS chain. It is important to note that most model PDMS networks are experimentally prepared using vinyl terminated PDMS chains. However, the MD potential used in this work provides a better characterization of silanol terminated PDMS chains and thus the simulation is conducted with such a chain [11]. The by-product of the above reaction is the escaping hydrogen gas. In this study, the hydrogen atoms are not explicitly simulated avoiding the complexity of dealing with quantum effects when

simulating light atoms like hydrogen. Also, a crosslinking approach similar to the one employed by Heine et al. [11] is adopted. In this dynamic approach to crosslinking, a bond between the crosslinker and PDMS chain is formed with unit probability if they are within a specified cutoff distance. This distance is specified to be 6.5 Å and a new potential, which is linear at large distances and harmonic at distances near equilibrium bond lengths, is specified for the purpose of crosslinking. The harmonic bond potential, provides a large potential energy for large bond separations leading to high energy unstable networks. Therefore, the employment of this new potential for crosslinking is essential and is described by the following equations:

$$
U_{bond}^{xlink}(r) = \begin{cases} \dfrac{1}{2}k_{bond}(r-r_0)^2 \ , \ r \leq r_{cut} \\ \dfrac{1}{2}k_{bond}(r_{cut}-r_0)^2 \ + \ \dfrac{1}{2}k_{bond}(r-r_{cut}) \ , \ r > r_{cut} \end{cases}
\tag{35}
$$

In the above equation, the spring constant k_{bond} is set to 35.01 kcal/mol and r_{cut} is fixed to be 1.71 Å [11]. Therefore, structural instabilities resulting from stretched bonds, which could adversely affect the system's bond, angle, and dihedral configurations is avoided through the use of this new potential. In order to better illustrate the crosslinking algorithm used in this study, the following flowchart is presented:
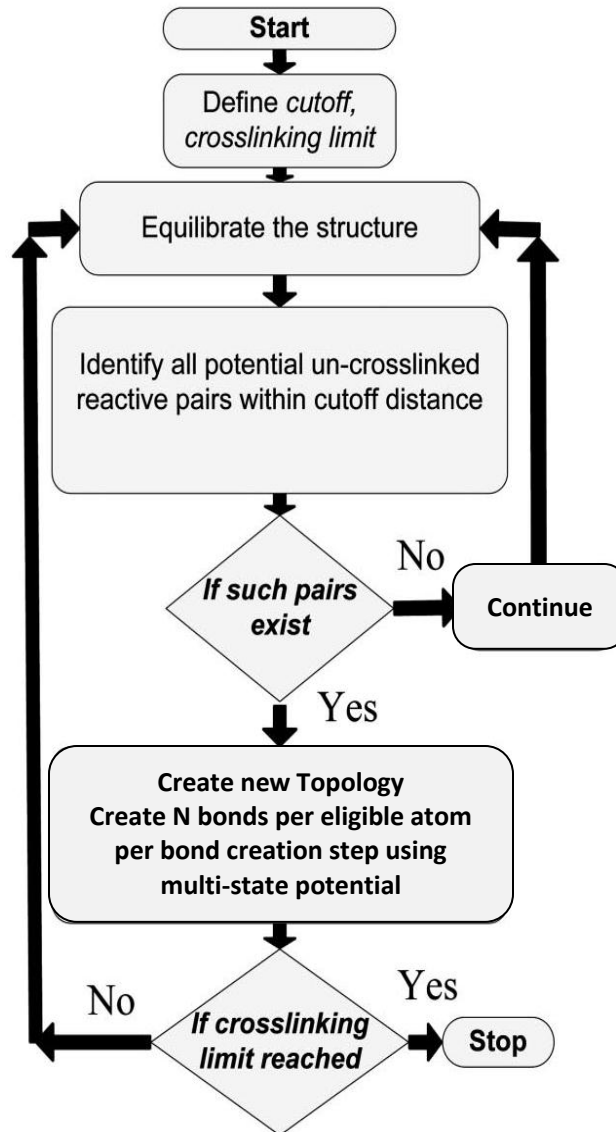
Figure 10: Schematic of the crosslinking algorithm implemented in this study. Modified from Varshney et al. [47].

III.5.3 Crosslinked PDMS Models

In this study, the crosslinked PDMS models consist of 50 silanol terminated PDMS chains and an appropriate number of crosslinker molecules determined by weight ratio. Recall from Chapter I that silanol (Si-OH) terminated PDMS chains consist of a Si-O backbone with

two methyl groups attached to the Si atoms. The chains considered in this study have molecular weights of 5,000 g/mol, 10,000 g/mol, 20,000 g/mol, and 40,000 g/mol while the PDMS to crosslinker weight ratios are of 5:1 and 10:1. In order to meet the desired weight ratios, the number of crosslink molecules varies for systems with varying molecular weights indicated in Table 3.

PDMS:CL	Molecular Weight (g/mol)			
	5,000	10,000	20,000	40,000
	Number of Crosslink molecules			
Weight Ratio 5:1	150	303	606	1215
Weight Ratio 10:1	75	151	303	607

Table 3: The number of crosslink molecules required to meet the given PDMS:CL weight ratio

These conformations are created using the Coupled-Decoupled CBMC formulation described in Chapter III.4 in a procedure identical to the pure uncrosslinked PDMS systems. Three independent conformations of the PDMS system are created with different initial random conformations of the chains. The CBMC simulations were run for 5 cycles, where a cycle equals N moves, with N being the number of molecules in the system (50 PDMS chain plus the appropriate number of crosslinkers).

III.5.4 Preliminary Simulation Setup for Crosslinked PDMS Models

The combined PDMS chain and crosslinker model undergoes an energy minimization, followed by the application of a purely repulsive soft potential (done in two stages) and a NPT equilibration (using LJ parameters in Table 2 to characterize non-bonded interactions) which restores the system to its proper equilibrium density in a procedure identical to the pure PDMS

models. Upon completion of this run, the new linear plus harmonic crosslinking potential is specified. The system is then crosslinked in the NPT ensemble with the system temperature and pressure specified at 300 K and 1 atm respectively. After every 10 picoseconds, all potential uncrosslinked reactive pairs are identified and crosslinks are generated between eligible pairs. The topological information is updated and the system is relaxed for 10 picoseconds avoiding abrupt changes in the spatial coordinates of atoms in the local region of the newly formed bonds. This is repeated until the system achieves an 80 % crosslink density (ratio of the number of bonded PDMS ends to the number of free PDMS ends) upon which the final crosslinked topology is equilibrated for a further period of 1 nanosecond in a NPT ensemble. Upon the completion of this equilibration, the system undergoes the diffusion part of the simulation analogous to the pure PDMS models.
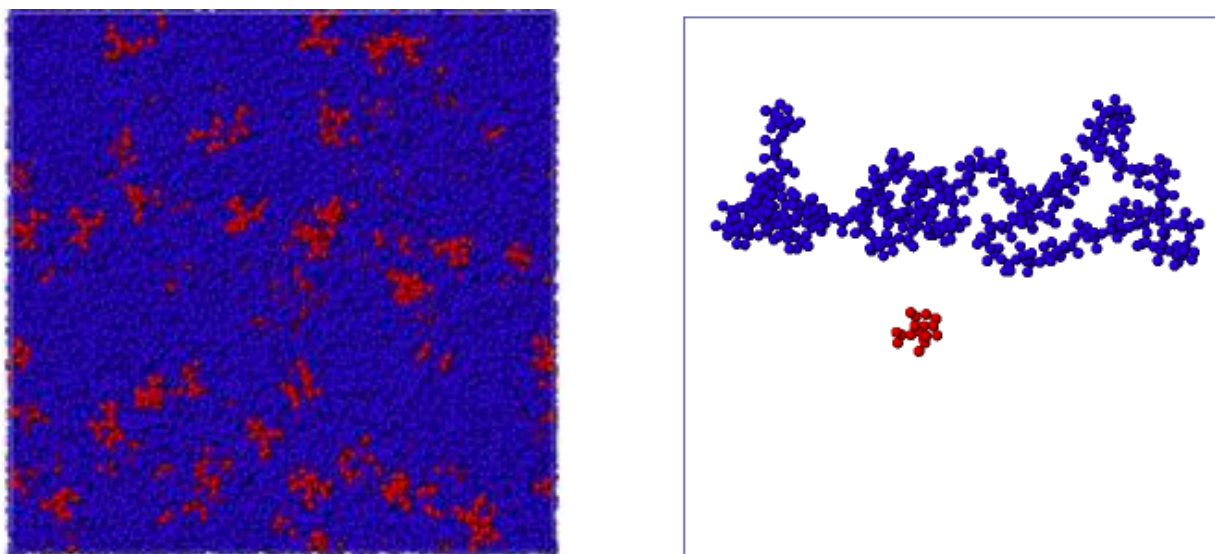
Figure 11: Illustration of a fully dense crosslinked PDMS system (left) and a single chain of molecular weight 10,000 g/mol and crosslink molecule (red) generated using Ovito [40].

III.6   Model Validation: Studying bond, angle, and dihedral distributions

Prior to computing diffusion-related data, in order to validate the appropriateness of the chain configurations due to the crosslinking process, two methods are employed. First, the bond, angle, and dihedral distributions of the system are analyzed using histograms after the crosslinking process. Second, glass transition temperatures are computed and compared to experiments for uncrosslinked and crosslinked structures.

Histograms are used to graphically display the distribution and variation of a given data set. The basic idea is to sort data into specified regions or bins and obtain a frequency distribution that can be displayed in a clear graphical format. They are typically used to find the center, spread, shape (symmetric or skewed), outliers etc. of the data set. As mentioned above, histograms are employed in this study to obtain the bond, angle, and dihedral distributions of the simulated systems.

The reaction radius (6.5Å in this study) is the limit within which PDMS chains and crosslinker atoms are allowed to bond, is much larger than the equilibrium bond distance (1.64 Å for Si-O bonds and 1.90 Å for Si-CH$_3$ bonds). Therefore, stretched bonds are created in simulations leading to a tremendous increase in the potential energy of the system (due to the harmonic nature of the potential used to describe interactions between bonded atoms). This is in contrast to experiments, where bond formation is a favorable process resulting in a decrease in energy. Also, the tendency of the harmonic potential to rapidly return these stretched bonds to their equilibrium configurations can result in increased internal strain causing the system's bonds, angles, and dihedrals to become distorted. Finally, crosslinking increases the molecular weight of the chains involved which adversely affects chain mobility and this reduced

configurational freedom limits the chain reorientation mechanism to damp out these excessive internal strains. Despite the increase in both bonded and non-bonded energy terms during crosslinking, Li and Stratchan [48] report that dihedral energy dominates the total increase in internal network strain by increasing over 100 percent of its original value. A combination of a low spring constant combined with reduced mobility after network formation is attributed to this dramatic increase in dihedral energies. In order to overcome these detrimental effects and generate a relaxed crosslinked topology, studies [11, 42, 45-48] have developed unique crosslinking algorithms which allow sufficient relaxation times. High temperature polymerization is also shown to reduce internal network strains due to the availability of added kinetic energy to the molecules.

To verify the validity of the generated crosslinked structures, a sample system consisting of 50 short silanol terminated PDMS chains (n = 10) and 25 crosslinkers is created using Towhee. Short chains (M_g = 900 g/mol) have enhanced mobility therefore their ability to dissipate internal strains due to crosslinking is better than long chains and hence their use is ideal for model validation. The polymerization process continues until a crosslink density of 50 percent is achieved. Four different simulations are performed: (1) Crosslinking with purely harmonic potential without relaxation (time to reestablish a state of equilibrium) allowed between crosslinks, (2) Crosslinking with linear plus harmonic potential without relaxation, (3) Crosslinking with harmonic potential allowing relaxation between crosslinks, (4) Crosslinking with linear plus harmonic potential with relaxation. A sample histogram showing the bond, angle, and dihedral distributions is shown below:
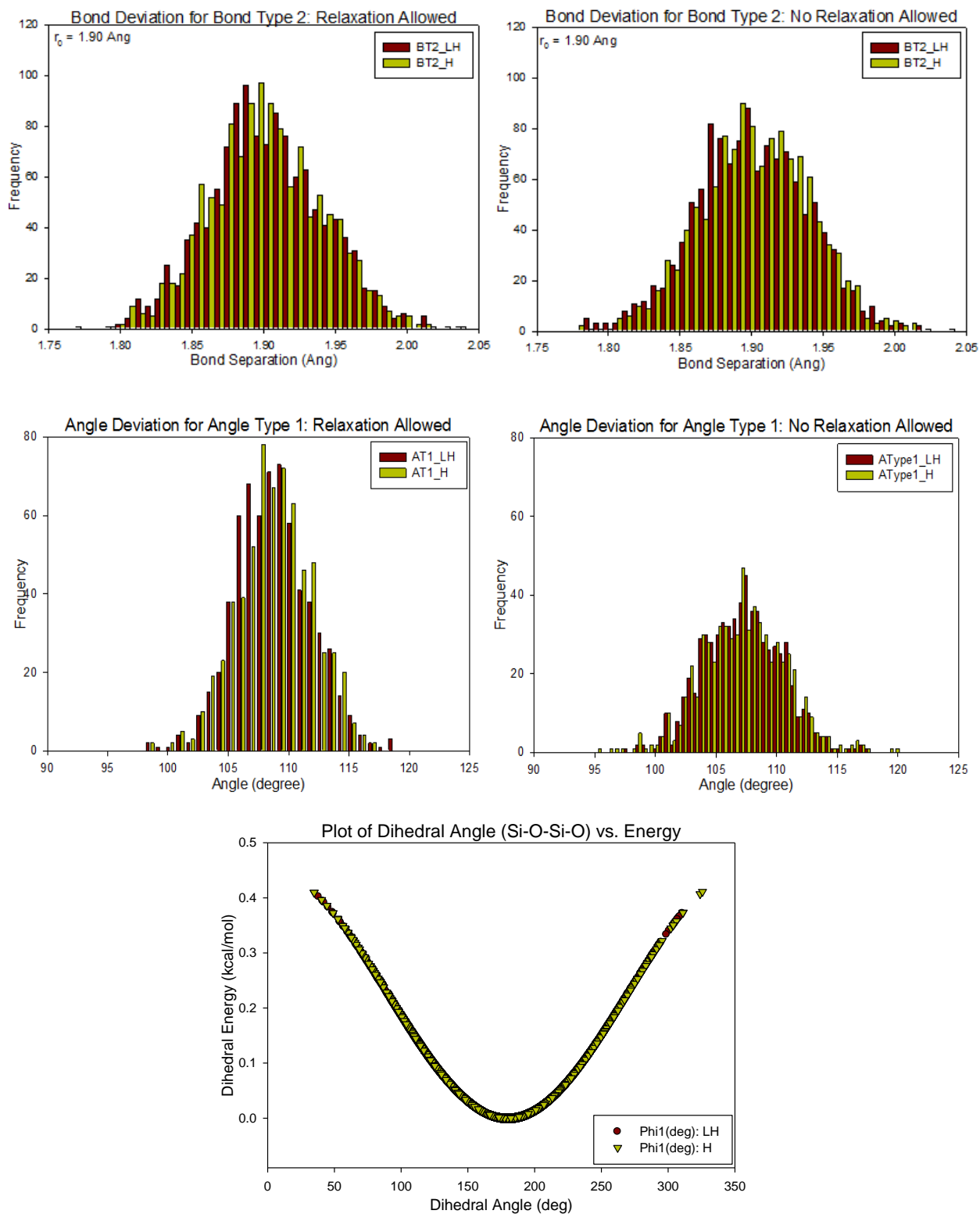
Figure 12: Histograms studying bond, angle, and dihedral distortion with relaxation (left) and without relaxation

The equilibrium angle for O-Si-O is 107.82 degrees. On comparison of the two histograms, the presence of outliers is evident for the case where crosslinking without relaxation is performed with the harmonic potential. When relaxation of the structure is allowed, the linear plus harmonic potential displays a nice distribution around the equilibrium angle for type O-Si-O. Similar trends are observed when analyzing bonds, angles, and dihedrals in larger systems. Although it is difficult to notice much difference with and without relaxation in the bond distortion histograms due to their high k value, there definitely is a presence of outliers in the dihedral distortion histogram. It can be observed that the purely harmonic potential provides extreme under and over-approximations owing to a really low k value. This validates that using the linear plus harmonic potential while appropriately relaxing the structure ensures the generation of undistorted networks.

III.7   Glass Transition Temperature

The glass transition, a unique property of amorphous polymers, is the temperature at which transition occurs from a soft 'rubbery' state to a solid 'glass' state upon cooling. Above the glass transition temperature (T_g), sufficient kinetic energy is available to allow for long range segmental motion resulting in an increase in free volume of the polymer. As a result, heat capacity, linear coefficient of thermal expansion, and elasticity increase [50]. Below T_g, internal adjustments of the segments are limited due the lack of mobility, and brittle behavior is exhibited. At this point, it is important to distinguish T_g from melting. Melting is a first order transition, characterized by both latent heat and change in heat capacity of the material, while

glass transition is a second order transition involving only a change in heat capacity but no latent heat.

Since contrasting behavior is displayed either side of T_g, understanding factors that affect glass transition are extremely important in the study of polymers and their application. Chemical composition, structure, chain flexibility, molecular weight, crosslinking, etc. are some of the common factors that affect the T_g of a polymer. Some of these are discussed further in order to understand their effect on T_g.

- Molecular Weight and Crosslinking: Chain ends have a certain free volume associated with them. Systems with shorter chains naturally have more free ends per unit volume and therefore more free volume compared to longer chains. This results in a lower T_g for shorter chains. Crosslinking increases the molecular weight, and therefore adds to the T_g of the polymer.

- Chain Flexibility and Side Groups: The flexibility of polymer chains is determined by the ease of rotation about primary valence bonds [51]. Groups tending to stiffen the backbone increase T_g, while a reduction in resistance to internal rotation lowers T_g. Bulky side groups close to the backbone hinder mobility by reducing free volume and therefore raise T_g. Note that the influence of the side group in increasing the stiffness of the chain is determined by their flexibility and not their size [51]. Flexible side groups have more molecular freedom resulting in increased free volume, consequently lowering T_g.

- Geometric Factors: Polymers with symmetric structures have a lower T_g than ones with an asymmetric structure. This is because the packing of additional side groups in a symmetric structure results in a "loose" configurational arrangement increasing free

volume resulting in a decrease of T_g [51]. The presence of double bonds and cis/trans configurations also affects T_g. Double bonds in the cis configuration reduce the energy barrier for adjacent bond rotation. This results in a softening of the chain thereby reducing T_g [51].

- Inter-chain Forces of Attraction: Intermolecular bonding in polymers is due to the presence of secondary attractive interactions. Therefore, strong intermolecular bonds result in a significant increase in T_g [51]. Note that these attractive forces are only effective over short distances; therefore side groups which increase distance between adjacent chains decrease the cohesive effect of these attractions reducing T_g.

- Rate of Cooling: The rate of cooling also heavily influences T_g and an increased T_g results with higher cooling rates. This behavior can be explained by analyzing the intermolecular relaxation process. Rapid cooling reduces the time available for molecules to reorient themselves and when combined with reduced cooperative molecular motion near glass transition results in a tangled chain structure (reduced free volume) increasing T_g. In simulations, the time scales are extremely small compared to the reduction in temperature, resulting in extremely high cooling rates. This is the reason why simulations tend to overestimate T_g when compared to experiment.

III.7.1 MD Studies of Glass Transition

The inability of experiments to provide details at the molecular level regarding structural changes and the reduced mobility phenomenon at temperatures near glass transition makes MD simulations, which can provide a detailed analysis of material structure and local dynamics, an appealing option. One of the earliest works in glass transition using MD was performed by Rigby and Roe [52] for polyethylene systems. The simulated system consisted of linear chains of upto 50 spherical segments subject to forces due to bond stretching, bending, torsion, nonbonded interactions through a truncated LJ potential between neighboring chains and between segments separated by three bonds on the same chain. They reported the liquid to glass transition phenomena in these systems were exhibited in the following steps: (1) cessation of trans-gauche conformational transitions (2) changes in the temperature coefficients of the density and internal energy, and (3) effective vanishing of the segmental diffusion coefficient. Although the chain length severely affected T_g when the chains were rigid, the effects of chain length on T_g for highly flexible chains was small. At the time, this feature was not corroborated by experiments. The study reports that the effect of chain length on T_g was qualitatively the same as that exhibited by the experimental T_g of polymers. It is interesting to note that these early studies refrained from a quantitative comparison with experimentally derived T_g values. Han et al. [53] performed glass transition studies using MD simulations on four polymers: cis-poly (1, 3-butadiene), polyisobutylene (PIB), atactic polypropylene, and (atactic) polystyrene. The authors conclude that the upward displacement of T_g due to time scale limitations in MD simulations is minor enough to allow useful materials predictions using MD techniques. A similar conclusion was made by Fried et al. [54] who studied PVT properties of polyphosphazenes using the COMPASS forcefield. A small break at a temperature near glass transition was reported for a

plot of internal energy versus temperature was observed lending credence to the fact that energy components need not be in equilibrium in the rubbery and glassy states. Sun et al. [55] investigated the effects of backbone chain flexibility and side groups on glass transition of polymers. The polymers included in this study were: polyethylene (C-C backbone, -H side group), polypropylene (C-C backbone, one –CH_3 side group), polyisobutylene (C-C backbone, two –CH_3 side groups), polyoxymethylene (C-O backbone, -H side group), and PDMS. Torsional and non-bond energy decrease linearly with temperature above T_g and a similar trend is observed below T_g with a slightly smaller slope indicating that these play important roles in the glass transition process of amorphous polymers. Their simulations report that the fraction of bonds in the trans-state (dihedrals in $\pm\ 180\ ^\circ \pm 30^\circ$ are in the trans state) are constant below T_g implying that glass transition is primarily associated with the freezing of the torsional degrees of polymer chains. Buchholz et al. [56] studied the cooling rate dependence of T_g using a coarse-grained bead spring model of polymers for a test of mode coupling theory for analysis of the relation between glassy dynamics and behavior of the Rouse modes, analyzing the effect of confinement on glass transition, etc. Yang et al. [57] conducted a study to understand the thermodynamics and kinetics of glass transition by comparing glass formation under isobaric and isochoric (constant volume process) conditions. The undergoing of an abrupt change of trans-state fractions and torsional contributions to the energy at glass transition temperature at both isobaric and isochoric conditions validated results from previous studies [54, 55] that glass transition is primarily associated with the freezing of torsional degrees of polymer chains which is coupled to the degree of freedom associated with the non-bonded LJ potential. Comparisons of the isobaric and isochoric data also yields that the thermodynamic is cooling path independent above T_g and path dependent below T_g. Aforementioned studies [47-49] on glass transition of

crosslinked epoxy systems using MD simulations show reasonable agreement with experimentally predicted T_g for such systems once the cooling rate is taken into account.

III.7.2 T_g Simulation Details and Comparison

Glass transition temperature simulations are carried out by lowering the system temperature from 300 K to 50 K using 25 K decrements every 1 nanosecond after the preliminary simulation setup for pure PDMS models is completed as described previously in Chapter III.4.1. This simulation is performed in an NPT ensemble under atmospheric pressure and results in a cooling rate of 2.5×10^{10} K/s. Although total simulation time was 1 nanosecond at each temperature, statistics were collected only over the last 200 picoseconds of the run at each temperature. Three equivalent, statistically independent runs were performed for each of the crosslinked and un-crosslinked models and the glass transition data presented is averaged over these three runs. The glass transition temperature is extracted at the kink occurring in the temperature versus volume plot by fitting a linear two segment piecewise function to the data using SigmaPlot. The results for the uncrosslinked case and the two crosslinked cases with varying PDMS to crosslinker weight ratio are presented in the Figure 13 and Table 4.
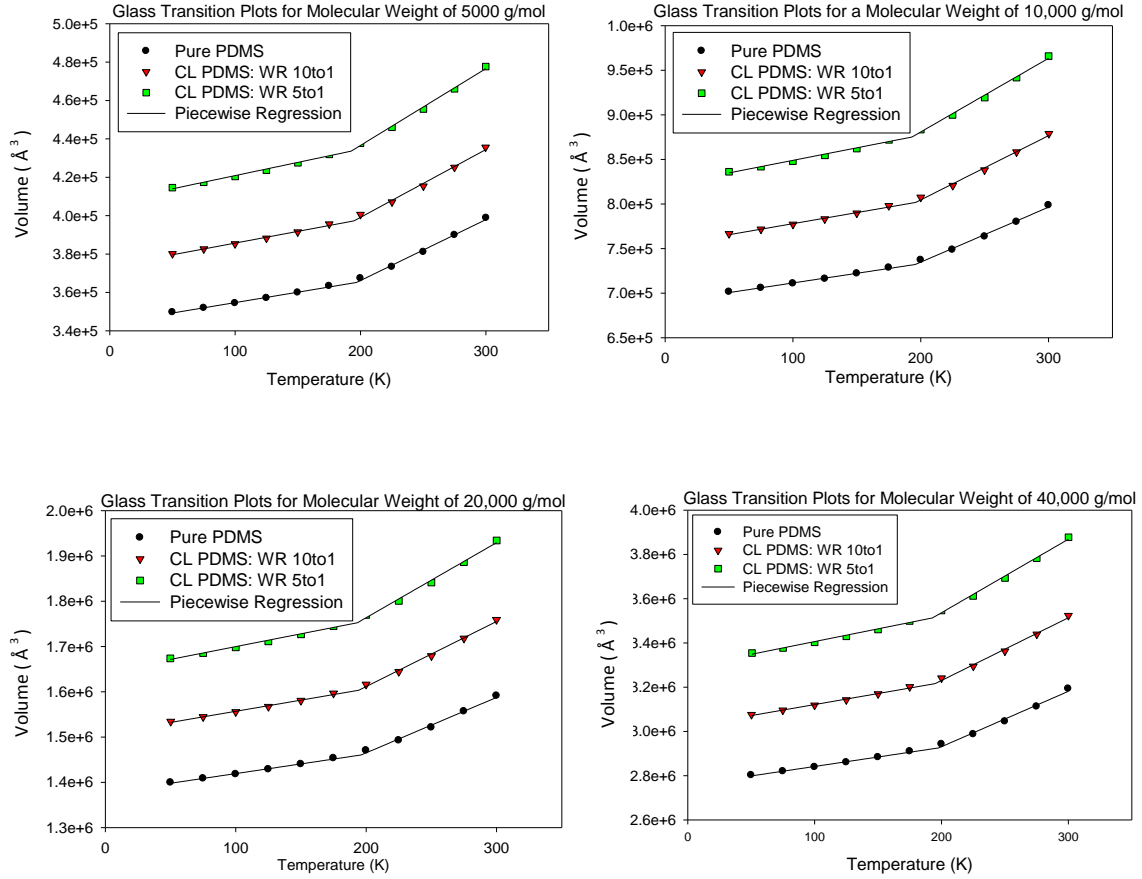
Figure 13: Volume versus temperature plots studying glass transition temperature for pure and crosslinked PDMS systems of varying weight ratios and molecular weights.

	5000	**10,000**	**20,000**	**40,000**
UCL	195.76	196.862	196.161	197.841
10:1	194.787	196.123	194.368	195.05
5:1	192.51	193.171	193.318	192.996

Table 4: Glass Transition Temperatures for various models.

Two trends are evident from Figure 13 and Table 4: (1) a very modest increase in T_g is observed with molecular weight, and (2) model having the most crosslinker molecules exhibits the lowest T_g within the respective molecular weight groups. These trends indicate the lack of dependence of T_g of PDMS on crosslinking. Andrady et al. [58] report similar results derived from experiments and attribute this lack of dependence of T_g on crosslink density to the extreme flexibility of the PDMS chains. Even though crosslinking is known to introduce constraints on the mobility of the chains, in PDMS it fails to reduce the overall mobility of the system by an appreciable degree. Therefore, T_g of the networks remains roughly equivalent as the main chain flexibility overrides the constraining effect of crosslinks [58]. As mentioned above, T_g is a kinetic property and dependent on cooling/heating rate; an increase of 3 K is expected per order of magnitude increase in rate [59]. Therefore, the T_g determined using our MD simulation should roughly be 30 K higher than the experimental value. This should result in a T_g value of around 180 K which is close to the results obtained here. The time scale for overall relaxation of a typical chain in an entangled melt is approximately 10^{-6} seconds [55] and increases with chain length indicating equilibrium states are not achieved even at temperatures well above T_g. Therefore, importance should be given to the fact that experimental trends are successfully captured in MD rather than a quantitative agreement with experiments.

III.8 Nanocomposite Models

The nanocomposite models, which contain Cu nanoparticles in the PDMS matrix, are an extension of the crosslinked PDMS models. The objective of studying these models is to understand the role of nanoparticle length scale and volume fraction on steady state diffusion of

penetrants through PDMS. The generation of voids for the nanoparticles begins with the PDMS chain and crosslinker system at equilibrium density (before they are crosslinked) which are created as described in the previous section. Small voids are grown at specified locations within the system with a purely repulsive potential which exerts a force of magnitude:

$$F = K \left(r - R \right)^2 \tag{36}$$

where K is the force constant, r is the distance from the atom to the center of the repulsive sphere, and R is the radius of the repulsive potential. This radius is increased linearly to the appropriate distance (depending on the volume fraction we want to achieve) over the length of a 100 picosecond simulation in the NPT simulation at 300 K and 1 atmosphere. A slow growth of these voids is important to limit deviation from equilibrium. This repulsive potential pushes PDMS chains away from the center of these voids until no atoms exist within the radius of the sphere. The Cu nanoparticles are then created within these voids and care is taken to avoid overlaps with the PDMS chains. A 100 picosecond NPT equilibration is performed at 300 K to allow the PDMS chains to redistribute themselves in the matrix around the nanoparticles. A few atoms in the center of each sphere are fixed at zero force and velocity to prevent the nanoparticles from moving during this equilibration. The linear plus harmonic crosslinking potential is introduced and the system is crosslinked as described in the previous section. Upon attainment of the 80 % crosslink density, the system is ready to undergo the diffusion part of the simulation which is similar to the pure PDMS models.

Figure 14 provides a schematic illustration of the nanocomposite construction procedure employed in this study. Note that the atmospheric penetrates are enlarged for better viewing in Figure 14.
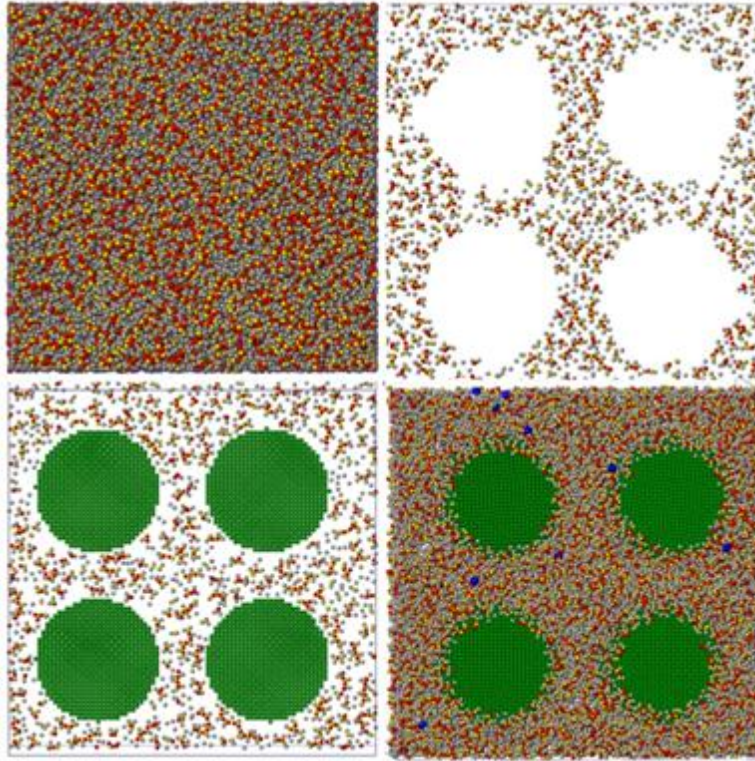
Figure 14: Illustration of nanocomposite construction procedure: 1) Fully dense system (top left) 2) Growing voids for placement of nanoparticles (top right) 3) Creation of nanoparticles in the voids 4) re-equilibrating the system and introducing penetrants.

The nanocomposite case is an extension of the crosslinked PDMS case with the inclusion of Cu nanoparticles. In this work, we study nanoparticle volume fractions of 5%, 10%, and 20%. Recall that Table 3 specifies the number of crosslink molecules in a given system of a specified weight ratio and molecular weight. Using the information in Table 3, the nanoparticle radius for varying volume fractions can be easily determined. This information is presented in Table 5 for all the systems in this study.

PDMS:CL	Molecular Weight (g/mol)				
	5000	**10000**	**20000**	**40000**	
PDMS:CL	**Nanoparticle Radius (Angstroms)**				**Volume Fraction**
Weight Ratio 5:1	8.9	11.3	14.2	17.9	**5 %**
	11.2	14.2	17.9	22.6	**10 %**
	14.2	17.9	22.6	28.5	**20%**
Weight Ratio 10:1	8.6	10.9	13.7	17.3	**5 %**
	10.9	13.7	17.3	21.9	**10 %**
	13.7	17.3	21.8	27.5	**20%**

Table 5: Nanoparticle radius for a given Molecular Weight and Weight Ratio to meet a certain volume fraction criterion.

Chapter IV DIFFUSION CALCULATIONS AND DISCUSSION

This chapter explains diffusion, calculation of mean-squared displacement in this thesis, capturing the role of temperature on diffusion using the WLF equation, background in diffusion studies using MD, simulation results and diffusion calculations for uncrosslinked, crosslinked, and nanocomposite models.

IV.1 Diffusion

Diffusion is a transport process through which mass flows from one place to another (due to a concentration gradient) caused by the molecular motion of particles. Diffusion has two primary properties: it is random in nature and the transport of mass is from regions of higher concentration to regions of lower concentration, with an equilibrium state of uniform concentration [60]. An appropriate example to verify this is the spraying of a perfume bottle in a closed room. Initially, the fragrance is stronger near the source however, with time due to the random molecular motion of the particles; the fragrance has traveled throughout the room. The classical definition of steady-state diffusion is provided by Fick's 1st Law, which states that the net flow of atoms by atomic diffusion is proportional to the negative gradient of the concentration of that species,

$$J = -D\left(\frac{dc}{dx}\right) \qquad (37)$$

where J is the flux or net flow of atoms, D is the proportionality constant called the diffusivity or diffusion coefficient, and (dc/dx) is the concentration gradient [61]. In this study, the terms diffusivity and diffusion coefficient will be used interchangeably.

IV.1.1 Mean-Squared Displacement: Significance and Calculation

As will be discussed in the results section, MD simulations can accurately compute data associated with small molecule diffusion through polymers. The observation of the trajectory of a diffusing molecule through a system leads to the conclusion that its diffusion is random through the available free volume. This random motion, which is characterized by collisions of the diffusing species with other particles in the system, can be modeled with a random walk. Mathematically, a random walk can be described by a series of consecutive steps, where each following step is in a completely random direction from the one before. In order to correlate the distance traveled by random motion of these particles to the diffusion coefficient, a mean squared-displacement method is used. The mean-squared displacement is the measure of the average distance a molecule travels,

$$MSD(t) = \left\langle r_i(t) - r_i(0) \right\rangle \tag{38}$$

Where the term $[r_i(t) - r_i(0)]$ is the distance traveled by the molecule over a given time interval t. The angle brackets indicate that the squared magnitude of this vector is time and/or ensemble averaged over the 100 penetrates. The mean-squared displacement method is derived by relating Fick's 1st Law to the conservation of mass of the system. The diffusion coefficient, D, which is proportional to the slope of the mean-squared displacement with respect to time, can then be expressed as,

$$D = \frac{1}{2y} \frac{d}{dt} \left\langle \left[r(t) - r(0) \right]^2 \right\rangle \tag{39}$$

where $<r^2>$ is the ensemble average of the mean squared distance, y is the dimensionality of the system, D is the diffusion coefficient which defines the rate of diffusion. Due to this relation with the diffusion coefficient, the mean-squared displacement method is extremely important as it can be directly correlated to the underlying motion of the particles. It is important to note that an alternative method to compute diffusion coefficients from molecular dynamics simulations is to use the velocity auto-correlation function [17, 62-64]. This work will employ the MSD approach.

In the simulations employed in this study to observe diffusion, a NPT production run is performed for 1 nanosecond with the time origin for the MSD reset every 100 picoseconds during the production run. This resetting of the time origin is similar to performing 10 production runs to obtain MSD of the diffusing species and hence allows the obtainment of better statistics. The MSD of the penetrants at temperatures ranging from 225 K to 400 K, which is presented as an average over these 10 runs, is presented in Figure 15.
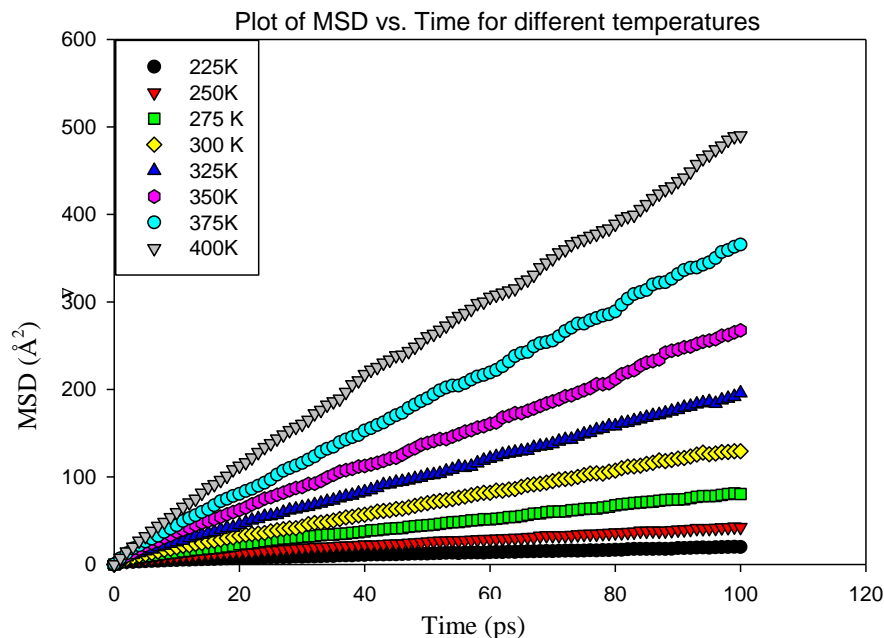
Figure 15: Sample plot of averaged MSD of 100 O_2 penetrants versus Time at various temperatures

Although the linear dependence of MSD at long times is apparent, it is important to observe that at very short times the plot is non-linear. Initially, penetrates move with constant velocity until the first collision with other atoms in the system takes place. At a constant velocity, the distance traveled is directly proportional to time making MSD proportional to the square of time. Therefore, at short times, there is a quadratic dependence in MSD with time. This initial non-linear portion of the MSD data is associated with the ballistic motion of the penetrant molecules as their motion is within their initial pockets of free volume within the PDMS matrix. Thus, a resemblance of the molecular motion of these penetrants to a random walk takes place only after the collision process is initiated resulting in a linear increase in MSD with time. In this study, the slope of MSD is computed after removing the first 30 ps of the MSD data in order to ensure the least squared fits to obtain the diffusion coefficients are performed over the linear portion of the MSD plot. This is illustrated in Figure 16.
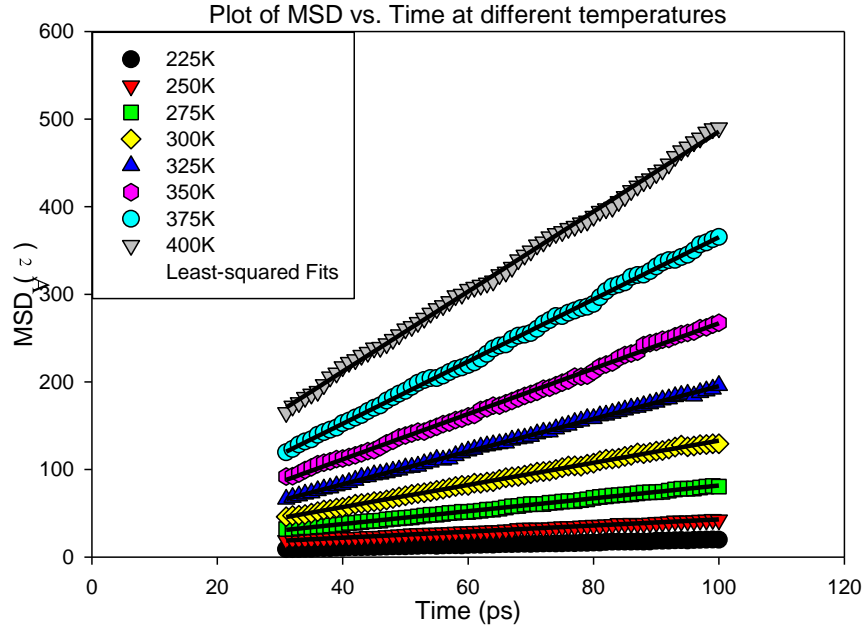
Figure 16: Sample MSD of 100 O$_2$ penetrants versus time plot after removal of the transient portion of the data. The diffusion coefficient at each temperature is proportional to the least-squared linear fit.

IV.1.2 Role of Temperature: Arrhenius vs. WLF

In order for diffusion to occur, the atoms must overcome the energy barrier associated with changing their position. The greater the kinetic energy of the system, which is related directly to temperature, the easier it is for the diffusing species to overcome the energy barrier. Therefore, temperature has a significant role on diffusion and it can be characterized in certain situations by an Arrhenius relation

$$D \ = \ D_0 \ \exp \left(\ \frac{-Q}{RT} \ \right) \qquad (40)$$

where D is the diffusion coefficient, D$_0$ is the diffusion constant, Q is the activation energy of the diffusing species, R is the molar gas constant, and T is the temperature. However, the WLF equation provides a better description of diffusion than the Arrhenius equation, especially at temperatures near glass transition [65], where free volume fraction is considered to be

66

approximately constant [59]. Therefore, in situations where free volume availability is the critical factor which determines molecular mobility, the WLF model is appropriate to describe temperature dependence of a process [66, 67]. The models observed in this study show a similar tendency to deviate from Arrhenius behavior as the simulation temperature approaches glass transition temperature, and therefore a WLF equation is fit to our diffusion data. This will be shown in the following sections.

The viscoelastic nature of polymers requires their analysis at long times and the WLF equation was derived from these studies. Due to the nature of the viscoelastic relaxation process, the effect of increasing the temperature is analogous to the allotment of more time in a given test [68]. This is expressed through the time-temperature superposition principle which states that a given property measured for short times at a certain temperature is identical to one measured for longer times at a lower temperature, except that the curves are shifted on a logarithmic time axis [69]. The WLF equation is associated to this time-temperature superposition and is described by

$$\log\left(a_T\right) \;=\; y_0 \;-\; \frac{c_1\left(T - T_g\right)}{c_2 + \left(T - T_g\right)} \tag{41}$$

where a_T is the ratio between the time for a given viscoelastic response at temperature T and the time for the same viscoelastic response at temperature T_0, T_g is the glass transition temperature, T is some reference temperature, and C_1 and C_2 are material constants. These material constants are sometimes considered universal for a wide range of polymers [66]. However, Angell [70] argues that although these parameters are fairly robust, with C_1 being more universal than C_2, it is best to fit the WLF equation to a given set of data. Also, the shift factor is meaningful in terms of material properties like diffusivity and viscosity [71]. Therefore, the WLF equation can be rewritten to characterize the diffusivity as:

$$\log(D) = y_0 - \frac{c_1(T - T_g)}{c_2 + (T - T_g)}$$ (42)

where y_0 is a shift variable that can be tailored to specific phenomenon, such as viscosity in Urakawa et al. [72]. Their work analyzed the self-diffusion coefficient, D, and the viscosity of low molecular weight polystyrene over a wide range of temperatures above glass transition temperature. A WLF model is used to describe the self-diffusivity of the molecular chains in their system as the temperature was cooled towards T_g.

IV.2 Diffusion Studies Using MD

One of the first works to study diffusion through polymers using simulations was performed by Trohalaki et al. [73] which simulated the diffusion of 4 penetrants (CO_2) in a system of 25 chains containing 20 united atom CH_2 units. The obtained diffusion coefficients were larger than experiments and attributed to the presence of crystallites in the real polymer. Sok et al. [74] analyzed the effect of penetrate size on the diffusion coefficient citing the numerous simulations concentrating on temperature effects on diffusion. Their small system consisting of five chains of 30 monomer units was simulated using the GROMOS potential in constant NPT conditions and diffusion constants were calculated with MSD. Calculated diffusion constants for methane (CH_4) and helium (He) penetrants are in good agreement with experiment. Similarly using the GROMOS forcefield, Tamai et al. [75] analyzed effects of free volume distribution on the diffusion coefficient for various polymers. Takeuchi et al. [76] studied diffusion of O_2 in two models: (1) torsional potential mimicked polymethylene, and (2) torsional potential was zero. The relaxation time of the dihedral angles, obtained from autocorrelation function of internal rotations, was found to be 30 times higher than the model in

68

which the torsional potential was zero. Upon elimination of the rotational barrier, O_2 diffused 5 times faster. Further investigation of the influence of the torsional barrier on diffusion by Pant and Boyd [77] showed that raising the torsional barrier completely halted the diffusion of O_2 in polyethylene. Charati and Stern [78] studied the influence of side groups on the diffusion coefficient of small molecular gases (He, O_2, N_2, CO_2, and CH4) at 300 K through five different silicone polymers. Their simulations concur with the experimental trend of decrease in diffusion coefficients with an increase in size of the polymer molecules and penetrant molecules. A similar MD study involving varying penetrant size to evaluate its effects on diffusion coefficients was performed by Jawalkar et al. [79] using four different penetrants (N_2, O_2, CO_2, and CH_4) in polymers at 298 K. Striolo et al. [80] studied thermodynamic and transport porperties of Polyhedral Oligomeric Sislesquioxanes (POSS) which are cages of silicon and oxygen, with a chemical formula $(SiO_{1.5})_8R_8$ where R is an organic group, in PDMS. The study determined self-diffusion coefficients of POSS through PDMS using a MSD type approach at simulation temperature varying from 300-1000 K. Also, the diffusion coefficients for POSS obeyed Arrhenius behavior for all temperatures studied here except 300 K. Shemella et al. [81] conducted all atom classical molecular dynamics simulations investigating the effects of structural and electrostatic environments on the local period of molecular motion. In order to accomplish this, self-diffusion of the crosslinker molecules was tracked through the system and self-diffusion constant calculated. The system consisted of 100 long PDMS chains with a degree of polymerization (DP is equal to the total molecular weight of polymer divided by molecular weight of the monomer) of 978 and 200 PHMS crosslinker molecules with DP of 32 considering various crosslink densities with a maximum of 50 percent. The crosslinked system showed self-diffusion characteristics that were considerably attenuated because (1) extremely large degree of

polymerization of the PDMS chains, and (2) few free crosslinkers were present. Therefore, MSD calculations were performed for pre-crosslinked systems. The long-time MSD of the crosslinker molecule can be accurately described by the self-diffusion coefficient. The origin of fast molecular motion as a function of temperature was studied along with the enhanced diffusion of fast moving crosslinker molecules (attributed to attractive electrostatic environment and reduced local density).

IV.3   Diffusion Results for Pure PDMS Models

The following sections provide plots and discussions regarding the results of diffusion for the pure PDMS systems. There is also a discussion of the trends in the WLF fit parameters for the aforementioned model.

IV.3.1 Effect of Chain Length on Diffusivity in Pure PDMS Models

As mentioned in the previous section, diffusion coefficients are extracted from the slope of the MSD linear least-squared regressions performed after the removal of the transient portion of the data. As mentioned in Chapter IV.1.2, free volume availability becomes critical at temperatures near glass transition for the models studied here; therefore the WLF equation provides a better fit to the diffusion data than an Arrhenius type equation. Perfect Arrhenius behavior is represented on the plots below with a straight blue line. The following plot, for a system of 50 PDMS chains of varying molecular weights, displays the computed diffusion coefficients as a function of temperature. Error bars in the figure designate +/- 1 standard

deviation in the diffusion coefficient at each temperature calculated from the three independent

realizations.
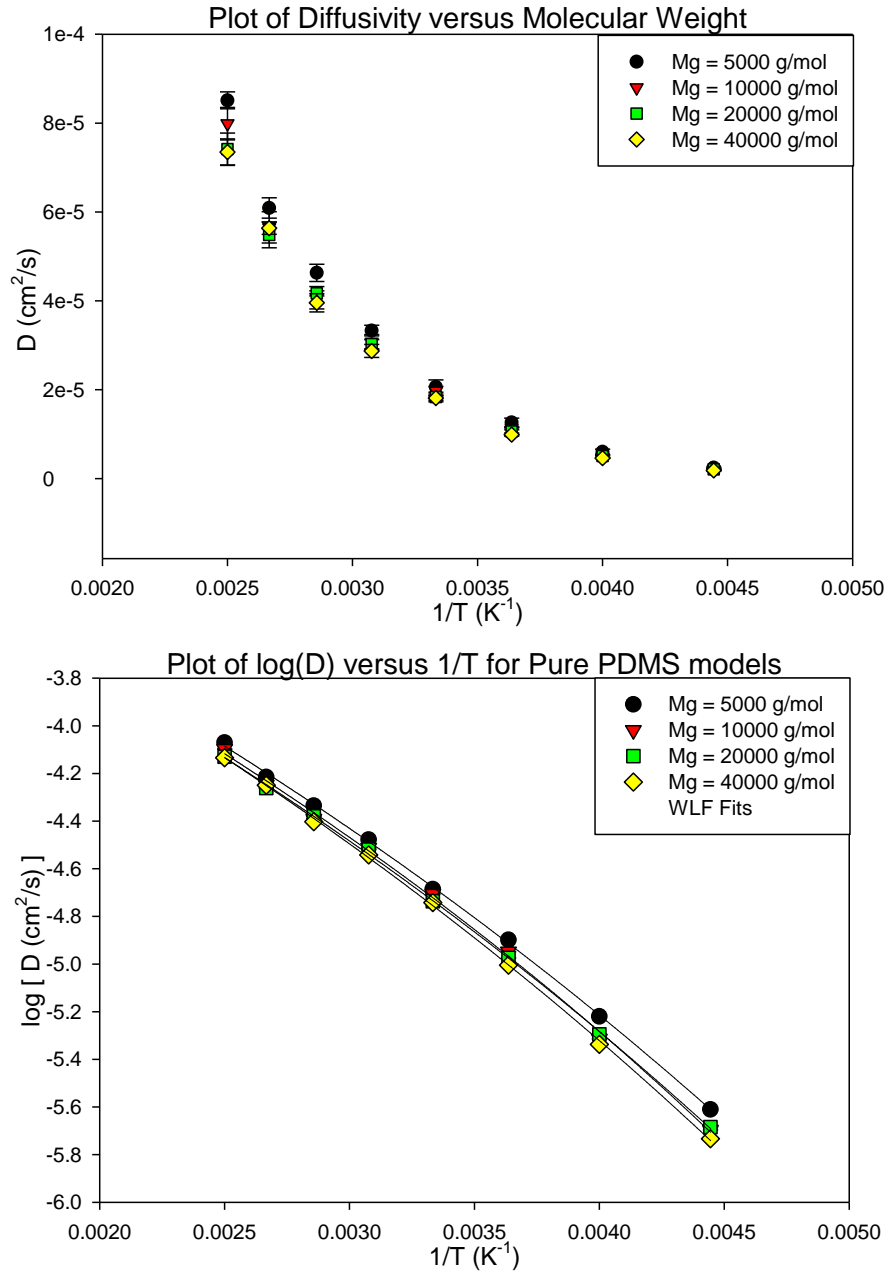
Figure 17. Temperature dependence of the diffusion coefficient for O_2 diffusion through pure PDMS models of varying molecular weights. The WLF fit captures the role of temperature while the Arrhenius relationship (valid well above T_g) is illustrated with a dashed line (blue).

The above figures clearly show that (1) the diffusion coefficient increases with increasing temperature, (2) increasing chain length reduces the ability of O_2 molecules to diffuse through the PDMS matrix thereby resulting in a decrease in D, (3) the variation in D for models with varying molecular weight is more pronounced at higher temperatures, and (4) the WLF equation provides an excellent fit to the diffusion data in this study. The reduction in diffusivity can be attributed to greater possibilities for physical entanglements with increasing chain length. Entanglements tend to restrict movement of the chains reducing available diffusion paths in the system, thereby serving as potential obstruction to the diffusion of penetrants. This is clearly represented in the above plots. Also, short chains have more potential for self-diffusion than longer chains resulting in a higher displacement of these short chains especially at higher temperatures. This added evolution of free volume in the system enhances penetrate diffusion through the PDMS matrix. Therefore, these simulations supplement the experimentally observed trend of an inverse relationship between diffusivity and chain length.

A previous MD [8] study of diffusion of atmospheric penetrates through short chain pure PDMS systems consisting 50 chains of 10 repeating units reported a diffusion coefficient for O_2 of 5.3776×10^{-5} cm^2/s at 300 K. In this study, for the pure PDMS model with a molecular weight of 5000 g/mol (n = 66), the diffusion coefficient obtained at 300 K is 2.0632×10^{-5} cm^2/s. The reduction in diffusion coefficient can be logically explained by (1) the molecular weight in this study is much larger than the previous study and this increase in chain length could serve as a possible obstruction to the flow of penetrants, and (2) a higher penetrant weight percent could provide a higher flux aiding diffusion. Other studies for O_2 diffusion [78, 79] reported diffusion coefficients of 1.8×10^{-5} and 3.7×10^{-5} cm^2/s respectively.

IV.3.2 Relationship between Chain Length and WLF Parameters

As mentioned above, the WLF equation is fit to the O_2 diffusion data and provides good agreement with the molecular dynamics simulation results. Figure 18 shows a plot of the variation of the WLF parameters with molecular weight for the pure PDMS models.
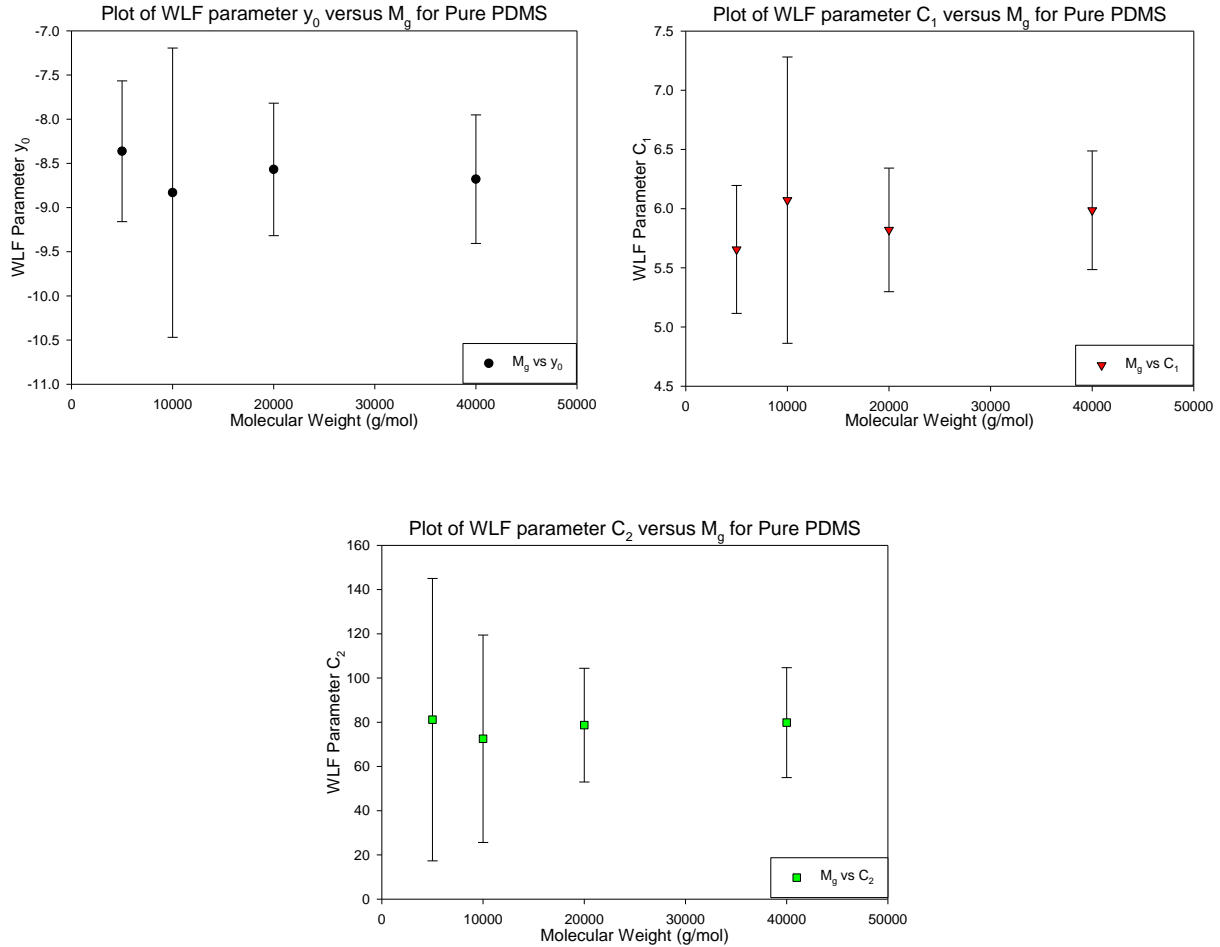
Figure 18. Relationship between chain lengths versus WLF parameters for pure PDMS systems.

For O_2 diffusion through pure PDMS models, the following trends can be observed: (1) a decrease in the y_0 WLF parameter with increasing molecular weight, (2) a very modest increase in the C_1 parameter, (3) the C_2 parameter staying fairly constant with increasing molecular

weight, and (4) the increase/decrease with an increase in molecular weight appears linear especially when the tolerances due to standard deviation are considered. For the four different molecular weight models, O_2 diffusion through pure PDMS, a fit to the WLF equation provides C_1 values ranging from 5.65 to 6.07, which is relatively close to the value of 6.1 reported by Angell [70]. The C_2 parameter value varies from 72.51 to 81.17 and the y_0 parameter ranges from -8.83 to -8.36. The author is not aware of reported C_2 and y_0 values for PDMS in literature.

IV.4 Diffusion Results for Crosslinked PDMS Models

The following sections provide plots and discussions regarding the results of diffusion for the crosslinked PDMS systems in this study. Recall that the crosslinked systems are of molecular weights 5,000, 10,000, 20,000, and 40,000 g/mol with weight ratios of 5:1 and 10:1. There is also a discussion of the trends in the WLF fit parameters for the aforementioned model.

IV.4.1 Effect of Crosslinking and Weight Ratio on Diffusion

Figure 19 shows the influence of crosslinking and weight ratio on the diffusion coefficient for each of the molecular weights studied.
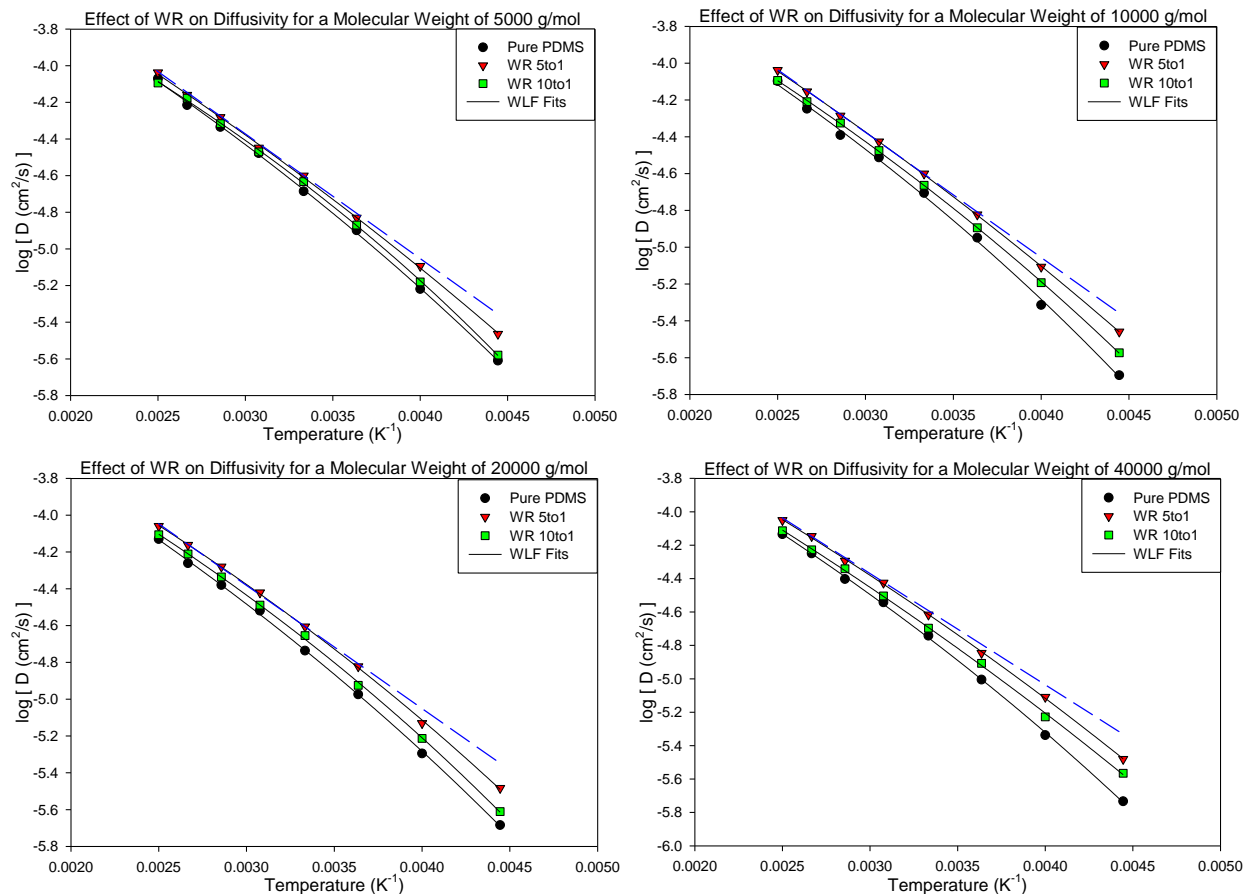
Figure 19. Temperature dependence of the diffusion coefficient for O_2 diffusion through crosslinked PDMS models with weight ratios of 5:1 and 10:1 for varying molecular weights. The WLF fit captures the role of temperature while the Arrhenius relationship (valid well above T_g) is illustrated with a dashed line (blue).

MD simulation data in the above figure indicates that the crosslinked PDMS systems display higher diffusivity than the pure uncrosslinked PDMS system at all temperatures and molecular weights studied. This seems counter-intuitive because crosslinking increases the molecular weight of the chains restricting their motion and evolution of free volume resulting in reduced diffusion paths and even trapped penetrants. This phenomenon of enhanced diffusivity in crosslinked PDMS systems is attributed to the presence of free or unbonded crosslink molecules in these systems, which is discussed in greater detail in the following section (IV.4.2).

Also, analyzing the diffusion data for only the crosslinked PDMS systems, it can be concluded that the system with a PDMS: crosslink molecule weight ratio of 5:1 shows higher diffusivity than the 10:1 system at all temperatures and molecular weights studied. Recall from Table 3 that at any given molecular weight, the crosslinked system with a weight ratio of 5:1 has more crosslink molecules than the 10:1 system. Therefore, our initial hypothesis of free crosslink molecules enhancing diffusivities in crosslinked systems is further consolidated by observing the trend in the above plots which indicate the system with the most crosslink molecules shows highest diffusivity. It is also interesting to note the strong deviation from Arrhenius behavior at lower temperatures (225 K and 250 K) for pure PDMS systems as compared to the crosslinked systems. Recall that glass transition temperatures obtained through MD simulation in this study for all the systems studied here are roughly 190 K. Also, when approaching this transition temperature, the segmental motion of polymers is severely restricted. Therefore, it is natural that the crosslinked systems will tend to display a more Arrhenius-like behavior as compared to the pure PDMS chain systems due to the presence of extremely mobile crosslink molecules in the former system.

IV.4.2 Crosslink Distribution: Crosslinked Models

In order to justify the diffusion data for crosslinked systems and the validity of the hypothesis presented in Section IV.4.1, we analyze the effect of the dynamic crosslinking process itself employed in this work to ascertain the number of bonds added to each crosslink molecule (ranging from 0 to 4) during the generation of the crosslinked network.
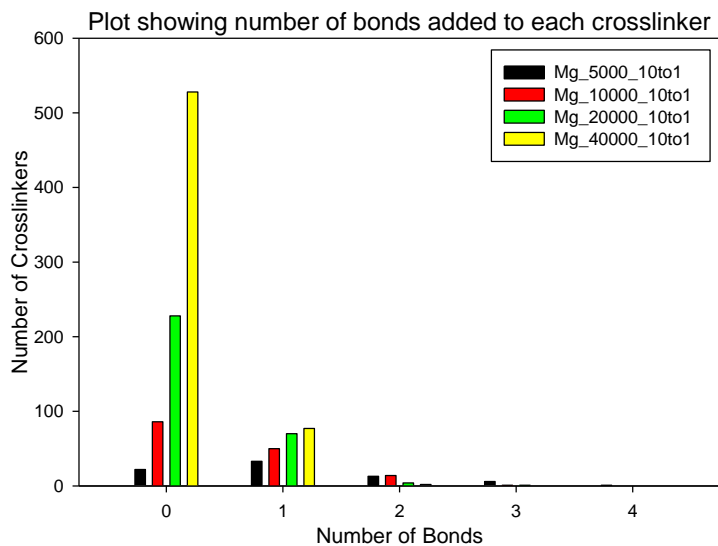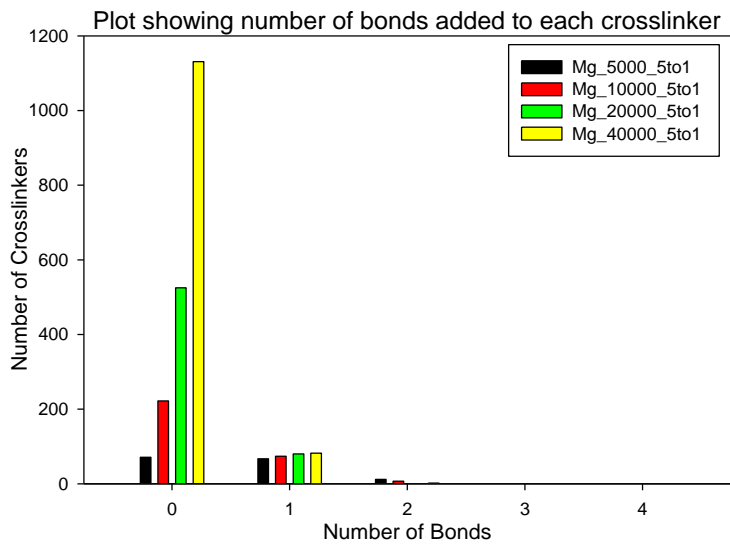
Figure 20. Crosslink Distribution represented via grouped bar charts for CL models with weight ratios of 5:1 (top) and 10:1 (bottom) display the number of bonds added to each crosslinker to illustrate the underlying network structure.

.

Figure 21, a grouped bar chart, enables the analysis of the number of bonds added to each crosslink molecule in a given system for weight ratios of 5:1 and 10:1 for the four different molecular weights examined in this study. In this work, such an analysis is critical due to the

possible existence of a large number of potentially unbonded crosslinkers after the completion of the crosslinking process especially in models with higher molecular weights.

In Figure 21, the zero on the x-axis represents the number of free crosslink molecules present in the system. The largest model in the above plot (molecular weight of 40,000 g/mol and weight ratio of 5:1) has 1,131 free crosslinker molecules as compared to the 22 free crosslinker molecules the smallest model (molecular weight of 5,000 g/mol and weight ratio of 10:1). The large number of unbonded crosslinker molecules in the models with higher molecular weights result in enhanced diffusivity. Although this would seem counterintuitive, analyzing crosslink density of the structure would help explain this phenomenon. Now, it is important to realize that just because a PDMS and crosslinker bond, it is only the bonding of this pair to another chain that will severely increase the viscosity of the melt. A mere 4.65% of the crosslink molecules form two or more bonds in the largest model while that statistic rises to 59.25% in the smallest case. Therefore, a dense network structure is generated in these smaller models with fewer unbonded crosslink molecules. These entanglements due to crosslinks potentially act as a barrier to the flow of penetrants through the smaller (low molecular weight) systems resulting in a decline in diffusivity. Hence, the increased diffusion in models with higher molecular weight (and therefore more unbonded crosslink molecules) is logical and explained through conducting crosslink distribution analysis of the various models.

IV.4.3 Effect of Chain Length for Crosslinked Systems with the same Weight Ratio

Figure 20 shows the influence of chain length on diffusivity for a constant crosslink density and weight ratios studied:
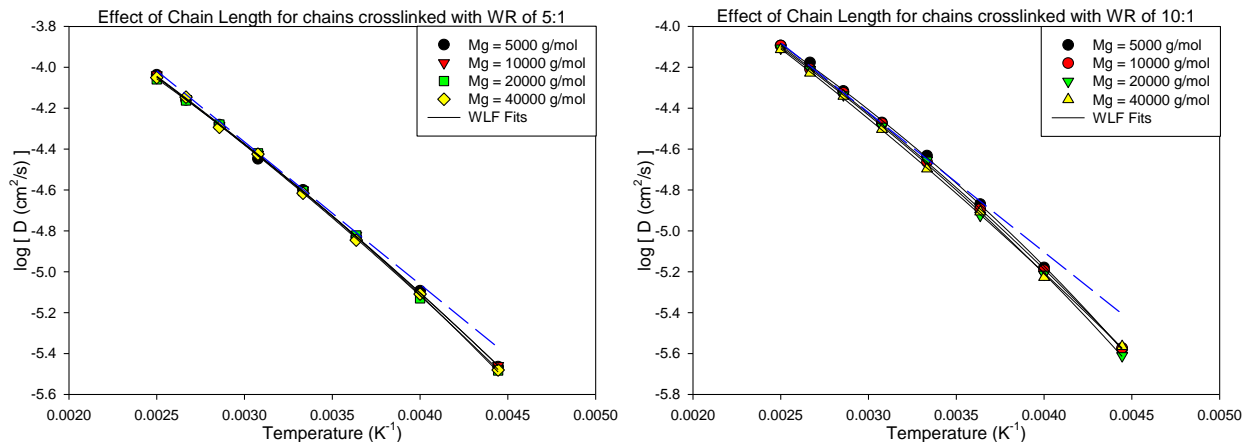
Figure 21. Temperature dependence of the diffusion coefficient for O_2 diffusion through crosslinked PDMS models with weight ratios of 5:1 (left) and 10:1 (right) for varying molecular weights. The plots specifically analyze the effect of chain length for crosslinked chains with varying weight ratios. The WLF fit captures the role of temperature while the Arrhenius relationship (valid well above T_g) is illustrated with a dashed line (blue).

MD simulation data in the figure above indicates the effect of molecular weight for crosslinked systems of similar weight ratios. It can be concluded that for a given weight ratio, the diffusivity decreases with an increase in molecular weight of the PDMS chains. This effect is more pronounced in the case with weight ratio of 10:1, which is logical as the case with weight ratio of 5:1 has more crosslinker molecules at each molecular weight. The enhanced mobility of these low molecular weight species along with their excessive presence in the 5:1 case tends to alleviate the effect of molecular weight on diffusivity. Therefore, the crosslinked models obey the experimentally observed trend of an inverse relationship between molecular weight and diffusivity just like the pure PDMS models in this study. Even though deviation from perfect Arrhenius behavior is observed in the crosslinked systems, it is not as severe as the pure PDMS systems. Crosslinked systems with a weight ratio of 10:1 show a greater deviation from Arrhenius behavior from the 5:1 weight ratio systems especially in the region of glass transition.

IV.4.4 Relationship between M_g, Weight Ratio, and WLF Parameters

As mentioned previously, the WLF equation is fit to the O_2 diffusion data and provides good agreement with the molecular dynamics simulation results. Figure 22 shows a plot of the variation of the WLF parameters at a given weight ratio for crosslinked systems of varying molecular weights.

For O_2 diffusion through crosslinked PDMS models at the two different weight ratios studied, no definitive trend in the variation of the WLF parameters is noticed. Analyzing Figure 22, it can be stated that the trends shown in pure PDMS systems are eliminated in the crosslinked PDMS models at both the weight ratios studied. This lack of dependence of WLF parameters for crosslinked PDMS models is attributed to the excessive free crosslink molecules in these systems, which mitigate any dependence of chain length and weight ratio on the y_0, C_1, and C_2 parameters. For O_2 diffusion through crosslinked PDMS systems, a fit to the WLF equation provides C_1 values ranging from 5.06 to 5.39, C_2 values range from 76.72 to 95.66, and the shift parameter y_0 varies from -8.19 to -7.71 for the case with weight ratio of 5:1 at the four different molecular weights studied. For the 10:1 case, C_1 values range from 5.24 to 6.01, C_2 values range from 62.14 to 95.72, and y_0 varies from -8.90 to -7.91. Note that these values are for varying molecular weight systems at a given weight ratio.
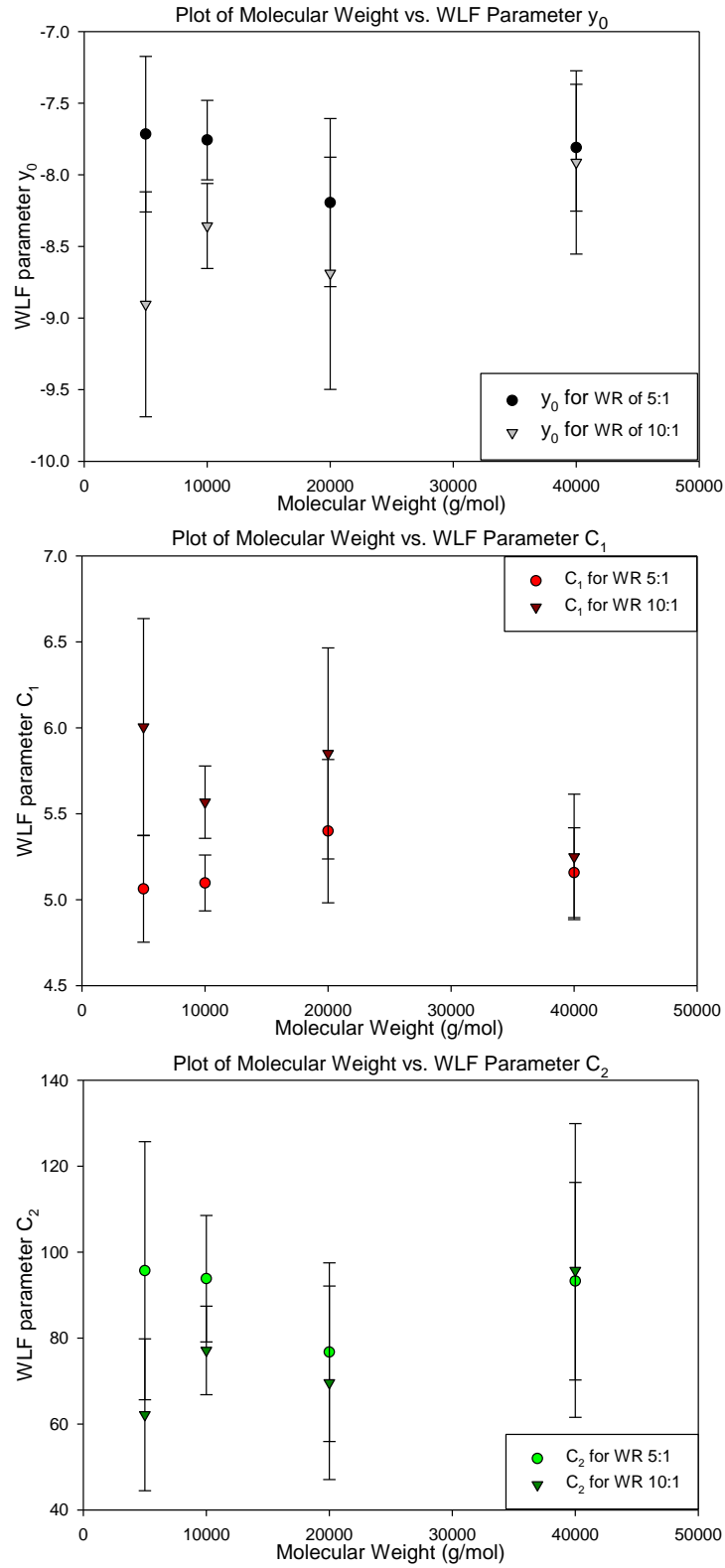
Figure 22. Relationship between WLF parameters for various chain lengths at a weight ratio of 5:1 (top) and 10:1 (bottom) for crosslinked PDMS systems.

IV.5 Diffusion Results for Crosslinked PDMS-based Nanocomposite Models

The following sections provide plots and discussions regarding the results of diffusion for the crosslinked PDMS-based nanocomposite systems in this study. The PDMS-based nanocomposite models are identical to the crosslinked systems discussed in Chapter IV.4 with the inclusion of Cu nanoparticles at 5%, 10%, and 20% volume fraction. There is also a discussion of the trends in the WLF fit parameters for the aforementioned model.

IV.5.1 Effect of Chain Length for a WR of 5:1 at varying Nanoparticle Volume Fraction

Figure 23 shows the plot of the log of diffusivity as a function of inverse temperature for O_2 diffusion through PDMS-based nanocomposites with varying nanoparticle volume fractions and molecular weights for a weight ratio of 5:1. The plots indicate that increasing the nanoparticle volume fraction decreases the diffusivity of small atmospheric penetrates through PDMS-based nanocomposites. Therefore, the presence of Cu nanoparticles reduces the ability of O_2 molecules to diffuse through the PDMS matrix. This reduction in diffusivity with increasing volume fraction is more pronounced at higher temperatures. An increase in molecular weight (and therefore in the number of crosslinkers present) results in an enhanced diffusivity at higher temperatures. Although not clearly evident in the 5 and 10 percent volume fraction cases, the 20 percent volume fraction case clearly displays a certain "crossover" behavior resulting in increased diffusivities (compared to the 5% and 10% VF cases) at lower temperatures.
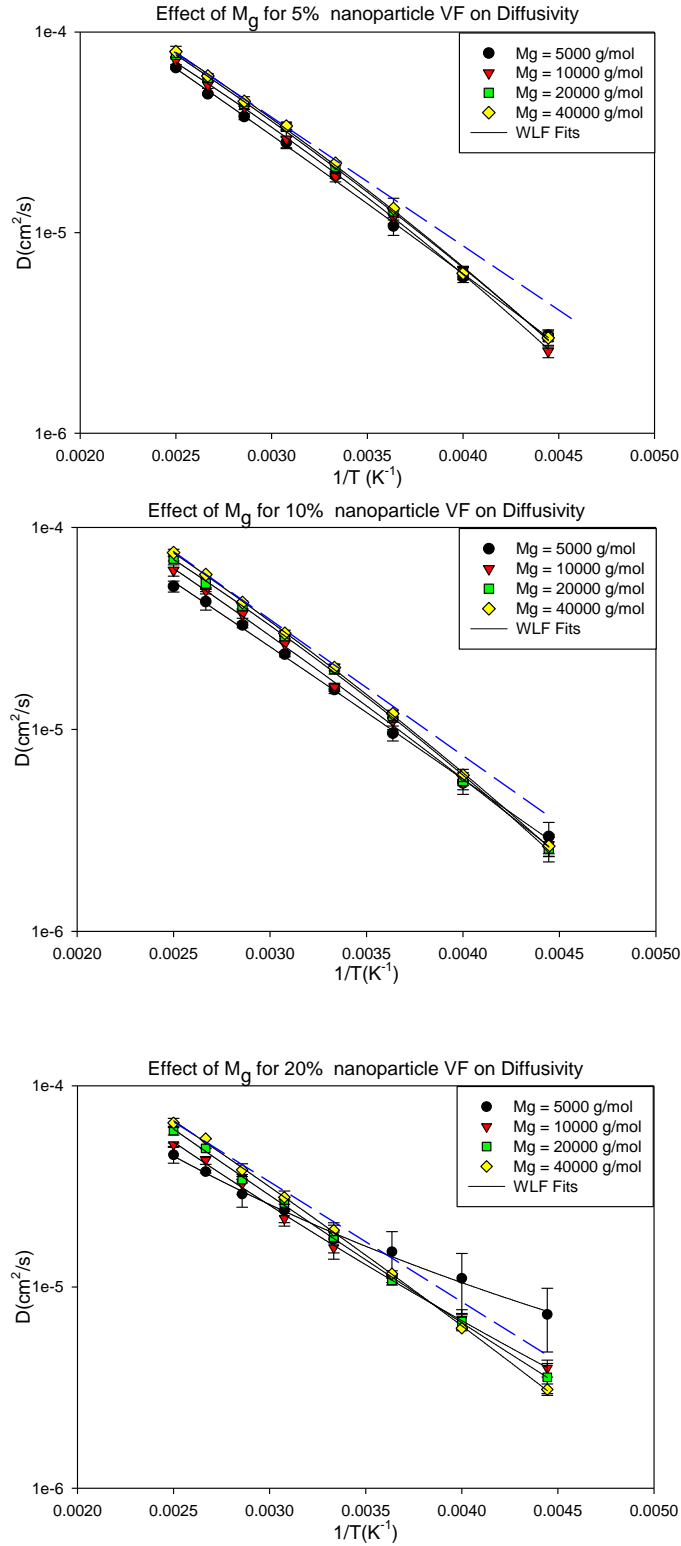
Figure 23. Temperature dependence of the diffusion coefficient for O_2 diffusion through PDMS nanocomposites as a function of Cu nanoparticle volume fraction. The WLF model captures the role of temperature while the blue dashed line illustrates perfect Arrhenius behavior.

Similar "crossover" behavior was observed in a previous study [9] and this characteristic

was attributed to the reduced spacing between nanosized inclusions with an increase in volume

fraction. In general, as glass transition temperature is approached, the segmental motion of the

polymer ceases. A combination of limited mobility and interactions between nanoparticle

surfaces and crystalline polymer surfaces results in the creation of high density envelopes of

PDMS around the nanoparticles which likely increase in thickness as the temperature approaches

T_g. However, as the spacing between nanoparticles decreases, PDMS chains are "trapped" in

these gaps resulting in low density pockets of PDMS. Therefore, increased diffusivity in models

with the smallest gap between nanoparticles at lower temperatures (closer to T_g) is attributed to

the preferential diffusion of the penetrants through localized regions of low density according to

this previous study [9]. This probable behavior of PDMS chains that are essentially "trapped" in

these low density pockets is schematically illustrated in Figure 24.

Cu Nanoparticles

PDMS regions with
higher density due to
nanoparticle surfaces

PDMS regions of low density
due to nanoparticles

Figure 24. Schematic illustration of the variation in PDMS density within the nanocomposite
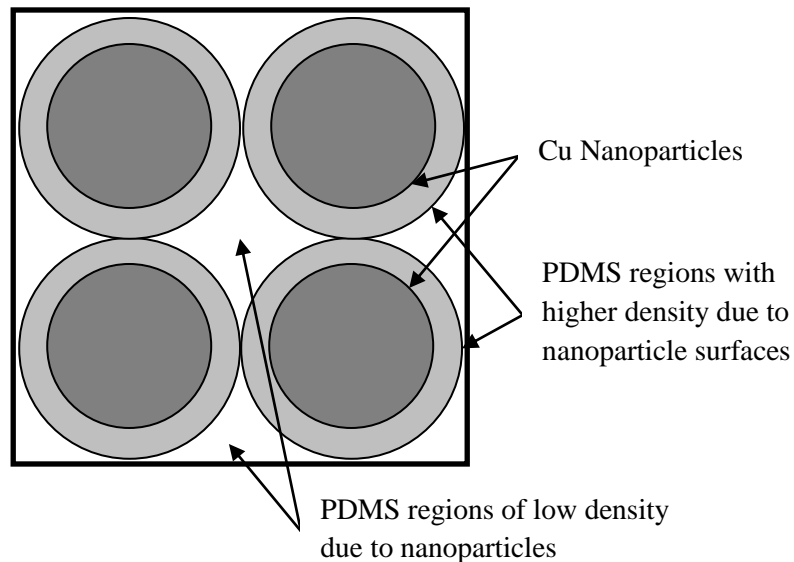models when PDMS regions strongly influenced by the nanoparticle surfaces overlap [9].

IV.5.2 Effect of Chain Length for a WR of 10:1 at varying Nanoparticle Volume Fraction

Figure 25 shows the plot of the log of diffusivity as a function of inverse temperature for O_2 diffusion through PDMS-based nanocomposites with varying nanoparticle volume fractions and molecular weights for a weight ratio of 10:1. Similar behavior to the previously studied case of weight ratio 5:1 is observed resulting in reduced diffusivity of atmospheric penetrants with increasing volume fraction.

The previously observed "crossover" behavior appears for 20% volume fraction for a weight ratio of 10:1. This "crossover" appears extreme for the case with PDMS chains with a molecular weight of 5000 g/mol. This configuration has the smallest gap between the Cu nanoparticles (9.95 Å) among all the different configurations studied here. This is further proof of the extreme sensitivity of these nanocomposite systems to the gap spacing between nanoparticles. Also, this configuration has the fewest number of crosslinker molecules (75) and analyzing the crosslink distribution for this case indicates that several of the crosslinkers form two or three bonds with some forming four. Therefore, the final structure that is generated is highly viscous with little scope for the evolution of free volume in the system due to this high crosslink density.
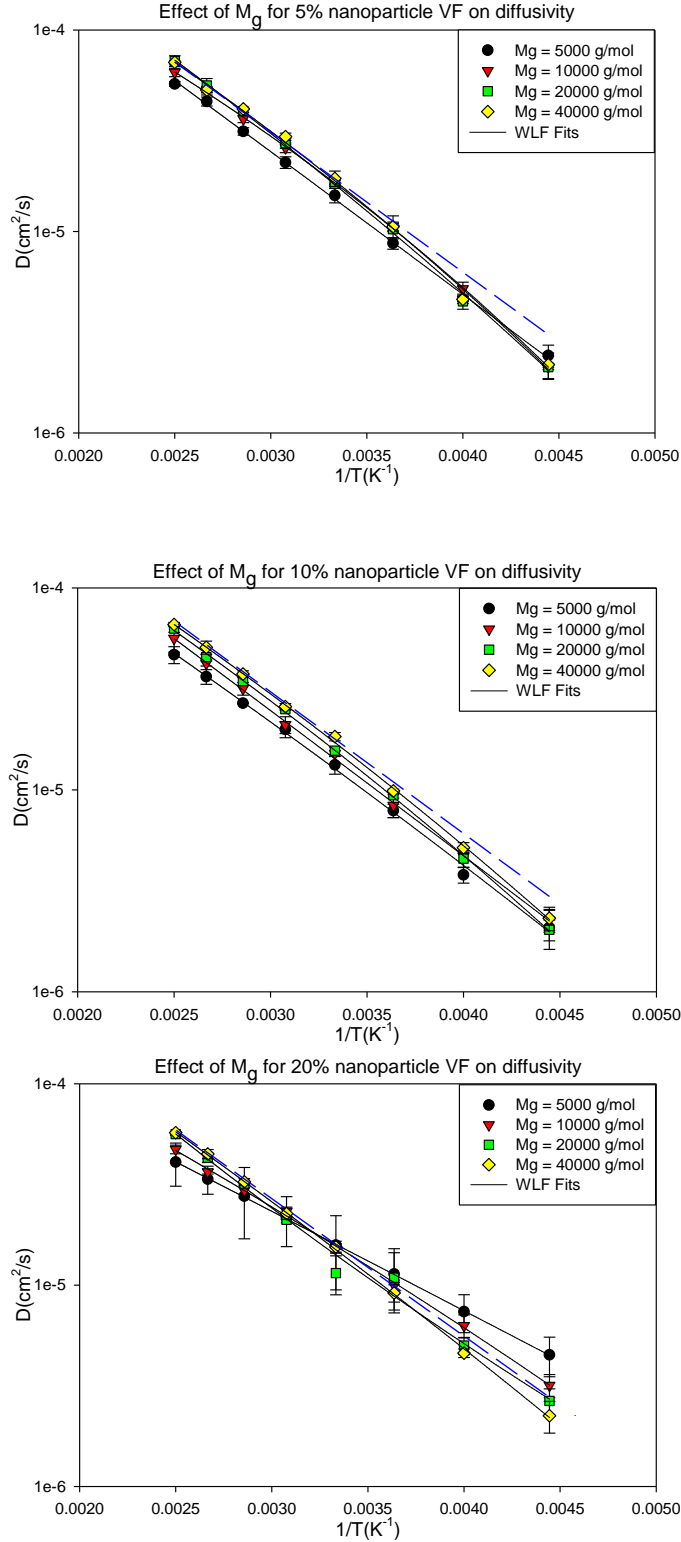
Figure 25. Temperature dependence of the diffusion coefficient for O_2 diffusion through PDMS nanocomposites as a function of Cu nanoparticle volume fraction. The WLF model captures the role of temperature while the blue dashed line illustrates perfect Arrhenius behavior.

IV.5.3 Crosslink Distribution: Nanocomposite Models

Similar to the crosslinked PDMS case, in order to justify the diffusion results for the PDMS-based nanocomposites case, we analyze the crosslink distribution in the network to ascertain the number of bonds added to each crosslink molecule (recall this ranges from 0 to 4). As described in Chapter IV.4.3, conducting such an analysis is crucial in explaining the diffusion results, the presence of a large number of crosslinker molecules for models with higher molecular weights leads to a higher probability of unbonded crosslink molecules in the system for such models. In order to present the underlying idea, Figure 26 studies the crosslink distribution for models with a 5% nanoparticle volume fraction at weight ratios of 5:1 and 10:1 for varying molecular weights. In this figure, the zero on the x-axis represents the number of free crosslinkers present in the system. The largest model in the above plot (molecular weight of 40,000 g/mol and weight ratio of 5:1) has 1,132 unbonded crosslinker molecules as compared to the 21 free crosslinker molecules the smallest model (molecular weight of 5,000 g/mol and weight ratio of 10:1). This would then imply enhanced diffusivity in larger models due to the added mobility of the crosslinkers. A mere 4.7% of the crosslinkers form two or more bonds in the largest model while that statistic rises to 59% in the smallest case. Therefore, a dense network structure is generated in these smaller models with fewer crosslinkers which potentially acts as a barrier to the flow of penetrants through the system resulting in a decline in diffusivity.
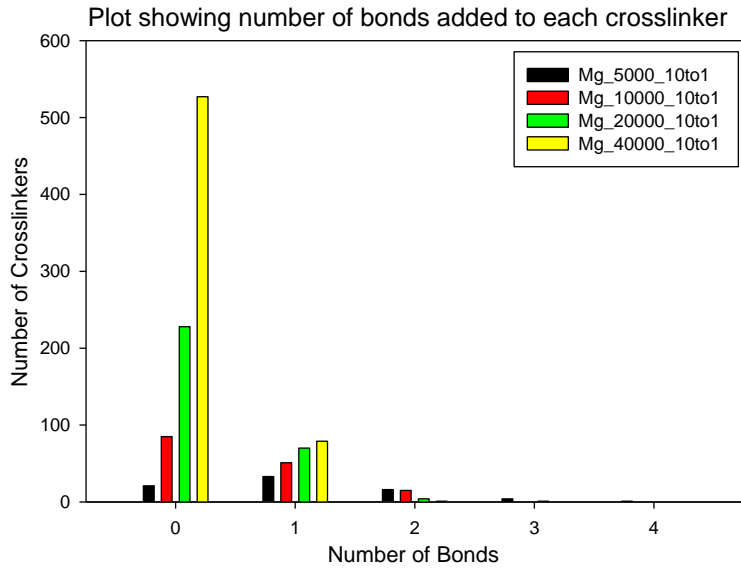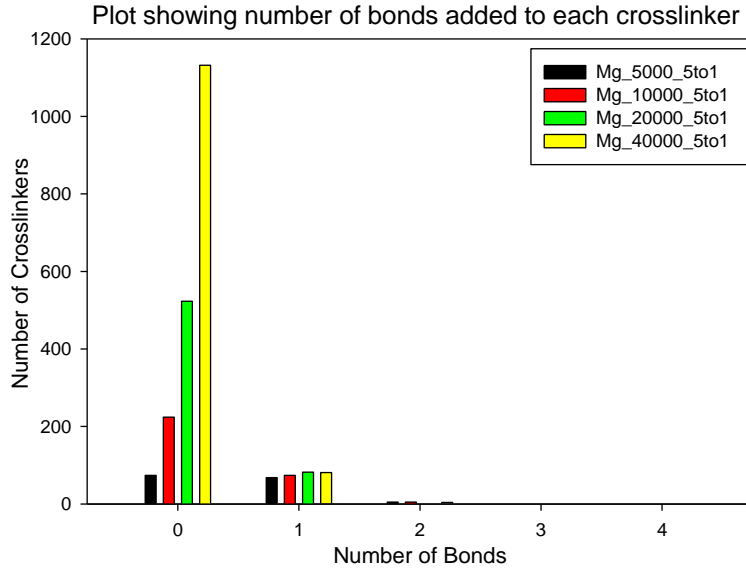
Figure 26. Crosslink Distribution represented via grouped bar charts for PDMS-based nanocomposite models with volume fraction of 5% and weight ratios of 5:1 (top) and 10:1 (bottom) display the number of bonds added to each crosslinker to illustrate the underlying network structure.

IV.5.4 Relationship between M_g, Weight Ratio, Volume Fraction, and WLF Parameters

As mentioned previously, the WLF equation is fit to the O_2 diffusion data and provides good agreement with the molecular dynamics simulation results. Figure 27 shows a plot of the variation of the WLF parameters at a 5:1 weight ratio for PDMS-based nanocomposite systems of different molecular weights at varying volume fraction. For O_2 diffusion through PDMS-based nanocomposite systems, the following trends can be observed for increasing nanoparticle volume fraction: (1) a decrease in the C_1 WLF parameter, (2) an increase in the y_0 and C_2 parameters, (3) the increase/decrease of all three WLF parameters is in a nonlinear fashion. It is interesting to note that for all three parameters, the D of the model with molecular weight of 40,000 g/mol experiences only a small shift when transitioning from 10% to 20% nanoparticle volume fraction while this transition for the three other models appears highly non-linear.

For O_2 diffusion through crosslinked PDMS-based nanocomposite systems, a fit to the WLF equation provides C_1 values ranging from 4.66 to 5.32, C_2 values range from 79.66 to 125.79, and the shift parameter y_0 varies from -8.19 to -7.29 for the case with weight ratio of 5:1 and 5% volume fraction at the four different molecular weights studied. For the system with weight ratio of 5:1 and 10% volume fraction, C_1 values range from 4.42 to 5.33, C_2 values range from 81.97 to 133.88, and y_0 varies from -8.18 to -7.16. The PDMS-based nanocomposite system with weight ratio 5:1 and 20% volume fraction has C_1 values ranging from 3.48 to 4.68, C_2 ranging from 118.58 to 414.13, and y_0 varying from -7.35 to -5.66.
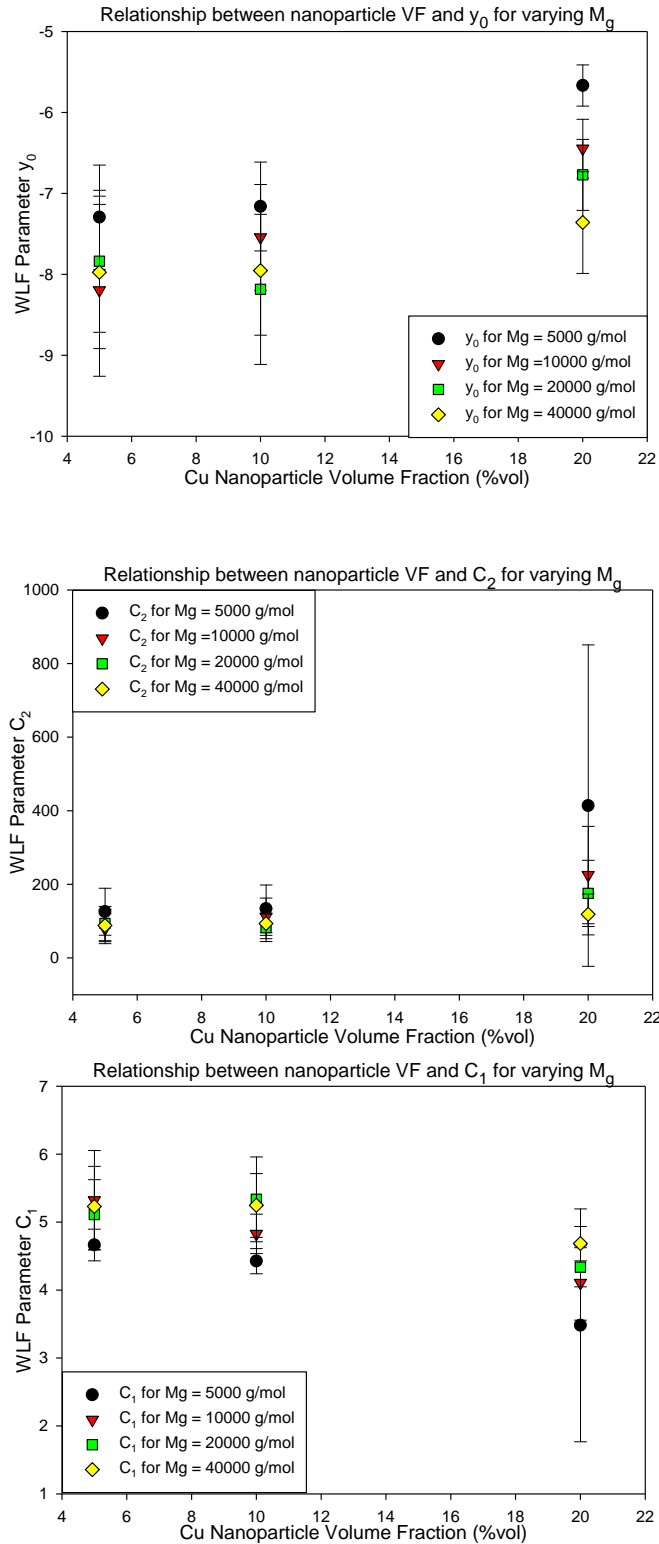
Figure 27. Relationship between WLF parameters for different chain lengths at a weight ratio of 5:1 for varying Cu nanoparticle volume fractions for PDMS-based nanocomposite systems.
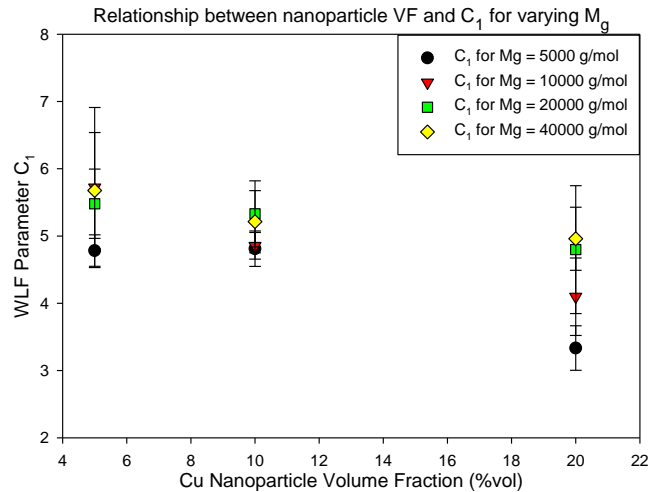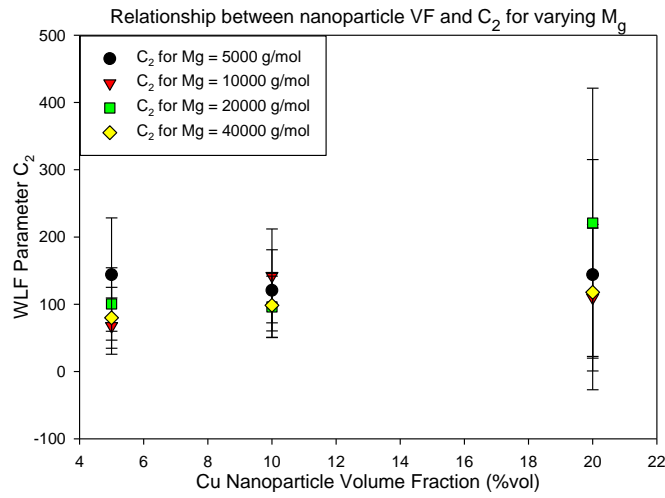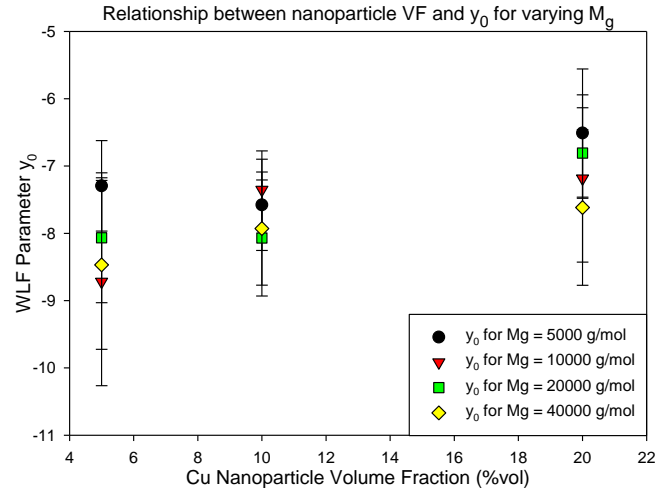
Figure 28. Relationship between WLF parameters for different chain lengths at a weight ratio of 10:1 for varying Cu nanoparticle volume fractions for PDMS-based nanocomposite systems.

Figure 28 shows a plot of the variation of the WLF parameters at a 10:1 weight ratio for PDMS-based nanocomposite systems of different molecular weights at varying volume fraction. For O_2 diffusion through PDMS-based nanocomposite systems, the following trends can be observed for increasing nanoparticle volume fraction: (1) a decrease in the C_1 WLF parameter, (2) an increase in the y_0 and C_2 parameters, (3) the increase/decrease of all three WLF parameters is in a nonlinear fashion. Similar to the case of a weight ratio of 5:1 for PDMS-based nanocomposites, the D of the model with molecular weight of 40,000 g/mol is the only one that consistently experiences a small shift when transitioning from 10% to 20% nanoparticle volume fraction for all three parameters. In the 10:1 case however, the transition from the 10% and 20% nanoparticle volume fraction is less non-linear as in the 5:1 case especially for the y_0 and C_2 parameters.

In summary, recall that the WLF parameters for pure PDMS showed an approximately linear increase/decrease while the crosslinked PDMS and PDMS-based nanocomposite cases displayed a nonlinear increase/decrease of the WLF parameters. Although it would require more data to develop a quantitative model, based on the data we have it could be concluded that the crosslinking induces this nonlinearity in the WLF parameters' variation with molecular weight for a given weight ratio. This trend is unchanged in the PDMS-based nanocomposite cases as well as described in Chapter IV.5.

IV.6 Comparison between Pure, CL, and PDMS-based Nanocomposite Models

As described in the thesis objectives, a unique feature of this study was to not only study diffusion through the pure, crosslinked, and PDMS-based nanocomposite models, but also to be able to compare between these models and observe changes in diffusivity due to chain length, weight ratio, and volume fraction. For clarity purposes, the WLF equation is not fit to the diffusion data for these comparisons.

IV.6.1 Comparing Diffusivity for Pure, CL, and NC models at WR of 5:1

Figure 29 compares diffusivity for all three models at a constant weight ratio of 5:1 at each of the molecular weights studied here. The plots indicate the following trend in diffusivity: (1) the crosslinked models show the highest diffusivity, (2) the effect of chain length on diffusivity can clearly be observed for models with molecular weight of 20,000, and 40,000 g/mol, as these models show minimal variation between pure PDMS and the 5% and 10% volume fraction cases while a hierarchy (CL PDMS, pure PDMS, 5%, 10%, 20%) is clearly observed for the cases with molecular weight of 5,000 and 10,000 g/mol, (3) the "crossover" behavior at lower temperatures is shown by all models with 20% nanocomposite volume fraction, and (4) the pure PDMS systems show a strong tendency to deviate from Arrhenius behavior at lower temperatures.
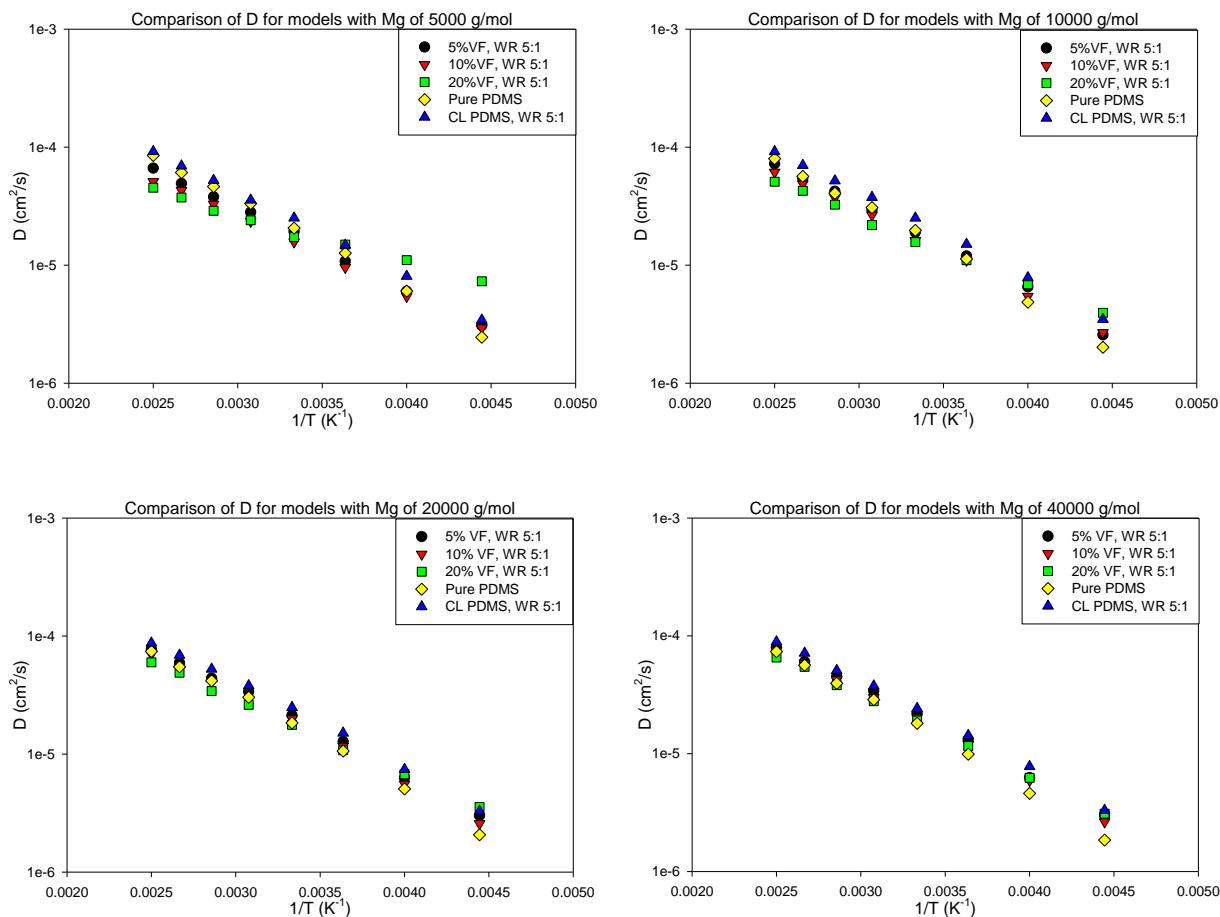
Figure 29. Comparison of D for pure, crosslinked, and PDMS-based nanocomposite systems for varying molecular weights and volume fractions and a weight ratio of 5:1

In short chain pure PDMS systems, the enhanced mobility of the chains along with a possibility of self-diffusion results in evolution of free volume within the system allowing for greater diffusivity for the penetrants. However, the presence of free crosslinkers in the crosslinked nanocomposite cases for these short chain models also results in enhanced diffusivity for the aforementioned reasons. Therefore, minimal differences are observed between the pure PDMS and the nanocomposite cases (5% and 10% VF) at higher molecular weights. As there is no available data for crosslinked PDMS models and PDMS-based nanocomposites, the results obtained cannot be compared to other studies.

IV.2.8 Comparing Diffusivity for Pure, CL, and NC models at WR of 10:1

In Figure 30, diffusivity for all three models at a constant weight ratio of 10:1 at each of the molecular weights studied. Similar behavior to the 5:1 case in Figure 29 is observed. It is important to note that the pronounced effects of chain length on diffusivity for the 20,000, and 40,000 g/mol characterized by the narrow distribution of the data points across various models. The 10:1 case has the fewer crosslink molecules for a given molecular weight compared to the 5:1 case and also a higher crosslink density. Both of these factors contribute by significantly lowering the diffusivity of these models as the aforementioned factors restrict the diffusion path.
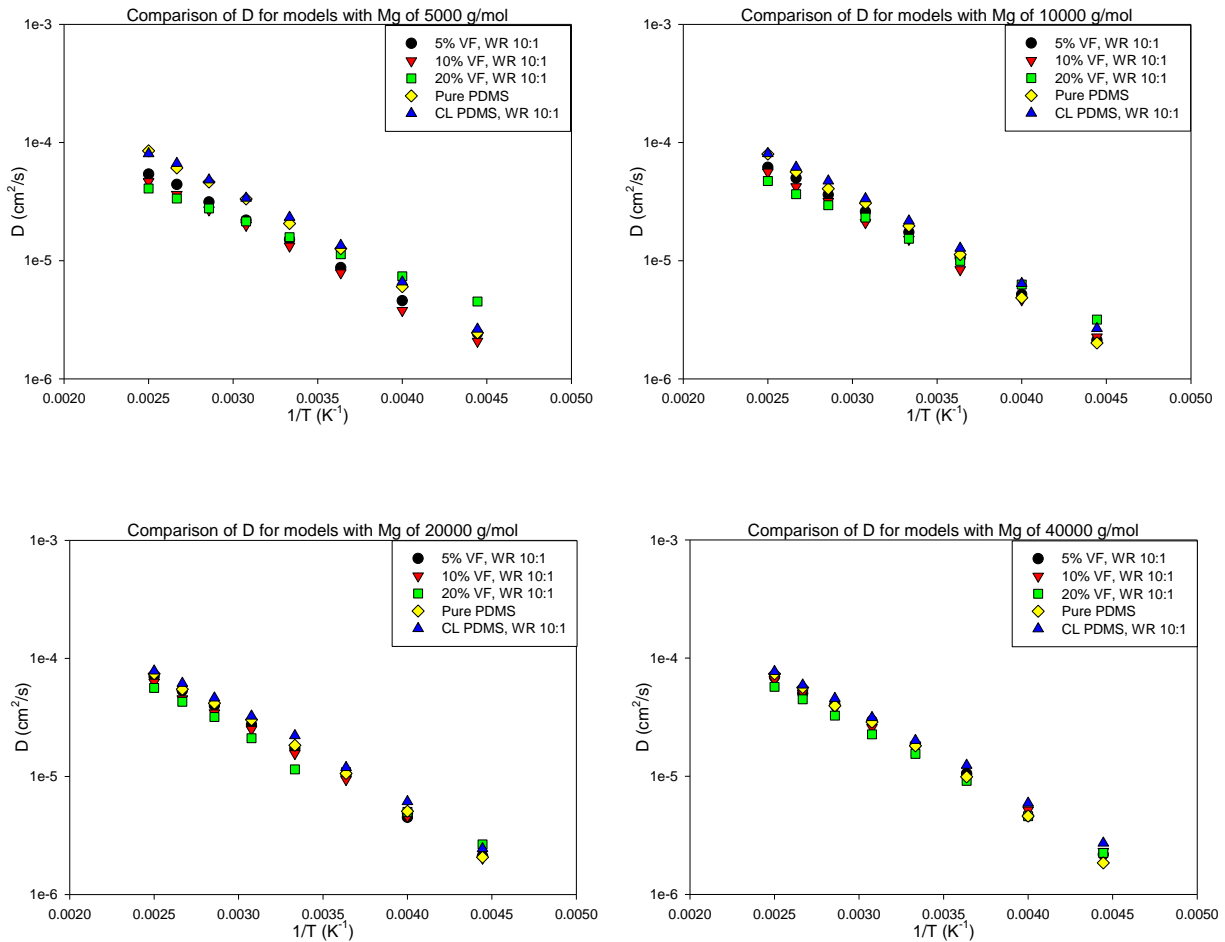

Figure 30. Comparison of D for pure, crosslinked, and PDMS-based nanocomposite systems for varying molecular weights and volume fractions and a weight ratio of 10:1

Chapter V. CONCLUSIONS AND FUTURE WORK

This chapter restates the thesis objectives, provides a detailed discussion of the steps used to accomplish these objectives and the conclusions that can be made on the basis of the results provided in the thesis. There is also a brief discussion of the future work that could supplement and elaborate some of the results presented this thesis.

V.1 Conclusions

In this study, MD simulations are performed to study the study of diffusion of an atmospheric penetrate (O_2) in pure PDMS, crosslinked PDMS, and PDMS-based nanocomposites. In order to understand the effect of chain length on diffusion in the aforementioned systems, models of four different molecular weights are constructed using a CD-CBMC code Towhee. These chain lengths are selected such that two of the models (5,000 and 10,000 g/mol) are below the entanglement length (24,500 g/mol), one is near entanglement (20,000 g/mol) and one is well above entanglement length (40,000 g/mol). The quantitative evaluation of diffusion coefficients is made by tracking the mean-squared displacement of the penetrants within the MD framework. The systems analyzed in this study tend to deviate from Arrhenius behavior at temperatures near glass transition (as shown in Figure 17 for example); therefore, the role of temperature on diffusion is captured using the WLF equation instead of the Arrhenius equation. The obtained diffusion results are validated with data from experiment and other simulations.

The crosslinked systems consist of models with the aforementioned molecular weights and two different PDMS: crosslink molecule weight ratios (5:1 and 10:1). The 10:1 weight ratio was chosen as it closely matches weight ratios used in corresponding experiments [82]. It is

important to note that the experimental sample used vinyl-terminated PDMS chains while this MD study uses silanol-terminated PDMS chains. In order to minimize network strains during network formation, a multistage potential is used simultaneously with the dynamic approach to crosslinking. In order to validate the generated crosslinked structure, histograms analyzing bond, angle, and dihedral distortions are constructed. In addition, the glass transition temperature of the crosslinked structure is also calculated by determining the exact location of the kink on the volume versus temperature curve by fitting a piecewise equation to the plot. Upon attaining 80% crosslink density (number of bonded PDMS chain ends to number of total PDMS chain ends), penetrants are randomly introduced in the system and diffusion results are computed as described previously.

The PDMS-based nanocomposites consist of crosslinked PDMS models containing Cu nanoparticles in varying volume fractions (5%, 10%, and 20%). As described in Section III.8, the objective of studying these models is to understand the role of nanoparticle length scale and volume fraction on the steady state diffusion of penetrants through PDMS. In this study, 8 FCC Cu spheres are inserted in a simple cubic arrangement (inside pre-grown voids created using repulsive potentials) within a unit cell of PDMS chains. After the growth of these voids and insertion of the nanoparticles, the system is crosslinked as described previously until the 80% crosslink density is achieved. Then, diffusion coefficients are calculated by tracking the mean-squared displacement of the atmospheric penetrates.

The conclusions derived from these diffusion simulations along with the summarizing thesis objectives stated in Section I.3 are as follows:

1) *Create a quantitative test matrix.* The diffusion of penetrants in the polymer membrane is affected by temperature, density, chain length, crosslink density, volume fraction of the nanoparticles, weight ratio of the PDMS chains and crosslink moelcules, etc. In this thesis, to study the aforementioned variables of primary importance, a test matrix is developed. This enables the isolation/reduction of these variables affecting the diffusion of O_2 penetrants in the pure, crosslinked, and PDMS-based nanocomposite systems.

2) *Create and validate an algorithm for crosslinking.* As described previously in this chapter, crosslinking can induce severe strain on the newly formed network structure. In order to avoid this situation, a multistage potential was employed which was linear above a predefined cutoff distance and harmonic otherwise. This objective was successfully achieved when analysis on the crosslinked network structure yielded close conformation to the equilibrium bond, angle, and dihedral values. Allowing sufficient relaxation of the crosslinked structure before crosslinking further enables the structure to dissipate the strain and return to a state of equilibrium conformation. Furthermore, in order to perform MD simulations on systems similar to experiments (which tend to be large considering MD length scales), the algorithm had to have the capability of being extended to large systems. The algorithm employed in this study uses a dynamic crosslinking algorithm allowing multiple pairs within a predefined cutoff to react and form bonds overcoming to a large degree the stress imposed by larger systems.

3) *Study the effect of chain length and unbonded crosslink molecule ends on the diffusion mechanism.* The properties of the PDMS chains vary with chain length: viscous jelly-like

behavior below the entanglement length and a higher viscosity solid-like state above entanglement. This transition is an important phenomenon as the physical behavior of the system is altered. Therefore, this change in the physical property can be correlated to changes in diffusivity for models above the entanglement length. This can be verified from Figure 17, where the model above entanglement length shows the following characteristics: (1) the lowest diffusivity at all temperatures compared to the three other lower molecular weight models in the pure PDMS case, and (2) the strongest deviation from Arrhenius behavior. An increase in chain length results in a system that has more entanglements and in the pure PDMS models these entanglements restrict the local motion of the PDMS chains. Consequently, this restricts the free volume evolution in the system which is essential for diffusion translating into reduced diffusivities. In the crosslinked systems, along with these physical entanglements, the crosslinks themselves create junctions restricting the evolution of free volume in the system which serves as an obstruction for penetrate diffusion. This would imply that crosslinking would lead to a reduction in diffusivity in the crosslinked system compared to the pure PDMS system. However, upon conducting further analysis on the crosslink distribution in the system (number of bonds added to each tetrafunctional crosslink molecule), it can be concluded that the presence of large number of unbonded crosslink molecules in the system leads to enhanced diffusivity compared to the pure PDMS case. This is because the crosslink molecule has a molecular weight of 324.7 g/mol which is much lower than the PDMS chains which gives it enhanced mobility enabling the evolution of free volume in the system even at lower temperatures. This can be verified in Figure 19, where for a given molecular weight; the diffusivity can be arranged in a descending order: crosslinked

99

system with weight ratio 5:1 (most crosslink molecules), crosslinked system with weight ratio 10:1, and pure PDMS systems.

4) *Create a crosslinked model of PDMS-based nanocomposites.* Upon successfully validating data from the pure PDMS and crosslinked PDMS systems, the challenge with the PDMS-based nanocomposite models lay in growing the voids to place the Cu nanoparticles. The growth of these voids, at specific locations in the system, is performed by using a purely repulsive potential. This slowly repels the PDMS chains away from the center of these voids until the radius of the sphere is devoid of any atoms. The Cu particles are then inserted into the voids and care is taken to ensure there is no overlap with the PDMS chains or crosslink molecules. A few atoms in the center of the nanoparticle are fixed at zero force and velocity to prevent their translation or rotation during simulation.

5) *Evaluate factors that will affect in the nanocomposite case.* For the nanocomposite models studied here, the weight ratio is a dominant factor contributing to diffusivity. This can be verified in Figures 24 and 25, where the systems with the most number of crosslink molecules show the highest diffusivity at a given nanoparticle volume fraction for all three systems of varying volume fractions studied. Although both chain length and nanoparticle volume fraction undoubtedly affect diffusivity, in this study weight ratio dominates due to the excessive number of unbonded crosslink molecules in the system. Therefore, at a given volume fraction, the model with the highest molecular weight (and

therefore the most crosslink molecules) shows the highest diffusivity. This trend, although still evident, is more subtle in the systems with weight ratio of 10:1 as these systems have fewer crosslink molecules than the cases with weight ratio of 5:1 and containing a denser network structure. The fewer unbonded crosslink molecules along with a dense network structure tend to diminish the dominating effect of weight ratio and the contribution of chain length to diffusivity is highlighted. At 20% nanoparticle volume fraction, regardless of the weight ratio, diffusivity of both models with molecular weights of 5,000 and 10,000 g/mol exhibit a crossover behavior at lower temperatures. Despite the presence of fewer crosslink molecules in these models, they show higher diffusivity than models with higher molecular weights (20,000 and 40,000 g/mol). This phenomenon is attributed to the reduced spacing between nanoparticles due to the increase in nanoparticle volume fraction. At these lower temperatures, which are close to the glass transition temperature, the segmental motion of these polymers ceases. A combination of limited mobility and interactions between nanoparticle surfaces and crystalline polymer surfaces results in the creation of high density envelopes of PDMS around the nanoparticles which likely increase as the temperature approaches T_g. However, as the spacing between nanoparticles decreases, PDMS chains are "trapped" in these gaps resulting in low density pockets of PDMS. Therefore, increased diffusivity in models with the smallest gap between nanoparticles at lower temperatures (closer to T_g) is attributed to the preferential diffusion of the penetrants through localized regions of low density. For a given weight ratio and molecular weight, comparing between the pure, crosslinked, and PDMS-based nanocomposite models, the diffusivity can be arranged in a descending order: crosslinked PDMS (most crosslinker molecules), pure

PDMS, and PDMS-based nanocompsite models with 5%, 10%, and 20% nanoparticle volume fraction respectively. This hierarchy is not maintained at lower temperatures due to the crossover behavior displayed at lower temperatures and 20% nanoparticle volume fraction.

V.2 Future Work

In this study, the WLF equation is fit to the diffusion data. The variation of the parameters in this equation are observed for changes in molecular weight (molecular weight at a given weight ratio for crosslinked models) and nanoparticle volume fraction. The trends identified are compared qualitatively. However, if further diffusion data could be obtained for systems of different molecular weights, weight ratios, and nanoparticle volume fractions, it would enable a quantitative analysis of the variation of these parameters for the aforementioned systems. Perhaps with the additional data to supplement the results in this thesis, these trends could be described with a mathematical model which would be an important breakthrough and provide greater understanding of PDMS and its characteristics in various systems.

In this initial study of PDMS-based nanocomposites, 8 FCC Cu nanoparticles were arranged in a simple cubic fashion in a PDMS unit cell. Perhaps, a potential future study could consider different aspects of particle inclusions varying the number of nanoparticles, their shape and size, their arrangement within the unit cell, the material of the nanoparticles. Choosing a different material for the nanoparticle will essentially alter its interactions with the rest of the system and the penetrants. Performing studies with different materials then would be crucial to understanding the effects of the nanoparticles themselves on the process of diffusion. Since in

the crosslinking portion of this study, there is a specific interest to conform to experiments, similar steps can be taken in future PDMS-based nanocomposite studies. The largest nanoparticle radius considered in this study is 2.85 nanometers (molecular weight of 40,000 g/mol and weight ratio of 5:1) whereas in experiments, nanoparticles are typically 20 nanometers. Assuming we want to maintain a 20% Cu nanoparticle volume fraction while scaling up the nanoparticles to experimental size, we would need to increase the number of chains in our system from 50 to approximately 2156. The number of atoms contributed by PDMS chains would then rise from 106,650 to 4,598,750. Therefore, computational challenges definitely accompany the scaling in size of the system, although models of this size are not unattainable.

Works Cited

1. Roberge, Pierre R. *Corrosion Engineering: Principles and Practice*. New York: McGraw-Hill, 2008. Print. Pages 10, 13

2. *Corrosion Basics: An Introduction.* Houston, TX: National Association of Corrosion Engineers, 1984. Print.

3. Schweitzer, Philip A. *Corrosion and Corrosion Protection Handbook*. New York: M. Dekker, 1983. Print.

4. Uhlig, Herbert Henry, and R. Winston Revie. *Corrosion and Corrosion Control: An Introduction to Corrosion Science and Engineering*. New York: Wiley, 1985. Print.

5. Roberge, Pierre R. *Handbook of Corrosion Engineering*. New York: McGraw-Hill, 2000. Print.

6. "Maintenance Strategies." National Association of Corrosion Engineers. Web. 5 July 2011. <http://events.nace.org/library/corrosion/Inspection/Strategies.asp>.

7. Pan, Feng, and A. Huang. *ASME International Mechanical Engineering Congress and Exposition Proceedings*. 2009. 12041. Print.

8. Sudibjo, A., and Douglas E. Spearot. "Molecular Dynamics Simulations of Diffusion of Small Atmoshperic Penetrates in Polydimethylsiloxane." *Molecular Simulation* 37.2 (2011): 115-22. Print.

9. Huang, A., and Douglas E. Spearot. *MEMS Based Corrosion Sensors*. Print.

10. Spearot, Douglas E., Alex Sudibjo, Varun N. Ullal, and Adam Huang. "Molecular Dynamics Simulations of Diffusion of O2 and N2 Penetrates in Polydimethylsiloxane-based Nanocomposites." *Journal of Engineering Materials and Technology*. Print.

11. Heine, David R., Gary S. Grest, Christian D. Lorenz, Mesfin Tsige, and Mark J. Stevens. "Atomistic Simulations of End-Linked Poly(dimethylsiloxane) Networks: Structure and Relaxation." *Macromolecules* 37.10 (2004): 3857-864. Print.

12. Chow, Winnie Wing Yin, Kin Fong Lei, Guangyi Shi, Wen Jung Li, and Qiang Huang. "Microfluidic Channel Fabrication by PDMS-interface Bonding." *Smart Materials and Structures* 15.1 (2006): S112-116. Print.

13. "Polydimethylsiloxane." *NationMaster.com*. Web. <http://www.nationmaster.com/encyclopedia/Polydimethylsiloxane>.

14. "Polymer Cross-Linking Information." Rockbestos-Surprenant Cable Corp., 2003. Web. <http://www.r-scc.com/pdf/tech-electronics.pdf>.

15. Sperling, L. H. *Introduction to Physical Polymer Science*. New York: Wiley, 2011. Print.

16. Allen, Michael P. *Introduction to Molecular Dynamics Simulations*. Tech. Vol. 23. John Von Neumann Institute for Computing, 2004. Print. NIC Ser.

17. Allen, M. P., and D. J. Tildesley. *Computer Simulation of Liquids*. Oxford: Clarendon, 2000. Print.

18. Ercolessi, Furio. *A Molecular Dynamics Primer*. Tech. Trieste, Italy: Spring College in Computational Physics, 1997. Print.

19. "Periodic Boundary Conditions." *Swiss EMBnet Node Server*. Web. <http://www.ch.embnet.org/MD_tutorial/pages/MD.Part3.html>.

20. Rothlisberger, Ursula. "Magic and Mysteries of Modern Molecular Dynamics Simulations: A Basic Introduction." *Infoscience*. 2002. Print.

21. Sprik, M. "Introduction to Molecular Dynamics Methods." *Monte Carlo and Molecular Dynamics of Condensed Matter Systems : Euroconference on Computer Simulation in Condensed Matter Physics and Chemistry* (1996): 43-88. Print.

22. Sudibjo, A. *Molecular Dynamics Study of Diffusion of Atmospheric Penetrates in Polydimethylsiloxane and Polydimethylsiloxane-based Nanocomposites*. Thesis. University of Arkansas, 2010. Print.

23. Frischknecht, Amalie L., and John G. Curro. "Improved United Atom Force Field for Poly(dimethylsiloxane)." *Macromolecules* 36.6 (2003): 2122-129. Print.

24. Erkoc, S. *Annual Reviews of Computational Physics.* Vol. IX. Singapore: World Scientific, 2001. Print. 1

25. Sok, R. M., H.J. C. Berendsen, and W.F. Van Gunsteren. "Molecular Dynamics Simulation of the Transport of Small Molecules across a Polymer Membrane." *Journal of Chemical Physics* 96.6 (1992): 4699. Print.

26. Spearot, Douglas E. *Atomistic Calculations of Nanoscale Interface Behavior in FCC Metals*. Diss. Georgia Tech, 2005. Print.

27. "Democritus: Integration Algorithms." *COMPSOC*. Web. <http://www.compsoc.man.ac.uk/~lucky/Democritus/Theory/verlet.html>.

28. Melchionna, S., G. Ciccotti, and B. L. Holian. "Hoover NPT Dynamics for Systems Varying in Shape and Size." *Molecular Physics* 78.3 (1993): 533-44. Print.

29. Sokal, Alan D. "Monte Carlo Methods in Statistical Mechanics: Foundations and New Algorithms." Functional Integration: Basics and Applications. Cargese Summer School. Sept. 1996. Lecture.

30. Spearot, Douglas E. "Computational Materials Science." University of Arkansas, Fayetteville. Jan. 2010. Lecture.

31. Frenkel, Daan. *Lecture Notes: Introduction to Monte Carlo Methods*. Vol. 23. Jülich: NIC, 2004. Print. Pages 29-60

32. Metropolis, N., A. W. Rosenbluth, M. N. Rosenbluth, A. N. Teller, and E. Teller. "Equation of State Calculations by Fast Computing Machines." *Journal of Chemical Physics* 21 (1953): 1087-092. Print.

33. Rosenbluth, M. N., and A. W. Rosenbluth. "Monte Carlo Calculation of the Average Extension of Molecular Chains." *The Journal of Chemical Physics* 23.2 (1955): 356. Print.

34. Siepmann, Jörn Ilja, and Daan Frenkel. "Configurational Bias Monte Carlo: A New Sampling Scheme for Flexible Chains." *Molecular Physics* 75.1 (1992): 59-70. Print.

35. Martin, Marcus G. "MCCCS Towhee (Configurational-bias Monte Carlo)." *MCCCS Towhee*. 11 Aug. 2010. Web. <http://towhee.sourceforge.net/algorithm/cbmc.html>.

36. Martin, Marcus G., and J. Ilja Siepmann. "Novel Configurational-Bias Monte Carlo Method for Branched Molecules. Transferable Potentials for Phase Equilibria. 2. United-Atom Description of Branched Alkanes." *The Journal of Physical Chemistry B* 103.21 (1999): 4508-517. Print.

37. Martin, Marcus G., and Aidan P. Thompson. "Industrial Property Prediction Using Towhee and LAMMPS." ScienceDirect, 2004. Web.

38. *LAMMPS Molecular Dynamics Simulator*. Web. <http://lammps.sandia.gov/>.

39. Polak, E. *Computational Methods in Optimization; a Unified Approach*. New York: Academic, 1971. Print.

40. Stukowski, A. "Visualization and Analysis of Atomistic Simulation Data with OVITO - the Open Visualization Tool." *OVITO - The Open Visualization Tool*. Web. <http://ovito.org/>.

41. Shy, L. Y., Y. K. Leung, and B. E. Eichinger. "Critical Exponents for Off-lattice Gelation of Polymer Chains." *Macromolecules* 18.5 (1985): 983-86. Print.

42. Doherty, D. "Polymerization Molecular Dynamics Simulations. I. Cross-linked Atomistic Models for Poly(methacrylate) Networks." *Computational and Theoretical Polymer Science* 8.1-2 (1998): 169-78. Print.

43. Schulz, Michael, and Harry L. Frisch. "Monte Carlo Studies of Interpenetrating Polymer Network Formation." *The Journal of Chemical Physics* 101.11 (1994): 10008. Print.

44. Tsige, Mesfin, Christian D. Lorenz, and Mark J. Stevens. "Role of Network Connectivity on the Mechanical Properties of Highly Cross-Linked Polymers." *Macromolecules* 37.22 (2004): 8466-472. Print.

45. Tsige, Mesfin, and Mark J. Stevens. "Effect of Cross-Linker Functionality on the Adhesion of Highly Cross-Linked Polymer Networks: A Molecular Dynamics Study of Epoxies." *Macromolecules* 37.2 (2004): 630-37. Print.

46. Komarov, Pavel, Chiu Yu Tsung, Chen Shih Ming, Pavel G. Khalatur, and Peter Reineker. "Highly Cross-Linked Epoxy Resins: An Atomistic Molecular Dynamics Simulation Combined with a Mapping/Reverse Mapping Procedure." *Macromolecules* 40.22 (2007): 8104-113. Print.

47. Varshney, Vikas, Soumya S. Patnaik, Ajit K. Roy, and Barry L. Farmer. "A Molecular Dynamics Study of Epoxy-Based Networks: Cross-Linking Procedure and Prediction of Molecular and Material Properties." *Macromolecules* 41.18 (2008): 6837-842. Print.

48. Li, Chunyu, and Alejandro Strachan. "Molecular Simulations of Crosslinking Process of Thermosetting Polymers." *Polymer* 51.25 (2010): 6058-070. Print.

49. Nouri, Nima, and Saeed Ziaei-Rad. "A Molecular Dynamics Investigation on Mechanical Properties of Cross-Linked Polymer Networks." *Macromolecules* 44.13 (2011): 5481-489. Print.

50. Schilling, Michael R. "The Glass Transition of Materials Used in Conservation." *Studies in Conservation* 34.3 (1989): 110-16. Print.

51. Ebewele, Robert Oboigbaotor. *Polymer Science and Technology*. Boca Raton: CRC, 2000. Print.

52. Rigby, David, and Ryong-Joon Roe. "Molecular Dynamics Simulation of Polymer Liquid and Glass. I. Glass Transition." *The Journal of Chemical Physics* 87.12 (1987): 7285. Print.

53. Han, Jie, Richard H. Gee, and Richard H. Boyd. "Glass Transition Temperatures of Polymers from Molecular Dynamics Simulations." *Macromolecules* 27.26 (1994): 7781-784. Print.

54. Fried, J. R., and P. Ren. "Molecular Simulation of the Glass Transition of Polyphosphazenes." *Computational and Theoretical Polymer Science* 9.2 (1999): 111-16. Print.

55. Yu, Kun-qian, Ze-sheng Li, and Jiazhong Sun. "Polymer Structures and Glass Transition: A Molecular Dynamics Simulation Study." *Macromolecular Theory and SImulation* 10.6 (2001): 624-33. Print.

56. Buchholz, Joachim. "Cooling Rate Dependence of the Glass Transition Temperature of Polymer Melts: Molecular Dynamics Study." *Journal of Chemical Physics* 117.15 (2002): 7364. Print.

57. Yang, Liu, David Srolovitz, and Albert Yee. "Molecular Dynamics Study of Isobaric and Isochoric Glass Transitions in a Model Amorphous Polymer." *Journal of Chemical Physics* 110.14 (1999): 7058. Print.

58. Andrady, A. L., M. A. Llorente, and J. E. Mark. "Some Dynamic Mechanical Properties of Unimodal and Bimodal Networks of Poly(dimethylsiloxane)." *Polymer Bulletin* 26.3 (1991): 357-62. Print.

59. Ferry, John D. *Viscoelastic Properties of Polymers*. New York: Wiley, 1980. Print.

60. "Concepts, Definition, and the Diffuison Equation." Web. <http://www.ifh.uni-karlsruhe.de/lehre/envflu_i/Downloads/course_script/ed2/ch1.PDF>.

61. Smith, William F. *Principles of Materials Science and Engineering*. New York: McGraw-Hill, 1996. Print.

62. Chitra, R., and S. Yashonath. "Estimation of Error in the Diffusion Coefficient from Molecular Dynamics Simulations." *The Journal of Physical Chemistry B* 101.27 (1997): 5437-445. Print.

63. Hunt, T. A., and B. D. Todd. "Diffusion of Linear Polymer Melts in Shear and Extensional Flows." *Journal of Chemical Physics* 131.5 (2009). Print.

64. Pikunic, J., and K. E. Gubbins. "Molecular Dynamics Simulations of Simple Fluids Confined in Realistic Models of Nanoporous Carbons." *The European Physical Journal E - Soft Matter* 12.1 (2003): 35-40. Print.

65. Gabbott, Paul. *Applications of Thermal Analysis*. Ames, IA: Blackwell Pub., 2007. Print.

66. William, Malcolm, Robert Landel, and John Ferry. "The Temperature Dependence of Relaxation Mechanisms in Amorphous Polymers and Other Glass-forming Liquids." *Journal of American Chemical Society* 77.14 (1955): 3701-707. Print.

67. Lomellini, P. "Williams-Landel-Ferry versus Arrhenius Behaviour: Polystyrene Melt Viscoelasticity Revised." *Polymer* 33.23 (1992): 4983-989. Print.

68. Packham, D. E. *Handbook of Adhesion*. Hoboken, NJ: John Wiley, 2005. Print.

69. Povolo, F., and M. Fontelos. "Time-temperature Superposition Principle and Scaling Behaviour." *Journal of Materials Science* 22.5 (1987): 1530-534. Print.

70. Angell, C. A. "Why C1 = 16-17 in the WLF Equation Is Physical-and the Fragility of Polymers." *Polymer* 38 (1997): 6261-266. Print.

71. Shaw, Montgomery T., and William J. MacKnight. *Introduction to Polymer Viscoelasticity*. Hoboken, NJ: Wiley-Interscience, 2005. Print.

72. Urakawa, Osamu, Stephen F. Swallen, M. D. Ediger, and Ernst D. Von Meerwall. "Self-Diffusion and Viscosity of Low Molecular Weight Polystyrene over a Wide Temperature Range." *Macromolecules* 37.4 (2004): 1558-564. Print.

73. Trohalaki, S., D. Rigby, A. Klockowski, J. E. Mark, and R. J. Roe. *Polymer Preprints (Am. Chem. Soc. Div. Polym. Chem)* 30.2 (1989): 23. Print.

74. Sok, Robert. *Permeation of Small Molecules across a Polymer Membrane: A Computer Simulation Study*. Diss. University of Groningen, 1964. Print.

75. Tamai, T., H. Tanaka, and K. Nakanishi. "Molecular Simulation of Permeation of Small Penetrants through Membranes. 1. Diffusion Coefficients." *Macromolecules* 27 (1994): 4498-508. Print.

76. Takeuchi, Hisao, and Keiji Okazaki. "Molecular Dynamics Simulation of Diffusion of Simple Gas Molecules in a Short Chain Polymer." *The Journal of Chemical Physics* 92.9 (1990): 5643. Print.

77. Boyd, Richard H., and P. V. Krishna Pant. "Molecular Packing and Diffusion in Polyisobutylene." *Macromolecules* 24.23 (1991): 6325-331. Print.

78. Charati, S. G., and S. A. Stern. "Diffusion of Gases in Silicone Polymers: Molecular Dynamics Simulations." *Macromolecules* 31.16 (1998): 5529-535. Print.

79. Jawalkar, Sheetal S., and Tejraj M. Aminabhavi. "Molecular Dynamics Simulations to Compute Diffusion Coefficients of Gases into Polydimethylsiloxane and Poly(1,5-Naphthalene)-co-[1,4-durene-2,2′-bis(3,4-dicarboxyl Phenyl)hexafluoropropane Diimide]." *Polymer International* 56.7 (2007): 928-34. Print.

80. Striolo, Alberto, Clare McCabe, and Peter Cummings. "Thermodynamic and Transport Properties of Polyhedral Oligomeric Sislesquioxanes in Poly(dimethylsiloxane)." *Journal of Chemical Physics* 109 (2005): 14300-4307. Print.

81. Shemella, Philip, Teodoro Laino, Oliver Fritz, and Alessandro Curioni. "Molecular Motion of Amorphous Silicone Polymers." *Journal of Physical Chemistry B* 115.12 (2011): 2831-835. Print.

82. "Information about Dow Corning Brand Silicone Encapsulants." *Dowcorning.com*. Dow Corning Corporation. Web. <http://www3.dowcorning.com/DataFiles/090007c88020bcca.pdf>.